

**Springer Theses**

Recognizing Outstanding Ph.D. Research

Mei Yan

# Development of New Catalytic Performance of Nanoporous Metals for Organic Reactions



Springer

# **Springer Theses**

Recognizing Outstanding Ph.D. Research

For further volumes:  
<http://www.springer.com/series/8790>

## **Aims and Scope**

The series “Springer Theses” brings together a selection of the very best Ph.D. theses from around the world and across the physical sciences. Nominated and endorsed by two recognized specialists, each published volume has been selected for its scientific excellence and the high impact of its contents for the pertinent field of research. For greater accessibility to non-specialists, the published versions include an extended introduction, as well as a foreword by the student’s supervisor explaining the special relevance of the work for the field. As a whole, the series will provide a valuable resource both for newcomers to the research fields described, and for other scientists seeking detailed background information on special questions. Finally, it provides an accredited documentation of the valuable contributions made by today’s younger generation of scientists.

### **Theses are accepted into the series by invited nomination only and must fulfill all of the following criteria**

- They must be written in good English.
- The topic should fall within the confines of Chemistry, Physics, Earth Sciences, Engineering and related interdisciplinary fields such as Materials, Nanoscience, Chemical Engineering, Complex Systems and Biophysics.
- The work reported in the thesis must represent a significant scientific advance.
- If the thesis includes previously published material, permission to reproduce this must be gained from the respective copyright holder.
- They must have been examined and passed during the 12 months prior to nomination.
- Each thesis should include a foreword by the supervisor outlining the significance of its content.
- The theses should have a clearly defined structure including an introduction accessible to scientists not expert in that particular field.

Mei Yan

# Development of New Catalytic Performance of Nanoporous Metals for Organic Reactions

Doctoral Thesis accepted by  
Tohoku University, Sendai, Japan

 Springer

*Author*

Dr. Mei Yan  
Key Laboratory of Microsystems and  
Micronanostructures Manufacturing  
Ministry of Education  
Harbin Institute of Technology  
Harbin  
China

*Supervisor*

Prof. Naoki Asao  
WPI Advanced Institute for Materials  
Research  
Tohoku University  
Sendai  
Japan

ISSN 2190-5053

ISSN 2190-5061 (electronic)

ISBN 978-4-431-54930-7

ISBN 978-4-431-54931-4 (eBook)

DOI 10.1007/978-4-431-54931-4

Springer Tokyo Heidelberg New York Dordrecht London

Library of Congress Control Number: 2014933779

© Springer Japan 2014

This work is subject to copyright. All rights are reserved by the Publisher, whether the whole or part of the material is concerned, specifically the rights of translation, reprinting, reuse of illustrations, recitation, broadcasting, reproduction on microfilms or in any other physical way, and transmission or information storage and retrieval, electronic adaptation, computer software, or by similar or dissimilar methodology now known or hereafter developed. Exempted from this legal reservation are brief excerpts in connection with reviews or scholarly analysis or material supplied specifically for the purpose of being entered and executed on a computer system, for exclusive use by the purchaser of the work. Duplication of this publication or parts thereof is permitted only under the provisions of the Copyright Law of the Publisher's location, in its current version, and permission for use must always be obtained from Springer. Permissions for use may be obtained through RightsLink at the Copyright Clearance Center. Violations are liable to prosecution under the respective Copyright Law. The use of general descriptive names, registered names, trademarks, service marks, etc. in this publication does not imply, even in the absence of a specific statement, that such names are exempt from the relevant protective laws and regulations and therefore free for general use.

While the advice and information in this book are believed to be true and accurate at the date of publication, neither the authors nor the editors nor the publisher can accept any legal responsibility for any errors or omissions that may be made. The publisher makes no warranty, express or implied, with respect to the material contained herein.

Printed on acid-free paper

Springer is part of Springer Science+Business Media ([www.springer.com](http://www.springer.com))

**Parts of this thesis have been published in the following journal articles:**

1. Jin, T.; Yan, M.; Menggenbateer.; Minato, T.; Bao, M.; Yamamoto, Y. Nanoporous Copper Metal Catalyst in Click Chemistry: Nanoporosity Dependent Activity without Supports and Bases. *Adv. Synth. Catal.* **2011**, *353*, 3095–3100.
2. Jin, T.; Yan, M.; Yamamoto, Y. Click Chemistry of Alkyne-Azide Cycloaddition Using Nano-structured Copper Catalysts. *ChemCatChem.* **2012**, *4*, 1217–1229.
3. Yan, M.; Jin, T.; Ishikawa, Y.; Minato, T.; Fujita, T.; Chen, L-Y.; Bao, M.; Asao, N.; Chen, M-W.; Yamamoto, Y. Nanoporous Gold Catalyst for Highly Selective Semihydrogenation of Alkynes: Remarkable Effect of Amine Additives. *J. Am. Chem. Soc.* **2012**, *134*, 17536–17542.
4. Yan, M.; Jin, T.; Chen, Q.; Ho, H. E.; Fujita, T.; Chen, L-Y.; Bao, M.; Chen, M-W.; Asao, N.; Yamamoto, Y. Unsupported Nanoporous Gold Catalyst for Highly Selective Hydrogenation of Quinolines. *Org. Lett.* **2013**, *15*, 1484–1487.

# Supervisor's Foreword

Studying the catalytic properties of nanostructured metals is of major interest in the catalytic research. For example, gold nanoparticles in the range of 2–5 nm on suitable oxide supports have attracted much attention over the last two decades owing to their remarkable catalytic activities. However, they have a tendency to agglomerate under reaction conditions, and this process often leads to poor long-term stability. Furthermore, the structural complexity including interaction with supports has limited the understanding of the catalytically important factors. On the other hand, unsupported nanoporous gold has emerged as an efficient catalyst with considerable synthetic potential for several types of molecular transformations. The material can be prepared by the leaching of Ag from an Au–Ag alloy by immersion in nitric acid. The monolithic material consists of a three-dimensional network of ligaments with 10–50 nm diameters, which are dependent on the dealloying conditions. Not only gold but also other metals are available for construction of sponge-like morphology by a similar etching process with corresponding alloys.

Mei Yan focused on nanoporous gold and copper as target materials, and revealed their remarkable catalytic properties in some molecular transformations such as semihydrogenation of alkynes and click reaction. Her work has been exceptionally well received, and her doctoral thesis, entitled *Development of New Catalytic Performances of Nanoporous Metals for Molecular Transformations*, is particularly well written.

From the wealth of the obtained results, I would like to highlight just a few. One research topic was the high catalytic efficiency of nanoporous copper in click chemistry. She succeeded in fabricating nanoporous copper catalysts with tunable nanoporosity from a Cu<sub>30</sub>Mn<sub>70</sub> alloy by controlling the dealloying temperature under free corrosion conditions. She found that the tunable nanoporosity of nanoporous copper led to a significant enhancement of catalytic activity in click chemistry without using any supports and bases. The catalyst exhibited a high reusability; it can be recycled 10 times without significant loss of activity.

A further highlight is that Dr. Yan was the first to succeed in catalyzing the highly selective semihydrogenation of alkynes by using the unsupported nanoporous gold catalyst with organosilanes and water as the hydrogen source, while nanoporous gold catalyst usually showed high catalytic efficiency for oxidative reaction in previous reports. Here, she found that the use of DMF as a solvent,

which generates amines in situ, or pyridine as an additive is crucial to suppress the association of hydrogen atoms on nanoporous gold to form H<sub>2</sub> gas, which is unable to reduce alkynes on the unsupported gold catalysts. Under the optimized reaction conditions, this catalyst showed excellent Z-selectivity for alkenes without any over-reduced alkanes.

Mei Yan's thesis contains outstanding results that are of interest to a broad audience ranging from organic chemists to catalytic chemists. The work for the thesis was performed at Tohoku University, leading to several publications and presentations in international conferences, and was honored with the Presidential Prize for Excellence by Tohoku University.

Sendai, December 2013

Prof. Naoki Asao

# Acknowledgments

The work for this thesis was carried out under the direction of Prof. Yoshinori Yamamoto and Prof. Naoki Asao in the Department of Chemistry, Graduate School of Science, Tohoku University, Japan.

I would like to express my sincere gratitude to Prof. Yamamoto for his encouragement, valuable suggestions, and strict guidance throughout this work. I also thank Prof. Asao for his valuable comments, suggestions, and probing questions, which caused me to learn much more and to know more about my work.

I am deeply grateful to Associate Professor Tienan Jin for his continuous guidance, valuable discussions, and technical advice, and also to Dr. Menggenbateer, Dr. Shirong Lu, and Dr. Fan Yang for their assistance not only with my work but also with my life.

I express my gratitude to Prof. Shaoqin Liu and Dr. Chongshen Guo (Harbin Institute of Technology, China) for their help with the revision of this thesis. I am also thankful to Dr. Qiang Chen, Mr. Yoshifumi Ishikawa, Dr. Jian Zhao, and every member of Prof. Asao's group for their kindness and constructive discussions.

I would like to thank Dr. Taketoshi Minato (Kyoto University) for assistance with the XPS experiments, and also Dr. Takeshi Fujita, Dr. Lu-Yang Chen, and Professor Ming-Wei Chen (WPI-Advanced Institute for Materials Research, Tohoku University) for their guidance in the characterization of nanoporous metals.

I am grateful to Prof. Ming Bao and Associate Professor Xiujuan Feng (Dalian University of Technology, China). Without them, I would not have been at Tohoku University for further study. I would also like to gratefully acknowledge China Scholarship Council, Global Centers of Excellence Program, and WPI-Advanced Institute of Materials Research for their financial support with my living expenses and tuition.

Last but not least, I want to express my deep appreciation to my family for their believing in my success and for their generous support.

# Contents

<b>1 The Fabrication of Nanoporous Metals (Au, Cu, Pd) and Their Application in Heterogeneous Molecular Transformations</b> . . . . .	1
1.1 Introduction . . . . .	1
1.2 Fabrication of Nanoporous Metals . . . . .	2
1.2.1 Fabrication of Nanoporous Gold . . . . .	2
1.2.2 Fabrication of Nanoporous Copper . . . . .	3
1.2.3 Fabrication of Nanoporous Palladium . . . . .	5
1.3 Application in Heterogeneous Molecular Transformations . . . . .	6
1.4 Summary and Outlook . . . . .	14
References . . . . .	14
<b>2 Nanoporous Copper Metal Catalyst in Click Chemistry: Nanoporosity Dependent Activity Without Supports and Bases</b> . . . . .	17
2.1 Introduction . . . . .	17
2.2 Results and Discussion . . . . .	18
2.2.1 Synthesis of Nanoporous Copper . . . . .	18
2.2.2 The Influence of CuNPore Structures on Catalytic Activity in the 1,3-dipolar Cycloaddition of Terminal Alkynes and Organic Azides . . . . .	22
2.2.3 Mechanistic Investigation . . . . .	25
2.3 Conclusion . . . . .	28
2.4 Experimental Section . . . . .	29
2.4.1 General Information . . . . .	29
2.4.2 Materials . . . . .	29
2.4.3 Calculation of TOF and TON . . . . .	30
2.4.4 Fabrication of Cu <sub>30</sub> Mn <sub>70</sub> Alloy . . . . .	30
2.4.5 Representative Fabrication Method of Nanoporous Copper (CuNPore, cat-1) Under Free Corrosion . . . . .	30
2.4.6 Representative Procedure for the CuNPore (cat-1)-Catalyzed Click Reaction of Phenyl Acetylene (1a) and Benzyl Azide (2a) (Tables 2.1 and 2.2) . . . . .	30

2.4.7	Neat Reaction Procedure (Eq. 2.2) . . . . .	31
2.4.8	Leaching Experiment (Fig. 2.9) . . . . .	31
2.4.9	Reusability (Fig. 2.5) . . . . .	32
2.4.10	Formation of Nanostructured Copper Acetylide (Figs. 2.10 and 2.11) . . . . .	32
2.4.11	Analytical Data . . . . .	32
2.4.12	$^1\text{H}$ and $^{13}\text{C}$ NMR Spectra . . . . .	36
	References . . . . .	51

### 3 Nanoporous Gold Catalyst for Highly Selective Semihydrogenation of Alkynes: Remarkable Effect of Amine Additives . . . . .

	of Amine Additives . . . . .	55
3.1	Introduction . . . . .	55
3.2	Results and Discussion . . . . .	56
3.2.1	Nanoporosity Characterization of AuNPore . . . . .	56
3.2.2	AuNPore-Catalyzed Oxidation of Organosilanes with Water . . . . .	59
3.2.3	Optimization of AuNPore-Catalyzed Semihydrogenation of Phenyl Acetylene with Various Organosilanes and Water Using DMF as Solvent (Method A) . . . . .	60
3.2.4	Optimization of Amine Additives on AuNPore- Catalyzed Semihydrogenation (Method B) . . . . .	61
3.2.5	Scope of Alkynes in AuNPore-Catalyzed Semihydrogenation . . . . .	62
3.2.6	Control Experiments and Reaction Pathways . . . . .	65
3.3	Conclusion . . . . .	68
3.4	Experimental Section . . . . .	69
3.4.1	General Information . . . . .	69
3.4.2	Materials . . . . .	69
3.4.3	Fabrication of AuNPore Catalyst . . . . .	69
3.4.4	Representative Procedure for the AuNPore-Catalyzed Semihydrogenation of 1j (Table 3.4, Entry 19): Method A . . . . .	70
3.4.5	Representative Procedure for the AuNPore- Catalyzed Semihydrogenation of 1d (Table 3.4, Entry 8): Method B . . . . .	70
3.4.6	Leaching Experiment . . . . .	70
3.4.7	Synthesis of Starting Materials . . . . .	71
3.4.8	Analytical Data of (1 and 2) . . . . .	72
3.4.9	$^1\text{H}$ and $^{13}\text{C}$ NMR Spectra . . . . .	75
	References . . . . .	88

<b>4 Unsupported Nanoporous Gold Catalyst for Highly Selective Hydrogenation of Quinolines</b> . . . . .	93
4.1 Introduction . . . . .	93
4.2 Results and Discussion . . . . .	94
4.2.1 Characterization of AuNPore . . . . .	94
4.2.2 AuNPore-Catalyzed Hydrogenation of Quinolines . . . . .	95
4.2.3 Proposed Reaction Pathway . . . . .	99
4.3 Conclusion . . . . .	101
4.4 Experimental Section . . . . .	101
4.4.1 General Information . . . . .	101
4.4.2 Materials . . . . .	101
4.4.3 Fabrication of AuNPore Catalyst . . . . .	102
4.4.4 Representative Procedure for the AuNPore-Catalyzed Hydrogenation of 1a (Table 4.1, Entry 5) . . . . .	102
4.4.5 Reaction Procedure for the Hydrogenation of Isoquinoline (1k) . . . . .	102
4.4.6 Deuterium-Labeling Experiment . . . . .	103
4.4.7 Leaching Experiments . . . . .	103
4.4.8 Synthesis of Starting Material (2-propylquinoline 1f) . . . . .	103
4.4.9 Analytical Data of (1 and 2) . . . . .	103
4.4.10 <sup>1</sup> H and <sup>13</sup> C NMR Spectra . . . . .	106
References . . . . .	117
<b>Curriculum Vitae</b> . . . . .	121
<b>Publications</b> . . . . .	123

# Abbreviations

Bn	Benzyl group
bz-THQ	5,6,7,8-tetrahydroquinoline
calcd	Calculated
cat.	Catalyst, catalytic amount
Conc.	Concentrated
CuAAS	Copper catalyzed cycloaddition of alkynes and azides
d	Day, doublet (spectral)
D	Deuterium ( $^2\text{H}$ )
DFT	Density functional theory
DHQ	Decahydroquinoline
DMF	N, N-dimethylformamide
EDX	Energy-dispersive X-ray spectroscopy
eq	Equation
equiv	Equivalent (s)
FTIR	Fourier transform infrared spectroscopy
GC-MS	Gas chromatography-mass spectroscopy
h	Hour
HAADF-STEM	A scanning TEM mode with a high-angle annular dark-field detector
HRMS	High-resolution mass spectrum
HRTEM	High-resolution transmission electron microscopy
HSA	High surface area
<i>i</i> -Pr	Isopropyl group
m	Multiplet (spectral)
M	Metal, moles per liter
Me	Methyl group
min	Minute (s)
<i>n</i> -Bu	Normal butyl group
NMR	Nuclear magnetic resonance
NPore	Nanoporous
NPs	Nanoparticles
Pd/C	Palladium on charcoal
Ph	Phenyl group
Py	Pyridine

py-THQ	1,2,3,4-tetrahydroquinoline
RT(rt)	Room temperature
s	Singlet (spectral)
SEM	Scanning electron microscopy
t	Triplet (spectral)
T	Temperature
TEM	Transmission electron microscopy
THF	Tetrahydrofuran
TOF	Turnover frequency
TON	Turnover number
Ts	Tosyl group
XPS	X-ray photoelectron spectroscopy

# Chapter 1

## The Fabrication of Nanoporous Metals (Au, Cu, Pd) and Their Application in Heterogeneous Molecular Transformations

**Abstract** Nanoporous metals (Au, Cu, Pd) fabricated by chemical or electrochemical dealloying, possess intriguing properties towards enormous promising potentials for heterogeneous catalysis, such as unique pore structure, tunable nanoporosity, large specific surface area, high density of atomic steps and kinks, as well as high thermal stability. Here, we summarized nanoporous metals fabricated from different alloys by dealloying and their applications in heterogeneous catalysis. They showed high catalytic activity and selectivity and could be reused several times without obvious loss of activity.

**Keywords** Dealloying · Heterogeneous catalysis · Nanoporous gold catalyst · Nanoporous copper catalyst · Nanoporous palladium catalyst

### 1.1 Introduction

Nanoscience has taught us that an assembly constructed by building blocks with sizes in the range of 1–100 nm can generate superior properties in comparison to their bulk counterparts, and thus it is essential to prescribe and alter the pore structures in such a nanoporous range. As a subset of nanostructured porous materials, nanoporous metals with highly ordered networks and narrow pore-size distributions are of particular interest for a wide range of important potential applications, such as electrocatalysts, chemical sensors and energy system [1]. In spite of the growing number of studies on various electrochemical applications of nanoporous metals, the catalytic properties in chemical reactions are still less explored, although the interesting features of nanoporous metals make them potentially attractive candidates for new heterogeneous catalysts; the three-dimensional open-pore network structures and metal ligaments allow the transport of molecules and ions, a high surface-to-volume ratio in comparison with bulk metals results in outstanding catalytic efficiency; furthermore, the potentially high reusability and rather simple work-up are favorable for practical synthetic methodology.

Moreover, in contrast to the supported nanoparticles (NPs) catalyst, a nanoporous metal without supports should be an ideal catalyst system to understand the relevant catalytic mechanism more easily and to extend the catalytic application widely by elimination of the support effect problems and relaxation of aggregation. Herein, the fabrication method of nanoporous metals and application in heterogeneous molecular transformations were summarized.

## 1.2 Fabrication of Nanoporous Metals

Nanoporous metals (Au, Cu, Pd) could be fabricated by chemical or electrochemical dealloying, which means selective dissolution of an active component in appropriate corrosion conditions from a homogeneous, single phase alloy that consists of two or multicomponent metals with different chemical activities, leading to a porous residue [1]. To obtain uniform nanoporosity by dealloying, it is essential to select suitable alloy precursors, which satisfy two basic requirements: homogeneous single phases and a large electrochemical potential difference between the alloy components. For example, the 1.477 V difference between Cu and Mn made Mn to be a suitable alloy precursor for fabrication of nanoporous copper material [2].

### 1.2.1 Fabrication of Nanoporous Gold

Chemical dealloying Au–Ag alloy in nitric acid is a common method for the fabrication of nanoporous gold material. By immersing Au<sub>50</sub>Ag<sub>50</sub> alloy in 50 % nitric acid for different time and then annealing at high temperature, Forty demonstrated that surface diffusion of gold played an important part in the corrosion process. As surface silver atoms were dissolved, the residual gold atoms reformed into gold-rich islands so that fresh silver atoms were continuously exposed to the environment layer by layer (Fig. 1.1) [3]. In 2001, Erlebacher demonstrated that nanoporosity in metals abided by an intrinsic dynamical pattern formation process. That is, pores form because the gold atoms are chemically driven to aggregate into two-dimensional clusters by a phase separation process at the solid-electrolyte interface, and the surface area continuously increase owing to etching [4].

To prepare nanoporous gold which would resist mechanical strains, Ag–Au alloy was immersed in aqueous HClO<sub>4</sub> solution. By optimizing the gold content of the Ag–Au alloy, staying below the threshold potential and increasing the temperature of the electrolyte, dealloyed membranes with a high degree of mechanical integrity have been prepared [5]. Immersing an ordered AuCu<sub>3</sub> intermetallic compound in 50 % HNO<sub>3</sub> aqueous solution at 50 °C could also fabricate fine porous gold catalyst with high catalytic activity [6].

When was chemical dealloying two-phase Al–Au alloy of Al<sub>2</sub>Au and Al–Au intermetallic compounds under free corrosion conditions, nanoporous gold

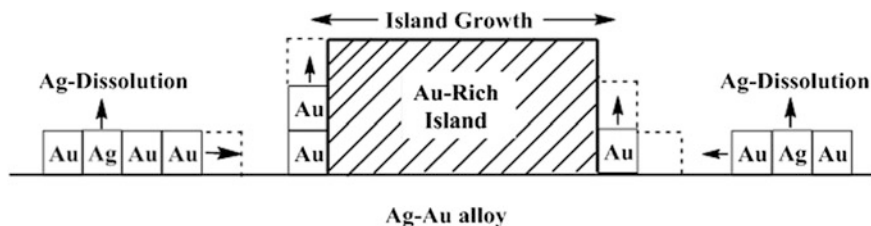


**Fig. 1.1** Gold island growth by the surface disordering, reordering mechanism

composites (NPGCs) formed. The microstructures of the NPGCs were composed of intracellular and intercellular areas which exhibited two kinds of nanoporous structures with different length scales of ligaments/channels. In addition, this length scales could be adjusted by simply changing the dealloying solution. The NPGCs showed abnormal coarsening behaviors when subjected to annealing at different temperatures. In comparison to nanoporous gold (AuNPore) with a homogeneous structure, the NPGCs exhibited higher Young's modulus and yield strength [7]. When was chemical dealloying of rapidly solidified (RS)  $\text{Al}_{66.6}\text{Au}_{33.4}$  alloys being composed of a single-phase  $\text{Al}_2\text{Au}$  intermetallic compound in the 20 wt% NaOH or 5 wt% HCl solution, nanoporous gold ribbons with an open, bicontinuous interpenetrating ligament-channel structure was fabricated [8]. The dealloying behavior of  $\text{Al}_2\text{Au}$  in organic acid solutions was also investigated. As compared with those in inorganic acids, the dealloying kinetics in organic acids became much slower even at elevated temperature. In addition, only the surface region of  $\text{Al}_2\text{Au}$  ribbon with the thickness of several microns could be dealloyed, and thus finally contributed to a kind of NPGF (nanoporous gold film)/ $\text{Al}_2\text{Au}$  composite [9].

Nanoporous gold films were fabricated by electrochemical etching of gold in a solution of hydrofluoric acid and dimethylformamide (DMF). As compared with dealloyed AuNPore, the electrochemically etched AuNPore exhibited controllable pore size and etching depth by adjusting the etching conditions [10]. Electrochemical dealloying of amorphous Au-Si co-deposited films on Si substrates could also produce nanoporous gold films. As the starting concentrations of Au decreased from 41 to 9 %, the pore sizes increased from 10 to 45 nm and the porosity increased from 45 to 70 % for the nanoporous Au films. The degree of film collapse due to dealloying also increased with decreasing Au concentration [11].

### ***1.2.2 Fabrication of Nanoporous Copper***

Uniform monolithic structures of nanoporous copper (CuNPore) can be created by dealloying  $\text{Mn}_{70}\text{Cu}_{30}$  via two distinct methods: potentiostatically driven dealloying and free corrosion. Both the ligament size and morphology were found to be highly dependent on the dealloying methods and conditions. Porous copper with

ligaments as small as 16 nm can be obtained when dealloyed potentiostatically in  $\text{H}_2\text{SO}_4$  and as large as 125 nm when dealloyed under free corrosion in acid chloride [12]. Nanoporous copper with tunable nanoporosity were fabricated by electrochemical dealloying the same alloy  $\text{Mn}_{70}\text{Cu}_{30}$  in hydrogen chloride. The influence of acid concentration and etching potential on the formation of nanoporosity was systematically investigated. The nanopore sizes can be tailored from about 15 to 120 nm by controlling the dealloying time (0.5 h to 32 h) in 0.025 M HCl [2].

We have shown that a large electrochemical potential difference is an important factor for selecting suitable mother alloys. The potential difference of Mg and Cu is markedly greater than that of Mn and Cu, thus the Mg–Cu alloy system were successfully developed to fabricate monolithic CuNPore ribbons and bulk CuNPore through chemical dealloying in a 5 wt% HCl solution. The compositions of starting Mg–Cu alloys do have an important effect on the dealloying process and microstructures of the CuNPore ribbons. The Mg–Cu alloys with 60 at. % Cu or less can be fully dealloyed, while the alloys with 67 at. % Cu or more cannot be completely dealloyed. The synergetic dealloying of  $\text{Mg}_2\text{Cu}$  and  $\text{MgCu}_2$  in two-phase Mg–Cu alloys results in the formation of CuNPore with a homogeneous structure [13].

Monolithic CuNPore ribbons can be fabricated through chemical dealloying of melt-spun Al–Cu alloys with 33–50 at. % Cu under free corrosion conditions (in a 5 wt % HCl or 20 wt % NaOH aqueous solution). The melt-spun Al–Cu alloys with 33–50 at. % Cu were composed of one or a combination of  $\text{Al}_2\text{Cu}$  and AlCu intermetallic compounds. Both  $\text{Al}_2\text{Cu}$  and AlCu can be fully dealloyed, and the synergetic dealloying of  $\text{Al}_2\text{Cu}$  and AlCu in the two-phase Al–Cu alloys resulted in the formation of CuNPore with a homogeneous porous structure. The fast surface diffusion of Cu along alloy/solution interfaces leads to the formation of CuNPore with large length scales of ligaments/channels (100–500 nm) [14]. Synthesis of monolithic CuNPore through dealloying of Al–Cu alloys with 15–35 at. % Cu have also been successfully developed. These alloys with different composition have different percentage of three phases:  $\alpha\text{-Al}$ ,  $\text{Al}_2\text{Cu}$  and AlCu. During dealloying, Al atoms in the  $\alpha\text{-Al}$  and  $\text{Al}_2\text{Cu}$  phases can be easily leached out, while those in the AlCu phase can hardly be eroded. Therefore, different percentage of these three phases ( $\alpha\text{-Al}$ ,  $\text{Al}_2\text{Cu}$  and AlCu) has a marked effect on dealloying process and morphology of the CuNPore ribbons. Monolithic CuNPore ribbons were fabricated by electroless dealloying of Al–Cu alloys in 10 wt% HCl and 10 wt% NaOH solution [15].

Nanoporous copper can also be fabricated from amorphous binary Ti–Cu ( $\text{Ti}_{30}\text{Cu}_{70}$ ,  $\text{Ti}_{40}\text{Cu}_{60}$ ,  $\text{Ti}_{50}\text{Cu}_{50}$ ,  $\text{Ti}_{60}\text{Cu}_{40}$ ) alloys in hydrofluoric acid solutions under a free corrosion condition. As-spun ribbons were dealloyed in various concentrations of HF solutions for different immersion times. An interpenetrating three-dimensional bicontinuous nanoporous structure of copper was formed after dealloying. The pore size was from tenths of nanometers to hundredths of nanometers, depending on the

alloy composition, HF concentration and the treatment time [16]. Multimodal nanoporous copper was fabricated through dealloying nanocrystallized  $\text{Ti}_{50}\text{Cu}_{50}$  ribbon alloy due to the presence of  $\text{Ti}_3\text{Cu}_4$  phase, which was co-precipitated with  $\text{Ti}_2\text{Cu}$  during the heat treatment at  $T = 400$  °C ( $T_g < T < T_x$ ) [17].

### 1.2.3 Fabrication of Nanoporous Palladium

Chen et al. have explored the synthesis of nanoporous palladium by electrochemically dealloying multicomponent  $\text{Pd}_{30}\text{Ni}_{50}\text{P}_{20}$  metallic glass ribbons in 1 mol/L sulfuric acid solution. In comparison with crystalline alloys, multicomponent metallic glasses are monolithic in phase with a homogeneous composition and structure down to subnanoscale. Nanoporous palladium with a rather uniform structure has been obtained. SEM image showed a bimodal porous Pd structure with two length-scale nanopores at  $\sim 50$  and 5 nm. TEM image showed that the size of the large pores was about 30–60 nm, and the ligaments among those big pores contained a large number of small pores with a size of about 5 nm. The formation mechanism of nanoporosity in the  $\text{Pd}_{30}\text{Ni}_{50}\text{P}_{20}$  metallic glass was analogous to that in the crystalline systems, such as Au–Ag alloys [18].

Nanoporous Pd with an average ligament size of 5–20 nm was fabricated by electrochemical dealloying  $\text{Pd}_{0.2}\text{C}_{0.8}$  in  $\text{H}_2\text{SO}_4$  aqueous solution. Heating nanoporous Pd above 573 K coarsened the nanoporous structure through a solid stated process like recrystallization, rather than melting which was typical for metallic nanoparticles [19].

Nanoporous palladium ribbons with bimodal channel size distributions could be fabricated by dealloying of the RS (rapidly solidified)  $\text{Al}_{80}\text{Pd}_{20}$  alloy in the 20 wt% NaOH solution. The RS  $\text{Al}_{80}\text{Pd}_{20}$  alloy was composed of two phases:  $\alpha$ -Al and  $\text{Al}_3\text{Pd}$ . After dealloying, only a fcc Pd phase could be identified in the as-dealloyed ribbons [8]. As compared with  $\text{Al}_{80}\text{Pd}_{20}$  alloy, the RS  $\text{Al}_{30}\text{Pd}_{70}$  alloy was composed of  $\text{Al}_3\text{Pd}$  and  $\text{Al}_3\text{Pd}_2$  intermetallic compounds. Chemical dealloying of the RS  $\text{Al}_{30}\text{Pd}_{70}$  alloy in 20 wt% NaOH or 5 wt% HCl aqueous solution formed nanoporous palladium composites with second phase embeddings. The resultant composites comprised the nanoporous palladium matrix dealloyed, forming  $\text{Al}_3\text{Pd}$  and the undealloyed  $\text{Al}_3\text{Pd}_2$  embeddings [20]. Dealloying a RS  $\text{Al}_{77}\text{Pd}_{23}$  alloy under free corrosion conditions could form nanoporous Pd ribbons with a typical bicontinuous interpenetrating cluster-channel structure. The clusters were composed of parallel rods, with large channels between them. The rods were also nanoporous and exhibited an ultrafine ligament/channel structure [21].

### 1.3 Application in Heterogeneous Molecular Transformations

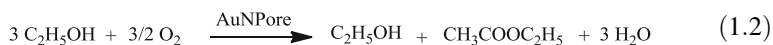
Nanoporous gold foams formed through the selective leaching of silver from  $\text{Au}_{30}\text{Ag}_{70}$  in nitric acid, has an unexpectedly high catalytic activity for CO oxidation at ambient pressures and temperatures or down to  $-20\text{ }^{\circ}\text{C}$ . Sintering can inhibit the catalytic applications of gold particles; in contrast, nanoporous gold has good thermal stability, and its morphology can be easily reproduced. X-ray photoelectron spectroscopy (XPS) revealed that, in addition to gold, 4.4 % metallic silver is present at the surface of the samples used for the catalytic studies. The distribution of silver was considered to have strong influence on the high catalytic activity of nanoporous gold [22]. Bäumer's data suggested that Ag played a significant role in promoting adsorption and dissociation of molecular oxygen [23–25]. When increasing the content of Ag, the activity of the nanoporous gold catalyst can be significantly enhanced [26]. Chen et al. reported that a very high density of atomic steps and kinks could be observed on the surface of nanoporous gold (average diameter of both gold ligaments and nanopores was  $\sim 30\text{ nm}$ ), comparable to 3–5 nm nanoparticles, and the residual Ag stabilized the atomic steps by suppressing {111} faceting kinetics. In situ TEM observations provided compelling evidence that the surface defects were active sites for the catalytic oxidation of CO [27].

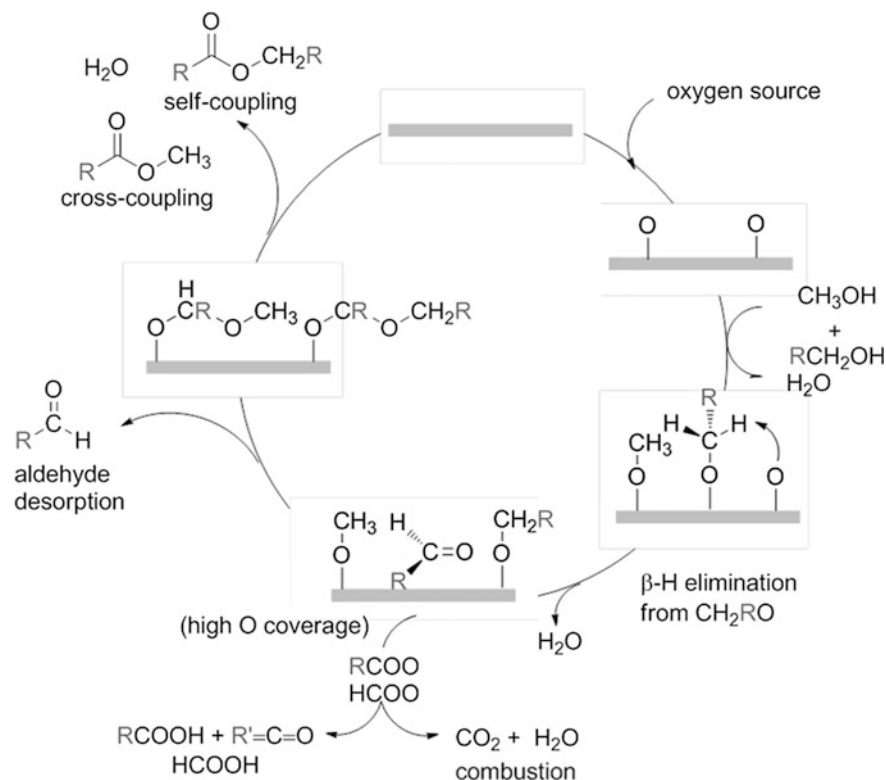
Ding et al. employed a modified dealloying by etching Ag/Au in concentrated nitric acid under applied anodic potential forming nanoporous gold with ligament sizes less than 6 nm. This AuNPore showed high catalytic activities for CO oxidation even at low temperatures, such as  $-30\text{ }^{\circ}\text{C}$ . The deactivation of the Au was observed at room temperature because of increased ligament size (around  $\sim 20\text{ nm}$ ) and clogging of pores in some areas. In contrast, the structure coarsening was significantly retarded at lower temperatures, and catalytic reaction at  $-30\text{ }^{\circ}\text{C}$  for over 30 h increased the pore size from the original 5 to  $\sim 8\text{ nm}$ . This property offered the AuNPore catalyst a unique advantage of performing at low temperatures with sustained stability. All AuNPore samples were tested as made without any activation pretreatment which was in sharp contrast to most supported Au catalysts [28]. Metallic gold atoms on AuNPore are the intrinsic active sites where the reaction of CO with  $\text{O}_2$  occurs. The kinetic study found that the reaction rate of CO oxidation on unsupported AuNPore depended significantly on CO concentration but only slightly on  $\text{O}_2$  concentration, consequently CO adsorption was suggested as the rate-limiting step in CO oxidation [29].

The reactivity of the alkaline pretreated nanoporous gold for the CO oxidation has been investigated. After being immersed in NaOH or ammonia solutions, the catalytic activity could be promoted dramatically for the room temperature reaction, and this promotional effect could be adjusted by varying the pH values of the alkaline solutions or immersing time. The roles of the alkaline were to provide  $\text{OH}^-$  anions to form Au– $\text{OH}^-$  sites, which were the active sites to form hydroxyl carbonyl ( $\text{Au}-\text{OCOH}^-$ ) with CO and activated the oxygen with hydroxyl carbonyl [30].

Nanoporous gold catalysts also exhibited effective catalytic activity and high selectivity ( $\sim 99\%$ ) for the aerobic oxidation of D-glucose to D-gluconic acid under mild conditions. AuNPore catalyst with a ligament size of 6 nm exhibited the highest catalytic activity and was more resistant to deactivation, while the 30 nm sample was found to have better structure stability during the whole catalytic process. The presence of residual Ag atoms does not seem to contribute to the activity of AuNPore for glucose oxidation. The Au atoms on the corners and step edges, that means the low-coordinated surface Au atoms, are the reaction active sites [31].

Besides the ability of gold to catalyze oxidation reactions already at very low temperatures, AuNPore is also a highly selective catalyst [32]. It catalyzed the selective oxidative coupling of methanol to methyl formate with 100% selectivity at 20 °C and high turnover frequencies ( $0.26\text{ s}^{-1}$ ) at 80 °C (Eq. 1.1). The residual Ag in AuNPore regulated the availability of reactive oxygen on the surface and thus controlled the selectivity. However, Ag was not directly involved in the coupling activity and Au surface sites were the real reactive sites [33]. When was increasing the content of Ag, the selectivity for the oxidation of methanol was shift from partial to total oxidation, that means only the product of  $\text{CO}_2$  was observed. Thus, in contrast to CO, in case of methanol increasing concentration of Ag were unfavorable, leading to more pronounced total oxidation and a decrease of total activity [26]. Other gas-phase aerobic oxidation and coupling of primary alcohols, ethanol and *n*-butanol, were also studied using nanoporous gold as an unsupported catalyst at ambient pressures and low temperatures [34]. The two predominant products for ethanol oxidation were acetaldehyde and ethyl acetate in a molar ratio of about 2:1, which formed at reaction temperatures as low as 40 °C (Eq. 1.2). The total oxidation of ethanol to  $\text{CO}_2$  was found to be close to the detection limit (ca.  $10^{-3}\text{ vol}\%$ ). The oxidation of *n*-butanol led exclusively to the production of the aldehyde, *n*-butanal (Eq. 1.3). The formation of  $\text{CO}_2$  was also close to the detection limit of about 10–3 vol%. One of the main intermediates was a surface-bonded carboxylate (i.e. formate, acetate; see Scheme 1.1) stemming from the oxidation of surface-bonded aldehyde. This carboxylate surface species could either desorb after reaction with water, forming the corresponding carboxylic acid, or be further oxidized to the ketene and eventually  $\text{CO}_2$ . With increasing chain length and increasing tendency to form a surface-bonded aldehyde (methanol < ethanol < *n*-butanol) the amount of this carboxylate species increased. Kong et al. examined the influence of Ag content, partial pressure of oxygen and temperature on the selectivity of gas-phase oxidation of ethanol over unsupported nanoporous gold. As similar with the cross-coupling of methanol, Ag in nanoporous gold promoted oxidation and so do high temperature and oxygen concentration [35].





**Scheme 1.1** Pattern of reactivity for oxidation and coupling of alcohols on Au. Surface oxygen initiates scission of the alcoholic O–H bond, forming an alkoxy unit. Subsequent  $\beta$ -H elimination from the alkoxy by reaction with surface oxygen or an adjacent alkoxy leads to adsorbed aldehyde which is then attacked by unreacted alkoxy, forming a hemiacetal species which eliminates a hydrogen to yield the ester



Our group reported the first example of nanoporous gold (AuNPore) catalyzed organic reactions [36]. It exhibited a remarkable catalytic activity in the oxidation of a wide range of organosilanes (Table 1.1). The corresponding silanols were produced in high yields under mild conditions together with the evolution of hydrogen gas without formation of the byproduct disiloxanes. In addition, aerobic oxidation of alcohols in both batch and flow systems proceeded smoothly in the presence of nanoporous gold catalys (Table 1.2). The reaction did not need any additives, such as bases, stabilizers, and ligands as well as any cumbersome work-up procedure like filtration or centrifugation [37]. Besides the above two reaction systems, the benzannulation reaction between *ortho*-alkynylbenzaldehydes and alkynes were successfully catalyzed by nanoporous gold catalyst. The catalytic

**Table 1.1** Scope of the oxidation of organosilane

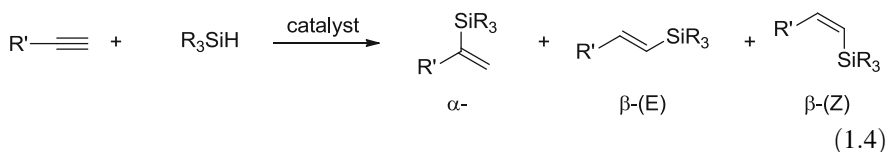
$\text{R}_{(4-n)}\text{SiH}_n + n \text{H}_2\text{O} \xrightarrow[\text{acetone, RT}]{\text{AuNPore cat.}} \text{R}_{(4-n)}\text{Si}(\text{OH})_n + n \text{H}_2$						
Entry	1	$\text{R}_{(4-n)}\text{SiH}_n$	AuNPore, mol%	Time, h	2	Yield, (%) <sup>a</sup>
1	1a	PhMe <sub>2</sub> SiH	1	1	2a	100
2	1b	Et <sub>3</sub> SiH	1	2	2b	94
3	1c	Bu <sub>3</sub> SiH	3	3	2c	95
4	1d	iPr <sub>3</sub> SiH	3	5	2d	88
5	1e	Ph <sub>3</sub> SiH	1	5	2e	99
6	1f	Ph <sub>2</sub> SiH <sub>2</sub>	1	9	2f	90
7	1g	PhSiH <sub>3</sub>	5	6	2g	80
8	1h	(H <sub>2</sub> C=CH)MePhSiH	1	1	2h	98
9	1i	(PhC≡C)Me <sub>2</sub> SiH	3	1.5	2i	92

Reactions were performed using 1 (1.0 mmol), H<sub>2</sub>O (0.1 mL), and AuNPore (n mol%) in 1.5 mL of acetone at room temperature

<sup>a</sup> Yield of isolated product

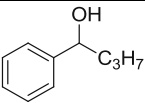
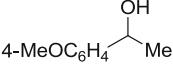
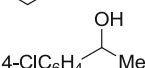
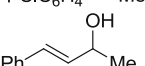
activity of nanoporous gold materials with different pore sizes from 25 nm to 100 nm was examined in this reaction. The results showed that the catalytic activity was highly dependent on the pore size, and the size should be less than 30 nm for this transformation, while the catalyst with larger sizes nearly inactive for this catalytic system (Table 1.3) [38]. The catalyst could be recycled several times in all above reactions and the work-up process was quite simple.

Since the hydrosilylation of terminal alkynes could possibly form three isomeric products,  $\alpha$ -,  $\beta$ -(E)-, and  $\beta$ -(Z)-isomers (Eq. 1.4), the control of regio- and stereoselectivity in this process is highly desirable for selective preparation of these vinylsilane compounds. Recently, we were successful in selective hydrosilylation of terminal alkynes using nanoporous gold, fabricated from an Au-Al alloy by dealloying in 20 % NaOH, leading to  $\beta$ -(E)-products with high regio- and stereoselectivities (Table 1.4). Nanoporous gold fabricated from Au-Ag alloy by dealloying in 70 % HNO<sub>3</sub> showed much lower catalytic activity than that from Au-Al alloy. We found the residual silver had inhibition effect while aluminum had no special activation effect on this reaction [39].



Nanoporous gold also showed high selectivity in synthesis of formamide by aerobic oxidation of methanol in the coexistence of various oxidizable primary and

**Table 1.2** Aerobic oxidation of alcohol with AuNPore catalyst

$\begin{array}{c} \text{OH} \\   \\ \text{R}^1\text{---C---C---R}^2 \\ \mathbf{1} \end{array} \xrightarrow[\text{MeOH, 60 }^\circ\text{C}]{\text{AuNPore cat, O}_2 \text{ balloon}} \begin{array}{c} \text{O} \\    \\ \text{R}^1\text{---C---C---R}^2 \\ \mathbf{2} \end{array}$					
Entry	Alcohol	1	Time, h	2	Yield, (%) <sup>a</sup>
1		1a	10	2a	96
2		1b	10	2b	88
3 <sup>b</sup>		1b	24	2b	88
4 <sup>c</sup>		1c	7	2c	85
5		1d	9	2d	97
6		1e	10	2e	94
7		1f	28	2f	91
8		1g	24	2g	98
9		1h	22	2h	83
10		1i	22	2i	81
11 <sup>c,d,e</sup>		1j	24	2j	85
12 <sup>c,d,e</sup>		1k	22	2k	82
13 <sup>e</sup>		1l	19	2l	96

Reactions were carried out with **1** (0.30 mmol) and O<sub>2</sub> balloon in the presence of 10 mol% of AuNPore catalyst at 60 °C unless otherwise noted

<sup>a</sup>Determined by <sup>1</sup>H NMR analysis with *p*-xylene as an internal standard

<sup>b</sup>Air balloon was used instead of O<sub>2</sub> balloon

<sup>c</sup>1,4-Dioxane was used as a solvent

<sup>d</sup>Reaction temperature was 80 °C

<sup>e</sup>20 mol% of catalyst was used

**Table 1.3** AuNPore-catalyzed benzannulation of **1a** with **2a**

Entry	Average pore size, nm	Yield of 3a, (%)	Yield of 4a, (%)	Recovery of 1a, (%)
1	AuNPore-1 (25)	62	14	0
2	Reuse 1	61	15	0
3	Reuse 2	60	17	0
4	AuNPore-2 (30)	61	13	0
5	AuNPore-3 (40)	12	Trace	66
6	AuNPore-4 (60)	Trace	0	83
7	AuNPore-5 (100)	0	0	93

**Table 1.4** AuNPore-catalyzed hydrosilylation with a variety of alkynes and hydrosilanes

Entry	R'	R <sub>3</sub> SiH	Cat, mol%	Time, h	Yield <sup>a</sup> , (%)			
					3	4		
1	C <sub>6</sub> H <sub>5</sub>	1a	Et <sub>3</sub> SiH	2a	2	3	98	1
2	p-FC <sub>6</sub> H <sub>4</sub>	1b	Et <sub>3</sub> SiH	2a	2	2	97	2
3	p-MeOC <sub>6</sub> H <sub>4</sub>	1c	Et <sub>3</sub> SiH	2a	2	6	97	2
4	C <sub>6</sub> H <sub>13</sub>	1d	Et <sub>3</sub> SiH	2a	2	3	99	2
5	PhCH <sub>2</sub>	1e	Et <sub>3</sub> SiH	2a	2	3	97	1
6	c-C <sub>6</sub> H <sub>11</sub>	1f	Et <sub>3</sub> SiH	2a	2	3	97	1
7	C <sub>6</sub> H <sub>5</sub>	1a	PhMe <sub>2</sub> SiH	2b	2	6	96	3
8	C <sub>6</sub> H <sub>5</sub>	1a	(EtO) <sub>3</sub> SiH	2c	5	12	85	3
9	C <sub>6</sub> H <sub>5</sub>	1a	Bu <sub>3</sub> SiH	2d	10	12	98	2
10	C <sub>6</sub> H <sub>5</sub>	1a	(i-Pr) <sub>3</sub> SiH	2e	20	18	80	2

Reactions were carried out with **1** (1 mmol) and **2** (1.5 mmol) in the presence of AuNPore catalyst at 70 °C

<sup>a</sup> Determined by <sup>1</sup>H NMR analysis with *p*-xylene as an internal standard

secondary amines under mild conditions (Table 1.5). This established a facile, direct formamide synthesis process. The current catalytic reaction can be conducted under mild conditions, such as ambient oxygen pressure and neutral solutions. The residual Ag enhanced the catalytic activity of gold through a synergistic effect with gold.

**Table 1.5** AuNPore-catalyzed N-formylation of various amines

Entry	1	Time, h	Product, yield, (%) <sup>a</sup>
1	1a	20	2a, 97
2	1b	20	2b, 99
3	1c	72	2c, 67
4	1d	72	2d, 77
5	1e	72	2e, 72
6	1f	72	2f, 70
7	1g	40	2g, 73
8	1h	30	2h, 95
9	1i	20	2i, 40
10	1j	20	2j, 98
11	1k	40	2k, 93
12	1l	48	2l, 91

Reaction conditions: **1** (0.30 mmol), AuNPore (0.03 mmol), MeOH (3.0 mL)

<sup>a</sup> Yield was determined by <sup>1</sup>H NMR spectroscopy using CH<sub>2</sub>Br<sub>2</sub> as an internal standard

Nanoporous metallic glass Pd, which was fabricated by dealloying of a glassy metallic alloy Pd<sub>30</sub>Ni<sub>50</sub>P<sub>20</sub>, exhibited a remarkable catalytic activity for the Suzuki-coupling reaction between iodoarenes and arylboronic acids under mild conditions (Table 1.6). Leaching test indicated that dissolved Pd species existed and catalyzed the reaction but its activity was much lower than that of the solid state of the catalyst, and the leaching amount was quite small. Meanwhile, nanoporous Pd formed from a Pd-Co alloy was also used to catalyze Suzuki coupling between **1a** and **2a**. The reaction proceeded and the product **3a** was obtained in nearly quantitative yield. Leaching test indicated this was a heterogeneous process [40].

**Table 1.6** Scope and limitations of the Suzuki-coupling reaction catalyzed by nanoporous metallic glass Pd

**1** +  $(\text{HO})_2\text{B}-\text{Ar}(\text{R}^2) \xrightarrow[\text{KOH, MeOH}]{\text{PdNPore cat}}$  **3**

**2a:**  $\text{R}^2 = \text{Me}$   
**2b:**  $\text{R}^2 = \text{Cl}$   
**2c:**  $\text{R}^2 = \text{OMe}$

**2d**

**2e**

**2f**

Entry	1	R <sup>1</sup> -I	2	Condition	Product, yield, % <sup>a</sup>
1	1a		2a	50 °C, 3 h	3a, 99
2	1b		2a	50 °C, 4 h	3b, 95
3	1b		2b	50 °C, 12 h	3c, 95
4	1b		2c	50 °C, 1 h	3d, 83
5	1c		2a	50 °C, 5 h	3e, 95
6	1d		2a	50 °C, 6 h	3f, 79
7	1e		2a	80 °C, 12 h	3g, 89
8	1f		2a	50 °C, 3 h	3h, 99
9	1g		2a	50 °C, 0.5 h	3i, 99
10	1h		2a	50 °C, 2 h	3j, 95
11	1i		2a	50 °C, 3 h	3k, 99
12	1a		2d	50 °C, 4 h <sup>b</sup>	3a, 87
13	1a		2e	80 °C, 3 h	3a, 78
14	1a		2f	80 °C, 4 h <sup>c</sup>	3a, 95

Reaction conditions: **1** (0.5 mmol), **2** (0.75 mmol), KOH (2.5 mmol), PdNPore (2 mol%), MeOH (2 mL)

<sup>a</sup> Isolated yield

<sup>b</sup> The reaction was conducted in a mixture of MeOH (1.2 mL) and H<sub>2</sub>O (0.6 mL)

<sup>c</sup> The reaction was conducted in the absence of KOH

## 1.4 Summary and Outlook

Nanoporous gold fabricated from different alloys showed distinct catalytic activity for the same reaction because of different nanostructures and synergistic effects between gold and residual metals. This means, choose a proper mother alloy is crucial for exploring high catalytic activity of nanoporous metals. In addition, for the same nanoporous metal catalyst, we can also explore new catalytic property for more reactions. Until now, nanoporous gold showed high catalytic activity for oxidation reactions, such as CO oxidation, but nanoporous copper and palladium have rarely been reported for catalyzing heterogeneous molecular transformations, especially for organic reactions. Within the reported catalyzed reactions, all of the nanoporous metals showed high selectivity and avoided the influence of stabilizer comparing with their corresponding nanoparticles. Therefore, it is necessary and promising for developing new catalytic performances of nanoporous metals for heterogeneous organic reactions.

## References

1. Zhang J, Li CM (2012) Nanoporous metals: fabrication strategies and advanced electrochemical applications in catalysis, sensing and energy systems. *Chem Soc Rev* 41:7016–7031
2. Chen LY, Yu JS, Fujita T et al (2009) Nanoporous copper with tunable nanoporosity for SERS applications. *Adv Funct Mater* 19:1221–1226
3. Forty AJ (1979) Corrosion micromorphology of noble metal alloys and depletion gilding. *Nature* 282:597–598
4. Erlebacher J, Aziz MJ, Karma A et al (2001) Evolution of nanoporosity in dealloying. *Nature* 410:450–453
5. Senior NA, Newman RC (2006) (2006) Synthesis of tough nanoporous metals by controlled electrolytic dealloying. *Nanotechnology* 17:2311–2316
6. Kameoka S, Tsai AP (2008) CO oxidation over a fine porous gold catalyst fabricated by selective leaching from an ordered AuCu<sub>3</sub> intermetallic compound. *Catal Lett* 121:337–341
7. Zhang Z, Wang Y, Qi Z (2009) Fabrication and characterization of nanoporous gold composites through chemical dealloying of two phase Al–Au alloys. *J Mater Chem* 19:6042–6050
8. Zhang Z, Wang Y, Qi Z et al (2009) Generalized fabrication of Nanoporous metals (Au, Pd, Pt, Ag, and Cu) through chemical dealloying. *J Phys Chem C* 113:12629–12636
9. Wang X, Zhang Z, Ji H et al (2012) Dealloying of single-phase Al<sub>2</sub>Au to nanoporous gold ribbon/film with tunable morphology in inorganic and organic acidic media. *Appl Surf Sci* 258:9073–9079
10. Fang C, Bandaru NM, Ellis AV et al (2012) Electrochemical fabrication of nanoporous gold. *J Mater Chem* 22:2952–2957
11. Gupta G, Thorp JC, Mara NA et al (2012) Morphology and porosity of nanoporous Au thin films formed by dealloying of Au<sub>x</sub>Si<sub>1-x</sub>. *J Appl Phys* 112:094320
12. Hayes JR, Hodge AM, Biener J et al (2006) Monolithic nanoporous copper by dealloying Mn–Cu. *J Mater Res* 21:2611–2616

13. Zhao C, Qi Z, Wang X et al (2009) Fabrication and characterization of monolithic nanoporous copper through chemical dealloying of Mg–Cu alloys. *Corros Sci* 51:2120–2125
14. Qi Z, Zhao C, Wang X et al (2009) Formation and characterization of monolithic Nanoporous copper by chemical dealloying of Al–Cu alloys. *J Phys Chem C* 113:6694–6698
15. Li M, Zhou Y, Geng H (2012) Fabrication of nanoporous copper ribbons by dealloying of Al–Cu alloys. *J Porous Mater* 19:791–796
16. Dan Z, Qin F, Sugawara Y et al (2012) Fabrication of nanoporous copper by dealloying amorphous binary Ti–Cu alloys in hydrofluoric acid solutions. *Intermetallics* 29:14–20
17. Dan Z, Qin F, Sugawara Y et al (2013) Nanoporous copper dealloyed from a nanocrystallized Ticu alloy. *Mater Sci Forum* 750:72–75
18. Yu J, Ding Y, Xu C et al (2008) Nanoporous metals by dealloying multicomponent metallic glasses. *Chem Mater* 20:4548–4550
19. Hakamada M, Mabuchi M (2009) Fabrication of nanoporous palladium by dealloying and its thermal coarsening. *J Alloys Compd* 479:326–329
20. Wang X, Wang W, Qi Z et al (2010) Fabrication, microstructure and electrocatalytic property of novel nanoporous palladium composites. *J Alloys Compd* 508:463–470
21. Zhang C, Ji H, Sun J et al (2013) Fabrication of nanoporous Pd with superior hydrogen sensing properties by dealloying. *Mater Lett* 92:369–371
22. Zielasek V, Jürgens B, Schulz C et al (2006) Gold catalysts: nanoporous gold foams. *Angew Chem Int Ed* 45:8241–8244
23. Wittstock A, Neumann B, Schaefer A et al (2009) Nanoporous Au: an unsupported pure gold catalyst? *J Phys Chem C* 113:5593–5600
24. Fajín JLC, Cordeiro MNDS, Gomes JRB (2011) On the theoretical understanding of the unexpected O<sub>2</sub> activation by nanoporous gold. *Chem Commun* 47:8403–8405
25. Moskaleva LV, Röhe S, Wittstock A et al (2011) Silver residues as a possible key to a remarkable oxidative catalytic activity of nanoporous gold. *Phys Chem Chem Phys* 13:4529–4539
26. Wittstock A, Wichmann A, Biener J et al (2011) Nanoporous gold: a new gold catalyst with tunable properties. *Faraday Discuss* 152:87–98
27. Fujita T, Guan P, McKenna K et al (2012) Atomic origins of the high catalytic activity of nanoporous gold. *Nat Mater* 11:775–780
28. Xu C, Su J, Xu X et al (2007) Low temperature CO oxidation over unsupported nanoporous gold. *J Am Chem Soc* 129:42–43
29. Xu C, Xu X, Su J et al (2007) Research on unsupported nanoporous gold catalyst for CO oxidation. *J Catal* 252:243–248
30. Han D-Q, Zhou C-Q, Yin H-M et al (2011) Reactivity of the alkaline pretreated nanoporous gold for the CO oxidation. *Catal Lett* 141:1026–1031
31. Yin H, Zhou C, Xu C et al (2008) Aerobic oxidation of d-Glucose on support-free nanoporous gold. *J Phys Chem C* 112:9673–9678
32. Wittstock A, Biener J, Bäumer M (2012) Nanoporous gold: a new material for catalytic and sensor applications. *Phys Chem Chem Phys* 12:12919–12930
33. Wittstock A, Zielasek V, Biener J et al (2010) Nanoporous gold catalysts for selective gas-phase oxidative coupling of methanol at low temperature. *Science* 327:319–322
34. Kosuda KM, Wittstock A, Friend CM et al (2012) Oxygen-mediated coupling of alcohols over nanoporous gold catalysts at ambient pressures. *Angew Chem Int Ed* 51:1698–1701
35. Kong X-M, Shen L-L (2012) Selectivity control of ethanol gas-phase oxidation over nanoporous gold. *Catal Commun* 24:34–37
36. Asao N, Ishikawa Y, Hatakeyama N et al (2010) Nanostructured materials as catalysts: nanoporous-gold-catalyzed oxidation of organosilanes with water. *Angew Chem Int Ed* 49:10093–10095
37. Asao N, Hatakeyama N, Menggenbateer et al (2012) Aerobic oxidation of alcohols in the liquid phase with nanoporous gold catalysts. *Chem Commun* 48:4540–4542

38. Asao N, Meggenbater, Seya Y et al (2012) Nanoporous gold-catalyzed [4 + 2] benzannulation between ortho-alkynylbenzaldehydes and alkynes. *Synlett* 23:66–69
39. Ishikawa Y, Yamamoto Y, Asao N et al (2013) Selective hydrosilylation of alkynes with a nanoporous gold catalyst. *Catal Sci Technol* 3:2902–2905
40. Tanaka S, Kaneko T, Asao N et al (2011) A nanostructured skeleton catalyst: Suzuki-coupling with a reusable and sustainable nanoporous metallic glass Pd-catalyst. *Chem Commun* 47:5985–5987

## Chapter 2

# Nanoporous Copper Metal Catalyst in Click Chemistry: Nanoporosity Dependent Activity Without Supports and Bases

**Abstract** Nanoporous copper catalysts with tunable nanoporosity were fabricated from Cu<sub>30</sub>Mn<sub>70</sub> alloy by controlling the dealloying temperature under free corrosion conditions. The tunable nanoporosity of CuNPore led to a significant enhancement of catalytic activity in click chemistry without using any supports and bases. Characterization of CuNPore surface, high reusability, leaching experiment, and formation of nanostructured copper acetylide revealed that the click reaction occurred at the catalyst surface and the Cu(I) species was the real catalytic active sites. The CuNPore catalyst system was also applied to the three-component coupling of terminal alkynes, tosyl azide and dialkylamines to afford the corresponding aminoimines in high yields.

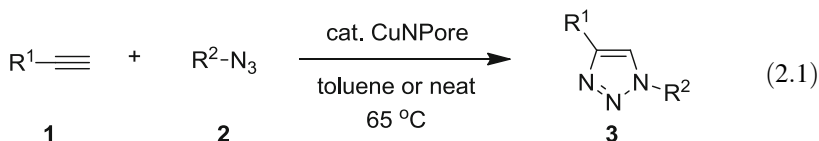
**Keywords** Click chemistry · Nanoporous copper catalyst · Heterogeneous catalysis · High reusability

## 2.1 Introduction

Nanoporous metals are promising materials for catalysis [1–9], sensing [10–12], and actuation [13, 14] applications due to their interesting structural, optical and surface properties. In spite of the growing number of studies on various applications of nanoporous metals, the catalytic properties in chemical reactions are still less explored, although the interesting features of nanoporous metals make them potentially attractive candidates for new heterogeneous catalysts [1–9]; the three-dimensional open-pore network structures and metal ligaments allow the transport of molecules and ions, a high surface-to-volume ratio in comparison with bulk metals results in outstanding catalytic efficiency; furthermore, the potentially high reusability and rather simple work-up are favorable for practical synthetic methodology. Moreover, in contrast to the supported nanoparticles (NPs) catalyst, a nanoporous metal without supports should be a challenging catalyst system to understand the relevant catalytic mechanism more easily and to extend the catalytic application widely by elimination of the support effect problems and

relaxation of aggregation. In this regard, we have focused on the study of the catalytic properties of unsupported nanoporous metals in organic molecular transformations under liquid phase conditions [15, 16]. Nanoporous gold exhibited a remarkable catalytic efficiency and reusability in the oxidation of organosilanes into silanols with water [15], and non-porous palladium without ligands and supports showed high catalytic activity and reusability in the Suzuki coupling [16]. Therefore, the design and synthesis of new and efficient nanoporous metal catalytic systems for development of molecular transformations are highly desirable.

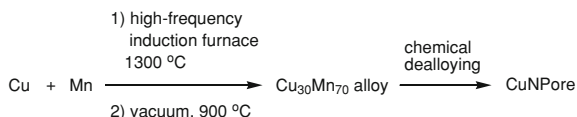
In 2002, Sharpless [17] and Meldal [18] reported independently the Huisgen [3 + 2] cycloaddition of terminal alkynes and organic azides catalyzed by homogeneous Cu(I) salts, the so-called click reaction. This methodology has been emerged as the most powerful tool for connecting the two useful functional groups. During the last few years, numerous applications of the click reaction have been reported in the field of material sciences, bio- and medicinal chemistry [19–21]. The click reaction can be catalyzed also by heterogeneous copper(I), such as immobilized copper nanoclusters and copper/cuprous oxide NPs, copper-in-charcoal NPs, copper zeolites, and copper nitride NPs supported on mesoporous SiO<sub>2</sub> with or without bases [22–30]. Copper metal alone also has been reported to catalyze this click reaction, while the reaction is relatively slow and requires high catalyst loading [31]. Recyclability of these heterogeneous copper catalysts was rarely reported [30]. Recently, it has been reported that the monolithic CuNPore is a promising high strength/low density material, which can be synthesized through the chemical or electrochemical de-alloying of various single-phase Cu/M (M = Al, Mg, Mn) alloys [32–36]. Herein, we report an efficient approach for the synthesis of CuNPore with tunable nanoporosity and its remarkable catalytic properties in click chemistry without using any supports and bases (Eq. 2.1). To the best of our knowledge, this is the first report on a monolithic CuNPore-catalyzed molecular transformation, while the non-monolithic CuNPore in the form of Raney copper is a well known catalyst in the water-gas shift reaction [37, 38].



## 2.2 Results and Discussion

### 2.2.1 Synthesis of Nanoporous Copper

Nanoporous metals with ideal bicontinuous structures can be synthesized by chemical or electrochemical dealloying of binary or ternary alloys by selective dissolution of one or more of the components of the alloy. To obtain uniform



**Scheme 2.1** Synthesis of  $\text{Cu}_{30}\text{Mn}_{70}$  alloy and CuNPore by chemical dealloying

nanoporosity upon dealloying, an alloy system is usually required to be in monolithic phase because the nanoporosity is formed by a self-assembly process through surface diffusion, not by the simple excavation of one phase from a pre-separated multiphase system. Surface diffusion of the less reactive component across the alloy/solution interface plays a key role in the formation of nanoporous metals and has a significant influence on size of ligament/pore. Furthermore, the electrochemical activities of elements in an alloy may be significantly different from the environment, which can strongly affect dissolution process and dealloying morphology; this relationship indicates that the compositions of starting alloys also have a significant influence on the nanostructure of porous metals.

CuNPore is a promising, high strength/low density material, because of its high porosity and yield strength of  $86 \pm 10$  MPa. Recently, it has been reported that monolithic CuNPores can be synthesized through the chemical or electrochemical dealloying of various Cu/M ( $M = \text{Al}, \text{Mg}, \text{Mn}, \text{etc.}$ ) alloys [32–36]. Hayes et al. [32] and Chen et al. [36] reported the synthesis of monolithic CuNPores by chemical/electrochemical dealloying of a single-phase  $\text{Cu}_{30}\text{Mn}_{70}$  alloy under acidic conditions with ligaments of length 10–125 nm. Zhang et al. have also synthesized monolithic CuNPores with a ligament length of several hundred nanometers from dual-phase Cu/Al and Cu/Mg alloys by chemical dealloying in HCl solution [33, 34]. Most recently, Liu et al. succeeded in synthesis of CuNPores with ligament lengths from 20–200 nm through chemical dealloying in an alkaline solution by altering the Cu/Al ratio of the initial alloys [45, 46]. In view of the industrial applications of these products, widespread use of the dealloying technique to make CuNPores is frequently hindered by the high cost of such unreactive metals and by the limited range of alloy systems. To date, little attention has been paid to the synthesis of CuNPores with tunable nanoporosity by means of changing the dealloying conditions; although it has been proved that materials with smaller nanostructure will offer higher surface area, which may significantly enhance catalytic properties. The Cu alloy that best fits these requirements is  $\text{Cu}_{30}\text{Mn}_{70}$ . Recently, Chen et al. obtained CuNPores with tunable nanopore sizes from Cu/Mn ribbons by controlling chemical dealloying time in a diluted HCl solution [36]. However, the small dimensions (thickness  $\approx 20$   $\mu\text{m}$ ; width  $\approx 1$  mm) of the ribbon used would cause it to be brittle during the catalytic transformations. Investigation of the synthesis of CuNPore catalysts with suitable dimensions and smaller pore/ligament size is highly desirable.

The alloy  $\text{Cu}_{30}\text{Mn}_{70}$  was synthesized from pure Cu (99.99 wt%) and Mn (99.99 wt%) at 1300  $^\circ\text{C}$  in a high-frequency induction furnace. The Cu/Mn alloy, sealed in quartz tube under vacuum, was heated at 900  $^\circ\text{C}$  for 72 h and then

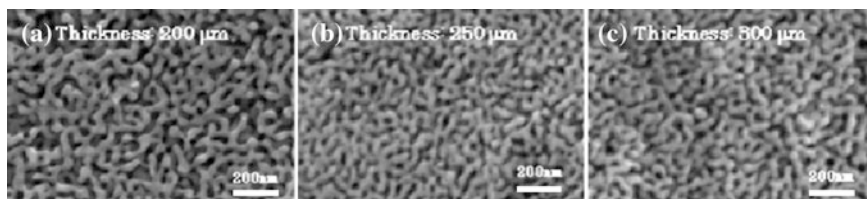


**Fig. 2.1** SEM images of CuNPore synthesized by dealloying of  $\text{Cu}_{30}\text{Mn}_{70}$  in  $1 \text{ M } (\text{NH}_4)_2\text{SO}_4$  and  $0.01 \text{ M } \text{MnSO}_4$  at  $25 \text{ }^\circ\text{C}$  from rolled alloys with thicknesses of **a**  $200 \text{ } \mu\text{m}$  (cat-1), **b**  $250 \text{ } \mu\text{m}$  (cat-2), **c**  $300 \text{ } \mu\text{m}$  (cat-3)

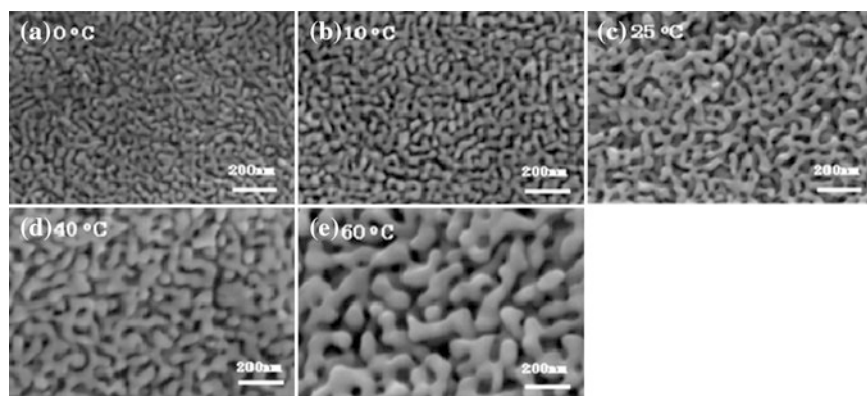


**Fig. 2.2** SEM images of CuNPore synthesized by dealloying of  $\text{Cu}_{30}\text{Mn}_{70}$  ( $200 \text{ } \mu\text{m}$  thickness) in  $1 \text{ M } (\text{NH}_4)_2\text{SO}_4$  and  $0.01 \text{ M } \text{MnSO}_4$  at **a**  $0 \text{ }^\circ\text{C}$  (cat-4), **b**  $10 \text{ }^\circ\text{C}$  (cat-5), **c**  $25 \text{ }^\circ\text{C}$  (cat-1), **d**  $40 \text{ }^\circ\text{C}$  (cat-6), **e**  $60 \text{ }^\circ\text{C}$  (cat-7)

quenched into water (Scheme 2.1). The resulting alloy was sectioned using a diamond saw into samples approximately  $1 \text{ mm}$  in thickness. The samples were rolled into films of thicknesses of about  $200$ ,  $250$ , and  $300 \text{ } \mu\text{m}$  for dealloying.

Various CuNPores with versatile ligament scales and morphologies were synthesized by chemical dealloying with two kinds of electrolytes following Hayes' method [32]  $5 \times 5 \text{ mm}$  pieces of the three thickness of rolled  $\text{Cu}_{30}\text{Mn}_{70}$  were placed directly in pre-prepared electrolyte  $1 \text{ M } (\text{NH}_4)_2\text{SO}_4$  and  $0.01 \text{ M } \text{MnSO}_4$  at room temperature for 6 days. SEM imaging (Fig. 2.1) showed that ligament and nanopore channels were formed uniformly. The average ligament diameters were estimated as  $\approx 40 \text{ nm}$  for the  $200 \text{ } \mu\text{m}$  thickness alloy (cat-1),  $\approx 35 \text{ nm}$  for both the  $250$  and  $300 \text{ } \mu\text{m}$  thickness alloys (cat-2 and cat-3). EDX analysis showed that the residual Mn composition of CuNPores remains approximately constant at  $1\text{--}2 \text{ at. } \%$ . In the same electrolytes, the rolled  $\text{Cu}_{30}\text{Mn}_{70}$  alloy with a thickness of  $\approx 200 \text{ } \mu\text{m}$  was treated at different temperatures, producing CuNPores with a tunable diameter;  $\approx 25 \text{ nm}$  at  $0 \text{ }^\circ\text{C}$  (cat-4),  $\approx 30 \text{ nm}$  at  $10 \text{ }^\circ\text{C}$  (cat-5),  $\approx 50 \text{ nm}$  at  $40 \text{ }^\circ\text{C}$  (cat-6),  $\approx 70 \text{ nm}$  at  $60 \text{ }^\circ\text{C}$  (cat-7) (Fig. 2.2). EDX analysis showed that the residual Mn composition of the  $0 \text{ }^\circ\text{C}$  dealloyed sample (cat-4) is  $\approx 4 \text{ at. } \%$ , and

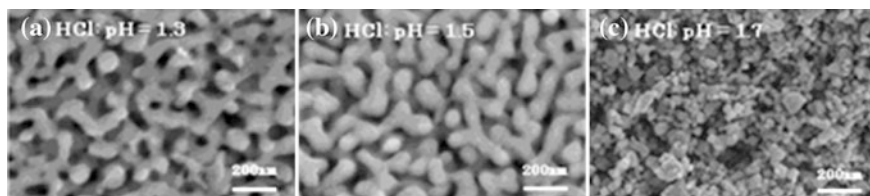


**Fig. 2.3** SEM images of CuNPore fabricated by dealloying of  $\text{Cu}_{30}\text{Mn}_{70}$  (200  $\mu\text{m}$  thickness) in HCl solution with pH **a** 1.3 (cat-8), **b** 1.5 (cat-9), **c** 1.7 (cat-10)

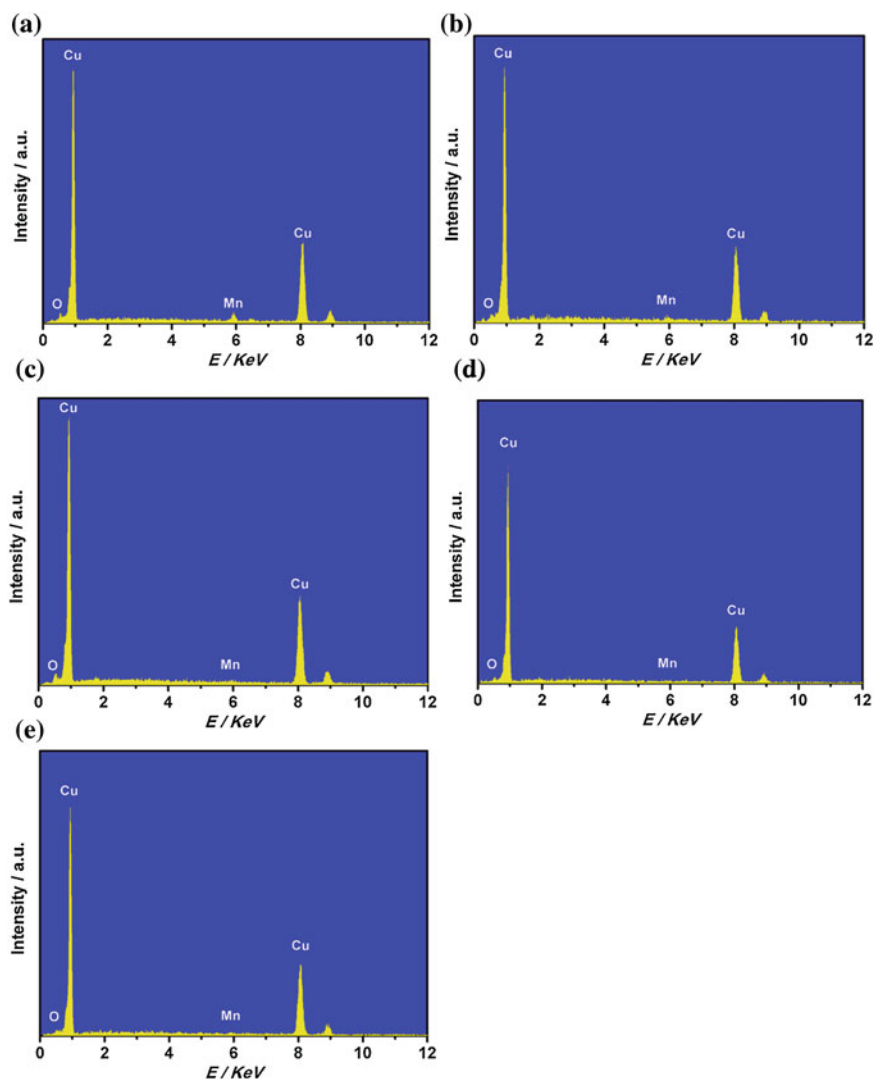


**Fig. 2.4** EDX spectra of **a** cat-4 made at 0 °C,  $\text{Cu}_{96}\text{Mn}_4$ , **b** cat-5 made at 10 °C,  $\text{Cu}_{98}\text{Mn}_2$ , **c** cat-1 made at 25 °C,  $\text{Cu}_{98}\text{Mn}_2$ , **d** cat-6 made at 40 °C,  $\text{Cu}_{98}\text{Mn}_2$ , **e** cat-7 made at 60 °C,  $\text{Cu}_{98}\text{Mn}_2$



**Table 2.2** CuNPore (cat-1)-catalyzed synthesis of various substituted triazoles

1	2	3		
Entry	R <sup>1</sup> 1	R <sup>2</sup> 2	Time, h	Yield, (%) <sup>a</sup>
1	2-pyridyl 1b	Bn 2a	4.5	3b, 96
2	3-thienyl 1c	Bn 2a	7	3c, 99
3	n-pentyl 1d	Bn 2a	6	3d, 99
4	c-hexyl 1e	Bn 2a	4	3e, 97
5	t-Bu 1f	Bn 2a	22	3f, 99
6	HOCH <sub>2</sub> 1g	Bn 2a	19	3 g, 94
7 <sup>b</sup>	Ph 1a	Ph 2b	22	3 h, 95
8 <sup>b</sup>	Ph 1a	Cinnamyl 2c	19	3i, 99
9	Ph 1a	EtO <sub>2</sub> CCH <sub>2</sub> 2d	3	3j, 99
10	BnNHCH <sub>2</sub> 1h	Ph 2b	3.5	3k, 95
11 <sup>c</sup>	TsNHCH <sub>2</sub> 1i	Ph 2b	6	3l, 98

To a toluene (2 M) solution of cat-1 (2 mol%) was added alkyne **1** and azide **2** (1 equiv.). The mixture was stirred at 65 °C for the time shown in the table

<sup>a</sup> Isolated yield

<sup>b</sup> 2 equiv. azide were used

<sup>c</sup> 1.2 equiv. azide were used

catalysts with controlled ligament sizes, cat-1, with a ligament size of about 40 nm, showed the greatest activity, affording the corresponding 1,2,3-triazoles in almost quantitative yield (entry 1 vs. entries 4–7). It is well known that nanocatalysts of smaller sizes exhibit greater catalytic activity as a result of their high surface areas; however, these results were unprecedented. The specific surface area of cat-3 was measured by the BET method to be 14 m<sup>2</sup>/g, the turnover frequency (TOF) thus reached to 0.26 s<sup>-1</sup>. It should be noticed that the reaction can be catalyzed by cat-3 at ambient temperature, although it required a longer reaction time (30 h). Cu-Mn alloy was totally inactive as a catalyst (entry 11). These results indicate that the tunable nanoporosity of CuNPore has a strong influence on catalytic activity in the click reaction, however the reason for this remains unresolved. Further examination of the dealloyed Cu catalysts synthesized in HCl solution (cat-8–10), revealed them to be less active (entries 8–10).

The catalytic activity of CuNPore (cat-1, 2 mol%) was further examined with various terminal alkynes and organic azides in toluene (2 M) at 65 °C (Table 2.2). Not only aromatic and heteroaromatic alkynes but also alkylalkynes were catalyzed regioselectively, affording 1,2,3-triazoles in excellent yields (entries 1–7). Various functional groups, such as alkene, ester, and protected amines were tolerated under the present heterogeneous conditions (entries 8–11). Under neat conditions, the catalytic loading can be decreased to 0.1 mol% without any significant influence on the reaction efficiency, and the TOF was increased up to 5.2 s<sup>-1</sup> (Eq. 2.2).

**Fig. 2.5** Reusability of CuNPore (cat-1) for the reaction of **1a** with **2a** was carried out in toluene (0.5 M) at 65 °C for 6 h

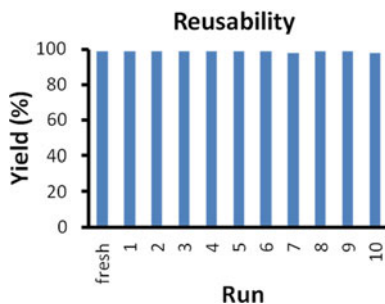
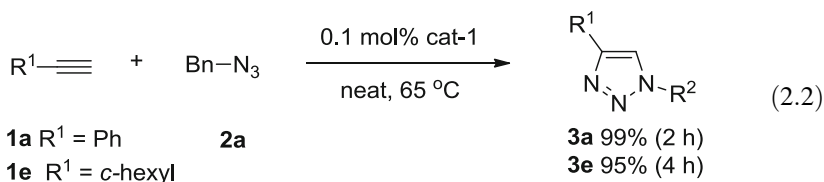
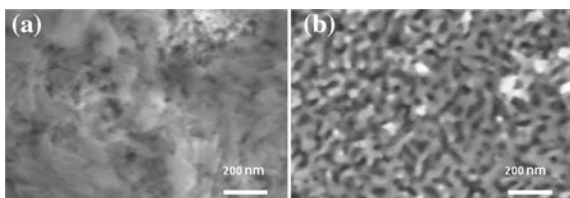
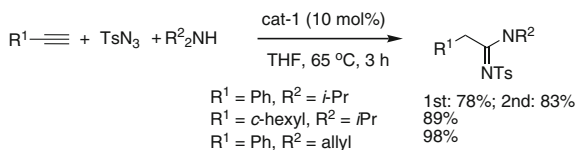


**Fig. 2.6** SEM images of cat-1 after tenth cycle. **a** Surface was not clear, **b** Cross-sectional nanostructure remained well



The CuNPore (cat-1) catalyst was reused for multiple cycles without significant loss of catalytic activity in the reaction of **1a** and **2a**; the yield was still 98 % in the tenth cycle (Fig. 2.5). After simple filtration of the reaction mixture, the catalyst was washed with acetone and reused without further purification. The product was produced almost quantitatively in every cycle and the turnover number (TON) reached up to 8200. It is noteworthy that the nanostructure of the recovered catalyst did not show significant changes after the fifth cycle, however, the nanostructure on surface was not clear after the tenth cycle while the cross-sectional nanostructure survived well (Fig. 2.6).

The CuNPore catalyst system can be further applied to the three-component coupling of terminal alkynes, tosyl azide and dialkylamines to afford the corresponding aminoimines in high yields; this was previously reported for homogeneous Cu catalysts (Scheme 2.2) [47]. The reactions tolerated different functional groups and the catalyst could be reused at least once without loss of catalytic activity. In addition, the three-component coupling gave an excellent yield, whereas the reaction over the reported homogeneous Cu catalyst afforded a mixture of products. This result implies that CuNPore catalysts can be applied to a range of other transformations with high activity and selectivity.



**Scheme 2.2** Application of a CuNPore catalyst to the three-component coupling of terminal alkynes, tosyl azide, and dialkylamines

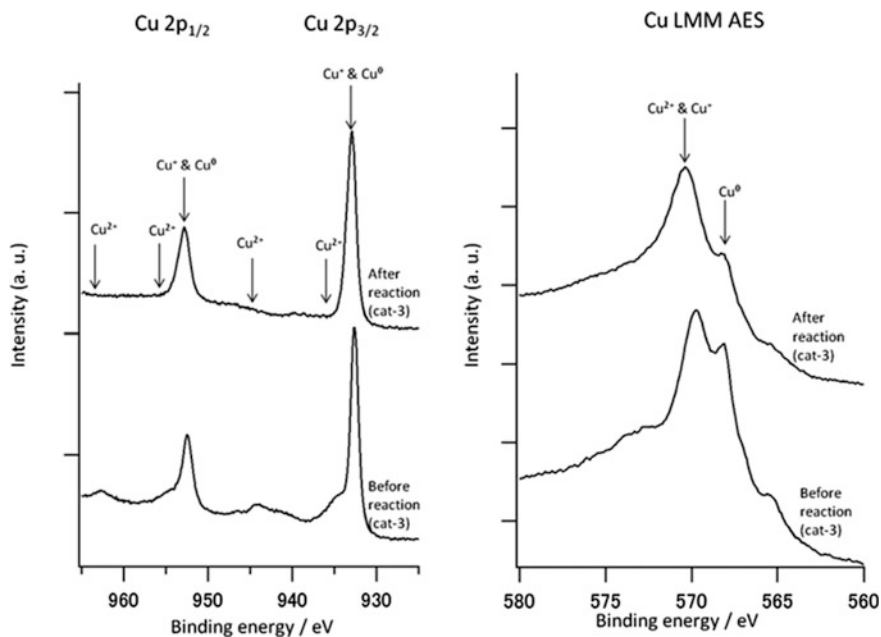


**Fig. 2.7** XPS spectra of CuNPore catalyst (cat-1) surface before reaction and after reaction

### 2.2.3 Mechanistic Investigation

A number of homogeneous and heterogeneous examples proved that the click reaction was catalyzed by Cu(I) species [17–30]. X-ray photoelectron spectroscopy (XPS) spectra showed that the fresh CuNPore (cat-1) surface is composed of Cu(0), Cu(I), and Cu(II) species, while Cu(I) is a predominant component (Fig. 2.7) [41]. The Cu 2*p* peaks at 932 and 953 eV and Cu LMM Auger peak at 568 eV were assigned to Cu(0); peaks at 570, 932, and 953 eV were ascribed to Cu(I); several satellite peaks at 935 eV, 944 eV, 955 eV, and 963 eV correspond to Cu(II). The Cu(I) and Cu(II) ions exist as the native Cu<sub>2</sub>O and CuO on CuNPore surface. The XPS spectra of cat-1, cat-4 to cat-7 having different ligament sizes did not show a significant difference on the surface component (Fig. 2.8). Moreover, after reaction, the satellite peaks of Cu(II) were almost disappeared while Cu(I)

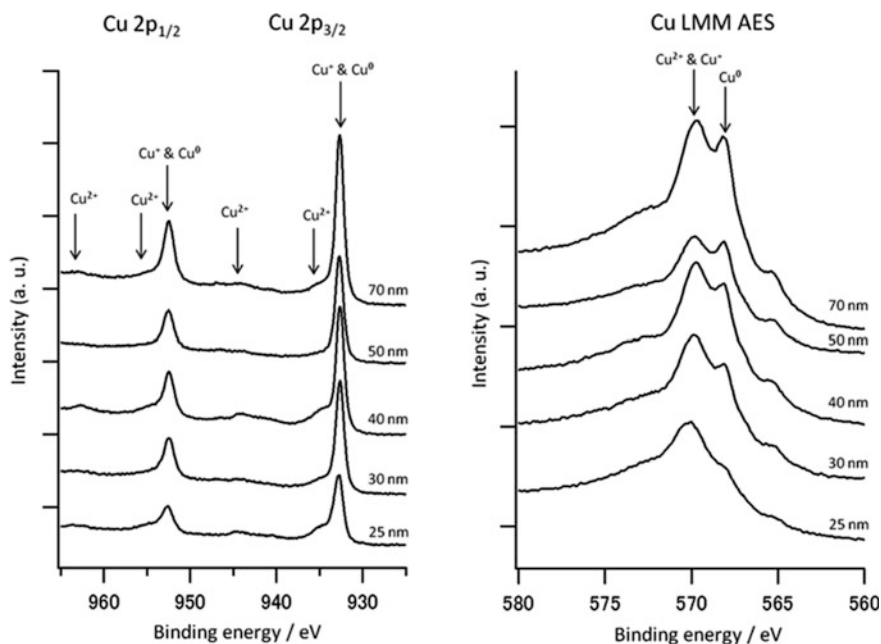


Fig. 2.8 XPS spectra of CuNPore materials with different ligament sizes

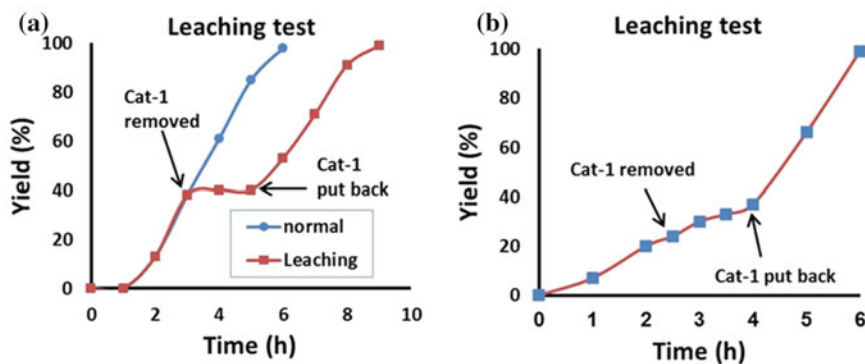
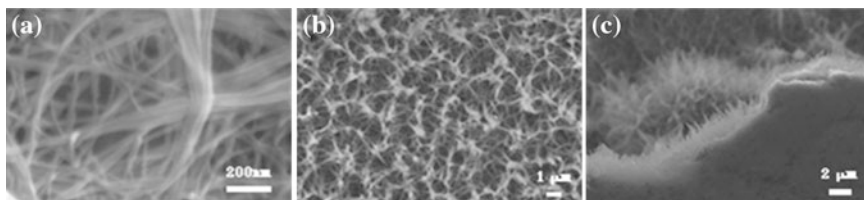
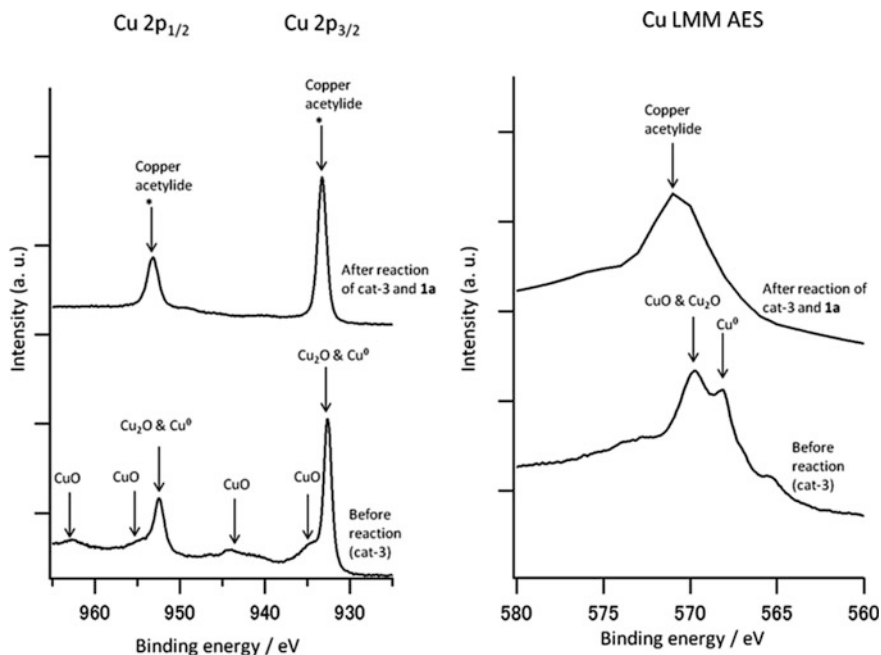


Fig. 2.9 Leaching test of CuNPore for the reaction of phenylacetylene and benzylazide with cat-1 at 65 °C **a** in toluene, **b** in THF

remained predominantly (Fig. 2.7). This result suggested that some amounts of Cu metal might be leached to the organic solvent. Indeed, the inductively coupled plasma (ICP-AES) analysis showed that only 0.2 ppm of Cu was leached after reaction. To clarify whether the leached Cu metal catalyzes the present reaction or not, we monitored the reaction with or without catalyst. The reaction of **1a** and **2a** was carried out by using 5 mol% of cat-1 in toluene (0.5 M) at 65 °C. After 3 h, CuNPore catalyst was removed from the reaction vessel and **3a** was produced in



**Fig. 2.10** SEM images of nanostructured copper acetylide **a** grass-like material on surface, **b** magnified surface, **c** cross sectional structure image



**Fig. 2.11** XPS spectra of nanostructured copper acetylide

38 %  $^1\text{H}$  NMR yield at this time (Fig. 2.9a, ■ symbols). The reaction mixture was continuously heated in the absence of the catalyst for 1 h, affording **3a** in 40 % yield, while the reaction was completely stopped in the next 1 h. The reaction restarted when cat-1 was put back into the mixture and finally gave **3a** in 99 % yield within 4 h. On the other hand, the control reaction without removal of catalyst was complete in 6 h, giving **3a** in 98 % yield (Fig. 2.9a, ● symbols). These results indicated that the leached copper was mainly Cu(II) species which was unable to catalyze the present click reaction, suggesting that the reaction is catalyzed by Cu(I) ions on the CuNPore surface. It should be noted that  $\text{Cu}_2\text{O}$  or  $\text{CuO}$  powder cannot catalyze this reaction without a base (Table 2.1, entries 12 and 13). These results further support that the nanoporous structure plays a crucial

role in the current catalysis. In contrast, when THF was used as solvent instead of toluene in the same control reaction, the reaction slowed down after removal the catalyst, but did not stop, implying that leached  $\text{Cu}^{\text{I}}$  species are stabilized by THF preventing easy oxidization to  $\text{Cu}^{\text{II}}$  (Fig. 2.9b). ICP analysis showed that only a negligible amounts of Cu were leached in the reaction in toluene and THF, 0.2 and 0.11 ppm, respectively.

Involvement of copper(I) acetylide species in the click reaction is well demonstrated by computational study and kinetic experiments [42–44]. During this study of the catalytic properties of CuNPore materials, we found that when cat-1 was treated with an excess amount of phenylacetylene in toluene without organic azides at room temperature, the CuNPore catalyst surface was turned to yellow after washing with acetone and dichloromethane. The SEM image showed that cat-1 surface was covered with a uniform grass-like material (Fig. 2.10). A binding energy peak appeared in between those of  $\text{CuO}$  and  $\text{Cu}_2\text{O}$ , and peaks of  $\text{Cu}(\text{II})$  and  $\text{Cu}(\text{O})$  were not detected in the XPS spectra, suggesting that the new peaks (marked by \*) of the grass-like material surface should be assigned to  $\text{Cu}(\text{I})$  species (Fig. 2.11). However, treatment of cat-1 with benzyl azide without phenylacetylene did not change the nanoporous structure of the catalyst. These results prompted us to examine the possibility of the nanostructured copper acetylide formation. When the grass-like material (Fig. 2.10) was treated with benzyl azide at  $65\text{ }^\circ\text{C}$  for 2 h, the grass-like material disappeared from the surface, and the nanoporous structure of cat-1 was recovered, and a very small amount of the corresponding triazole **3a** was detected by  $^1\text{H}$  NMR and GC-MS. Moreover, the recovered CuNPore remained its high catalytic activity in the reaction of **1a** and **2a** (99 % of **3a**), although the reaction with the grass-like material as a catalyst gave 58 % of **3a**. These results implied that the grass-like material should be the nanostructured *polymeric* copper acetylide which was less active than the copper acetylides with lower order aggregates generated in situ. The results were in good agreement with the previous DFT studies and experimental investigation reported by Fokin [42, 43] and Straub [44]. It is noteworthy that the nanostructured copper acetylide was very stable in air compared to the air-sensitive fresh CuNPore, suggesting that the polymeric copper acetylide can be used as a CuNPore metal storage to protect the nanoporosity of CuNPore from air.

## 2.3 Conclusion

we have developed an efficient approach for the fabrication of nanoporous copper materials with tunable nanoporosity, and demonstrated that CuNPore has an outstanding catalytic activity for the click chemistry without using any supports and bases. The catalytic activity was highly in dependence on the ligament (or pore) sizes of the CuNPore materials; ligament size about  $\sim 40$  nm significantly enhanced the catalytic efficiency. Characterization of the catalyst surface, leaching experiments, and the formation of nanostructured copper acetylide revealed that

the present click reaction is catalyzed by Cu(I) species on the CuNPore surface. The CuNPore catalyst exhibited a high reusability; it can be recycled for ten times without significant loss of activity. A wide range of alkynes and azides can be tolerated, giving the corresponding triazoles in excellent yields. The CuNPore catalyst system can also be applied to the three-component coupling of terminal alkynes, tosyl azide and dialkylamines to afford the corresponding aminoimines in high yields. Further studies on exploring new catalytic activities of CuNPore materials and extension of its utility to organic synthesis are in progress.

## 2.4 Experimental Section

### 2.4.1 General Information

$^1\text{H}$  NMR and  $^{13}\text{C}$  NMR spectra were recorded on JEOL JMTC-270/54/SS (JAS-TEC, 300, 400, 500 MHz) spectrometers.  $^1\text{H}$  NMR spectra are reported as follows: chemical shift in ppm ( $\delta$ ) relative to the chemical shift of  $\text{CDCl}_3$  at 7.26 ppm, integration, multiplicities (s = singlet, d = doublet, t = triplet, q = quartet, m = multiplet and br = broadened), and coupling constants (Hz).  $^{13}\text{C}$  NMR spectra reported in ppm ( $\delta$ ) relative to the central line of triplet for  $\text{CDCl}_3$  at 77 ppm. IR spectra were recorded on JASCO FT/IR-4100 spectrometer; absorptions are reported in  $\text{cm}^{-1}$ . High-resolution mass spectra were obtained on a BRUKER APEXIII spectrometer. The XPS measurements were carried out using a VG ESCALAB 250 spectrometer (Thermo Fisher Scientific K.K.) employing monochromatic Al K X-ray radiation. The system was operated at 15 kV and 200 W. The base pressure of the analysis chamber was less than 10 to 8 Pa. SEM observation was carried out using HITACHI FE-SEM S4300 operated at an accelerating voltage of 10 kV. EDX analysis was carried out using EDAX Genesis with HITACHI FE-SEM S4300 operated at an accelerating voltage of 20 kV. ICP-MS analysis was performed with Shimadzu ICPS-7510. Column chromatography was carried out employing Slica gel 60 N (spherical, neutral, 40 ~ 100  $\mu\text{m}$ , KANTO Chemical Co.). Analytical thin-layer chromatography (TLC) was performed on 0.2 mm precoated plate Kieselgel 60 F<sub>254</sub> (Merk).

### 2.4.2 Materials

Anhydrous toluene (WAKO), Cu (99.99 %, MITSUWA), Mn (99.99 %, MITSUWA), alkynes (**1**) and azides (**2**) were purchased and used as received. The structure of products were identified according to the reported literatures [48–52].

### 2.4.3 Calculation of TOF and TON

The surface area of CuNPore (cat-1, ligament size:  $\sim 40$  nm) dealloying at room temperature was measured by BET method to be  $14 \text{ m}^2/\text{g}$ , and the density of surface atoms for the energetically most stable Cu(111) surface is  $1.77 \times 10^{19}$  atoms/ $\text{m}^2$ . The reaction time was 2 h as shown in Table 2.1. Using these values the TOF was calculated to be  $936 \text{ h}^{-1}$  (Table 2.1, entry 1). On the other hand, TON was calculated to be 8200 by the number of the Cu atoms on the catalyst surface with the number of the product **3a** as shown in Fig. 2.5 [6].

### 2.4.4 Fabrication of $\text{Cu}_{30}\text{Mn}_{70}$ Alloy

$\text{Cu}_{30}\text{Mn}_{70}$  alloys was fabricated from pure Cu (99.99 wt%) and Mn (99.99 wt%) at  $1300 \text{ }^\circ\text{C}$  by high-frequency induction furnace. The Cu–Mn alloy sealed in quartz tube under vacuum was heated at  $900 \text{ }^\circ\text{C}$  for 72 h, and quenched into water [32]. The resulting alloy was sectioned, using a diamond saw, into samples approximately 1 mm thick. The alloy samples were rolled to about  $200 \text{ }\mu\text{m}$  thickness.

### 2.4.5 Representative Fabrication Method of Nanoporous Copper (CuNPore, cat-1) Under Free Corrosion

The rolled alloy sample with  $200 \text{ }\mu\text{m}$  thickness and  $5 \times 5 \text{ mm}$  size was placed directly in 1 M  $(\text{NH}_4)_2\text{SO}_4$  and 0.01 M  $\text{MnSO}_4$  electrolytes at room temperature ( $25 \text{ }^\circ\text{C}$ ) for 6 days [32]. All electrolytes were prepared with deionized (DI) water and reagent grade chemicals. After dealloying, the sample was removed from electrolytes and rinsed in DI water for few minutes. The sample was then washed with acetone and dried on vacuum. The dried CuNPore was stored in glove box (Fig. 2.12).

Under same electrolytes, cat-4 and cat-5 were fabricated at 0 and  $10 \text{ }^\circ\text{C}$  for 6 days, respectively. Cat-6 and cat-7 were dealloyed at 40 and  $60 \text{ }^\circ\text{C}$  for 4 days. Cat-2 and cat-3 were fabricated at  $25 \text{ }^\circ\text{C}$  for 6 days.

Under HCl solution, cat-8, cat-9 and cat-10 were fabricated at  $25 \text{ }^\circ\text{C}$  for 6 days.

### 2.4.6 Representative Procedure for the CuNPore (cat-1)-Catalyzed Click Reaction of Phenyl Acetylene (**1a**) and Benzyl Azide (**2a**) (Tables 2.1 and 2.2)

To a toluene (2 M, 0.5 mL) solution of CuNPore (cat-1, 2 mol%, 1.3 mg) was added phenyl acetylene **1a** (1 mmol, 112  $\mu\text{L}$ ) and benzyl azide **2a** (1 mmol, 125  $\mu\text{L}$ ) in a V-shape reactor vial. The reaction mixture was stirred at  $65 \text{ }^\circ\text{C}$  for 2 h by using a bulky round-shape magnetic stirring bar. After consumption of **1a** and **2a**

**Fig. 2.12** CuNPore (cat-3)  
size: 175  $\mu\text{m}$   
(thickness) $\times$ 5 mm $\times$ 5 mm



**Table 2.3** Reusability of cat-1

Run	Fresh	1	2	3	4	5	6	7	8	9	10
3a, yield (%) <sup>a</sup>	99	99	99	99	99	99	99	98	99	99	98

<sup>a</sup> <sup>1</sup>H NMR yield of **3a** determined using dibromomethane as an internal standard

which were monitored by TLC, the reaction mixture was cooled to room temperature. The mixture was filtered and washed with dichloromethane. The recovered CuNPore catalyst was washed with acetone and dried under vacuum. After concentration of the filtrate, the white solid was purified with a short silica gel chromatography, by using a 3:1 mixture of hexane and ethyl acetate as an eluent, to afford 233 mg of 1-benzyl-4-phenyl-1*H*-1,2,3-triazole **3a** (99 %) as a white solid.

#### 2.4.7 Neat Reaction Procedure (Eq. 2.2)

The reaction of **1a** (14.2 mmol, 1.59 mL) and **2a** (14.2 mmol, 1.77 mL) performed using 0.1 mol% of cat-1 (0.9 mg) in the absence of solvent at 65 °C for 2 h. The work-up procedure is same to above. **3a** was obtained in 99 % yield (3.33 g)

#### 2.4.8 Leaching Experiment (Fig. 2.9)

Figure 2.9a, leaching experiment for the reaction of **1a** and **2a** was carried out by using 5 mol% of cat-1 in toluene (0.5 M) at 65 °C. Cat-1 was removed from reaction vial after 3 h, giving **3a** in 38 % NMR yield. The reaction was continuously heated for 1 h in the absence of cat-1, producing **3a** in 40 %. After being heated another 1 h, the yield of **3a** was not changed (40 %). Then, cat-1 was put

back into the reaction mixture and heated for 1 h gave **3a** in 53 % yield. The reaction was finally complete within 3 h produced **3a** in 99 % yield.

On the other hand, under same reaction conditions, the controlled reaction without removal of cat-1 was complete in 6 h, giving **3a** in 98 % yield.

Figure 2.9b, leaching experiment for the reaction of **1a** and **2a** was carried out by using 5 mol% of cat-1 in THF (2 M) at 65 °C. Cat-1 was removed from reaction vial after 2.5 h, giving **3a** in 24 % NMR yield. The reaction was continuously heated for 1.5 h in the absence of cat-1, producing **3a** in 37 %. Then, cat-1 was put back into the reaction mixture and heated for 1 h gave **3a** in 66 % yield. The reaction was finally complete within 1 h produced **3a** in 99 % yield.

### 2.4.9 Reusability (Fig. 2.5)

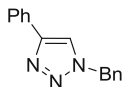
The reaction of **1a** and **2a** for the recycle was carried out in toluene (0.5 M) at 65 °C for 6 h in the presence of cat-1 catalyst. After filtration, cat-1 was washed with acetone and dried on vacuum. The recovered cat-1 was continuously used for 10 times. The <sup>1</sup>H NMR yield of **3a** for every cycle is shown in Table 2.3.

### 2.4.10 Formation of Nanostructured Copper Acetylide (Figs. 2.10 and 2.11)

A toluene (2 M, 0.7 mL) solution of cat-1 (2 mol%, 1.7 mg) and phenyl acetylene **1a** (1.34 mmol, 150 μL) was stirred for 3.5 h, the cat-1 surface was turned to yellow (Fig. 2.11). The SEM image showed that the surface was covered with a uniform grass-like material. When the grass-like material was treated with an excess amount of benzyl azide **2a**, the grass-like material was disappeared from SEM image. The nanoporous structure of cat-1 surface was recovered and a small amount of **3a** was observed from <sup>1</sup>H NMR and GC-MS. The grass-like material should be the nanostructured copper acetylide.

### 2.4.11 Analytical Data

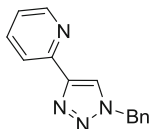
#### 1-Benzyl-4-phenyl-1H-1,2,3-triazole (**3a**) [48]



White solid; <sup>1</sup>H NMR (500 MHz, CDCl<sub>3</sub>) δ 7.77–7.75 (m, 2H), 7.64 (s, 1H), 7.36–7.30 (m, 5H), 7.28–7.22 (m, 3H), 5.49 (s, 2H); <sup>13</sup>C NMR (125 MHz,

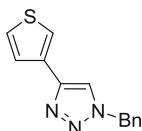
$\text{CDCl}_3$ )  $\delta$  148.0, 134.6, 130.4, 128.9, 128.6, 128.5, 128.0, 127.8, 125.5, 119.5, 54.0; HRMS (ESI positive) calcd for  $\text{C}_{15}\text{H}_{13}\text{N}_3$   $[\text{M} + \text{Na}]^+$ : 258.1002, found: 258.1001.

### 2-(1-Benzyl-1*H*-1,2,3-triazol-4-yl)pyridine (3b) [49]



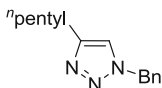
White solid;  $^1\text{H}$  NMR (300 MHz,  $\text{CDCl}_3$ )  $\delta$  8.45–8.42 (m, 1H), 8.10–8.06 (m, 1H), 7.97 (s, 1H), 7.68–7.63 (m, 1H), 7.27–7.21 (m, 5H), 7.12–7.07 (m, 1H), 5.48 (s, 2H);  $^{13}\text{C}$  NMR (75 MHz,  $\text{CDCl}_3$ )  $\delta$  150.0, 149.2, 148.5, 136.7, 134.2, 129.0, 128.6, 128.1, 122.7, 121.8, 120.0, 54.2; HRMS (ESI positive) calcd for  $\text{C}_{14}\text{H}_{12}\text{N}_4$   $[\text{M} + \text{Na}]^+$ : 259.0954, found: 259.0954.

### 1-Benzyl-4-(thiophen-3-yl)-1*H*-1,2,3-triazole (3c) [49]



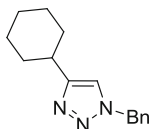
White solid;  $^1\text{H}$  NMR (400 MHz,  $\text{CDCl}_3$ )  $\delta$  7.61-7.60 (m, 1H), 7.54 (s, 1H), 7.38-7.23 (m, 7H), 5.50 (s, 2H);  $^{13}\text{C}$  NMR (100 MHz,  $\text{CDCl}_3$ )  $\delta$  144.2, 134.6, 131.7, 129.0, 128.6, 127.9, 126.2, 125.6, 120.9, 119.2, 54.0; HRMS (ESI positive) calcd for  $\text{C}_{13}\text{H}_{11}\text{N}_3\text{S}$   $[\text{M} + \text{Na}]^+$ : 264.0566, found: 264.0566.

### 1-Benzyl-4-pentyl-1*H*-1,2,3-triazole (3d) [50]



White solid;  $^1\text{H}$  NMR (400 MHz,  $\text{CDCl}_3$ )  $\delta$  7.29-7.24 (m, 3H), 7.17-7.15 (m, 2H), 7.12 (s, 1H), 5.39 (s, 2H), 2.59 (t,  $J = 7.6$  Hz, 2H), 1.57-1.53 (m, 2H), 1.24-1.21 (m, 4H), 0.79 (t,  $J = 7.2$  Hz, 3H);  $^{13}\text{C}$  NMR (100 MHz,  $\text{CDCl}_3$ )  $\delta$  148.7, 134.9, 128.8, 128.4, 127.7, 120.3, 53.7, 31.2, 28.9, 25.5, 22.2, 13.8; HRMS (ESI positive) calcd for  $\text{C}_{14}\text{H}_{19}\text{N}_3$   $[\text{M} + \text{Na}]^+$ : 252.1471, found: 252.1471.

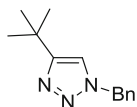
### 1-Benzyl-4-cyclohexyl-1*H*-1,2,3-triazole (3e) [51]



White solid;  $^1\text{H}$  NMR (300 MHz,  $\text{CDCl}_3$ )  $\delta$  7.31-7.20 (m, 3H), 7.18-7.15 (m, 2H), 7.09 (s, 1H), 5.40 (s, 2H), 2.69-2.62 (m, 1H), 1.95-1.94 (m, 2H), 1.71-1.60 (m, 3H), 1.37-1.10 (m, 5H);  $^{13}\text{C}$  NMR (75 MHz,  $\text{CDCl}_3$ )  $\delta$  154.0, 134.9, 128.8, 128.3,

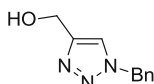
127.8, 119.0, 53.7, 35.1, 32.8, 25.9, 25.8; HRMS (ESI positive) calcd for  $C_{15}H_{19}N_3$   $[M + Na]^+$ : 264.1471, found: 264.1471.

**1-Benzyl-4-(tert-butyl)-1H-1,2,3-triazole (3f) [48]**



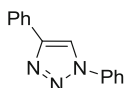
White solid;  $^1H$  NMR (500 MHz,  $CDCl_3$ )  $\delta$  7.35-7.32 (m, 3H), 7.26-7.24 (m, 2H), 7.19 (s, 1H), 5.46 (s, 1H), 1.31 (s, 9H);  $^{13}C$  NMR (125 MHz,  $CDCl_3$ )  $\delta$  157.9, 134.9, 128.8, 128.3, 127.8, 118.2, 53.6, 30.5, 30.1; HRMS (ESI positive) calcd for  $C_{15}H_{17}N_3$   $[M + Na]^+$ : 238.1315, found: 238.1314.

**(1-Benzyl-1H-1,2,3-triazol-4-yl)methanol (3g) [51]**



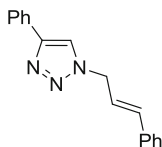
White solid;  $^1H$  NMR (300 MHz,  $CDCl_3$ )  $\delta$  7.40 (s, 1H), 7.28-7.26 (m, 3H), 7.19-7.16 (m, 2H), 5.39 (s, 2H), 4.64 (d,  $J = 5.1$  Hz, 2H), 4.20 (s, 1H);  $^{13}C$  NMR (75 MHz,  $CDCl_3$ )  $\delta$  148.1, 134.4, 128.9, 128.5, 127.9, 121.7, 55.8, 53.9; HRMS (ESI positive) calcd for  $C_{10}H_{11}N_3O$   $[M + Na]^+$ : 212.0794, found: 212.0793.

**1,4-Diphenyl-1H-1,2,3-triazole (3h) [48]**

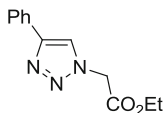


White solid;  $^1H$  NMR (300 MHz,  $CDCl_3$ )  $\delta$  8.19 (s, 1H), 7.91 (d,  $J = 7.2$  Hz, 2H), 7.79 (d,  $J = 7.8$  Hz, 2H), 7.56-7.51 (m, 2H), 7.48-7.43 (m, 3H), 7.39-7.34 (m, 1H);  $^{13}C$  NMR (75 MHz,  $CDCl_3$ )  $\delta$  148.3, 137.0, 130.2, 129.7, 128.8, 128.7, 128.3, 125.8, 120.4, 117.5; HRMS (ESI positive) calcd for  $C_{14}H_{11}N_3$   $[M + Na]^+$ : 244.0845, found: 244.0845.

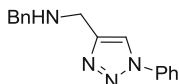
**1-Cinnamyl-4-phenyl-1H-1,2,3-triazole (3i) [52]**



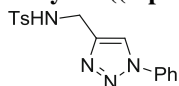
Light yellow solid;  $^1H$  NMR (500 MHz,  $CDCl_3$ )  $\delta$  7.80 (d,  $J = 7.5$  Hz, 2H), 7.76 (s, 1H), 7.38-7.35 (m, 4H), 7.33-7.21 (m, 4H), 6.30 (d,  $J = 16.0$  Hz, 1H), 6.31 (dt,  $J = 16.0$  Hz, 6.5 Hz, 1H), 5.09-5.08 (m, 2H);  $^{13}C$  NMR (125 MHz,  $CDCl_3$ )  $\delta$  147.9, 135.3, 135.1, 130.5, 128.7, 128.6, 128.4, 128.0, 126.5, 125.5, 121.8, 119.3, 52.2; HRMS (ESI positive) calcd for  $C_{17}H_{15}N_3$   $[M + Na]^+$ : 284.1158, found: 284.1158.

**Ethyl 2-(4-phenyl-1*H*-1,2,3-triazol-1-yl)acetate (3j) [51]**

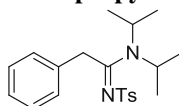
White solid;  $^1\text{H}$  NMR (400 MHz,  $\text{CDCl}_3$ )  $\delta$  7.90 (s, 1H), 7.82 (d,  $J = 7.2$  Hz, 2H), 7.40 (t,  $J = 7.6$  Hz, 2H), 7.32 (t,  $J = 7.6$  Hz, 1H), 5.17 (s, 2H), 4.24 (q,  $J = 7.2$  Hz, 2H), 1.27 (t,  $J = 7.2$  Hz, 3H);  $^{13}\text{C}$  NMR (100 MHz,  $\text{CDCl}_3$ )  $\delta$  166.2, 148.0, 130.2, 128.7, 128.1, 125.6, 120.9, 62.3, 50.8, 13.9; HRMS (ESI positive) calcd for  $\text{C}_{12}\text{H}_{13}\text{N}_3\text{O}_2$   $[\text{M} + \text{Na}]^+$ : 254.0900, found: 254.0900.

***N*-Benzyl-1-(1-phenyl-1*H*-1,2,3-triazol-4-yl)methanamine (3k)**

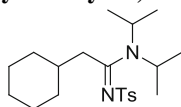
Brown solid;  $^1\text{H}$  NMR (300 MHz,  $\text{CDCl}_3$ )  $\delta$  7.66-7.62 (m, 2H), 7.46-7.39 (m, 2H), 7.37-7.16 (m, 6H), 3.93 (s, 2H), 3.81 (s, 2H), 1.86 (s, 1H);  $^{13}\text{C}$  NMR (75 MHz,  $\text{CDCl}_3$ )  $\delta$  147.4, 137.0, 129.5, 128.4, 128.3, 128.1, 126.9, 124.6, 120.3, 119.8, 53.2, 43.9; HRMS (ESI positive) calcd for  $\text{C}_{16}\text{H}_{16}\text{N}_4$   $[\text{M} + \text{Na}]^+$ : 287.1267, found: 287.1266.

**4-Methyl-*N*-((1-phenyl-1*H*-1,2,3-triazol-4-yl)methyl)benzenesulfonamide (3l)**

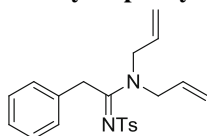
Yellow solid;  $^1\text{H}$  NMR (400 MHz,  $\text{CDCl}_3$ )  $\delta$  7.80 (s, 1H), 7.73 (d,  $J = 8.4$  Hz, 2H), 7.62-7.59 (m, 2H), 7.50-7.47 (m, 2H), 7.44-7.40 (m, 1H), 7.26-7.23 (m, 2H), 5.72 (s, 1H), 4.35 (d,  $J = 6.0$  Hz, 2H), 2.34 (s, 3H);  $^{13}\text{C}$  NMR (100 MHz,  $\text{CDCl}_3$ )  $\delta$  144.4, 143.6, 136.7, 129.7, 129.6, 128.8, 127.1, 124.8, 120.5, 120.3, 38.6, 21.3; HRMS (ESI positive) calcd for  $\text{C}_{16}\text{H}_{16}\text{N}_4\text{O}_2\text{S}$   $[\text{M} + \text{Na}]^+$ : 351.0886, found: 351.0885.

***N,N*-diisopropyl-2-phenyl-*N'*-tosylacetimidamide**

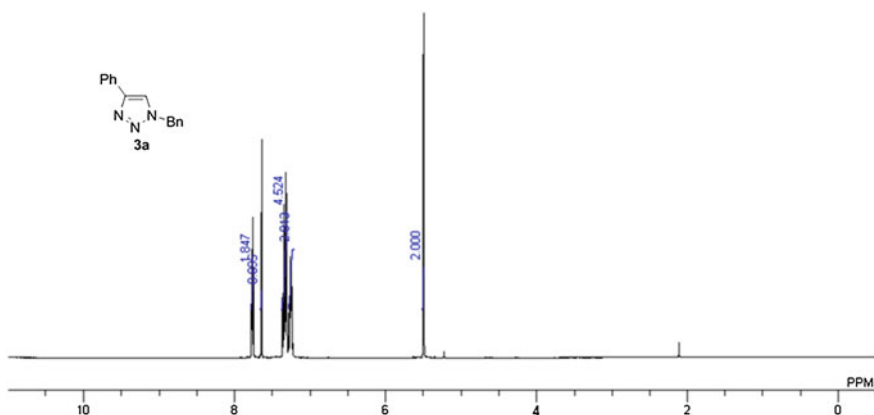
White solid;  $^1\text{H}$  NMR (300 MHz  $\text{CDCl}_3$ )  $\delta$  7.85 (d,  $J = 8.1$  Hz, 2H), 7.32-7.20 (m, 7H), 4.42 (s, 2H), 4.06-3.97 (m, 1H), 3.51-3.42 (m, 1H), 2.40 (s, 3H), 1.41 (d,  $J = 6.6$  Hz, 6H), 0.88 (d,  $J = 6.6$  Hz, 6H);  $^{13}\text{C}$  NMR (75 MHz,  $\text{CDCl}_3$ )  $\delta$  163.3, 141.4, 141.4, 134.8, 128.9, 128.6, 127.8, 126.6, 126.0, 50.3, 47.9, 38.5, 21.3, 19.6, 19.6; HRMS (ESI positive) calcd for  $\text{C}_{21}\text{H}_{28}\text{N}_2\text{O}_2\text{S}$   $[\text{M} + \text{Na}]^+$ : 395.1764, found: 395.1764.

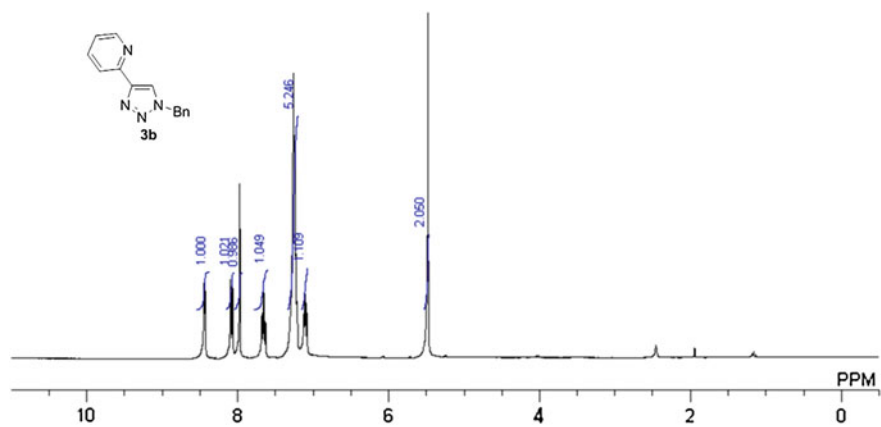
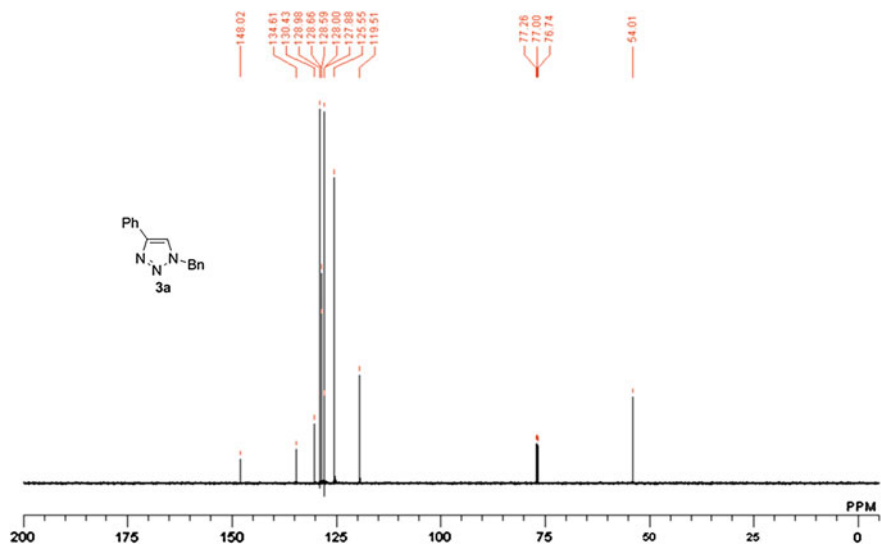
**2-cyclohexyl-N,N-diisopropyl-N'-tosylacetimidamide**

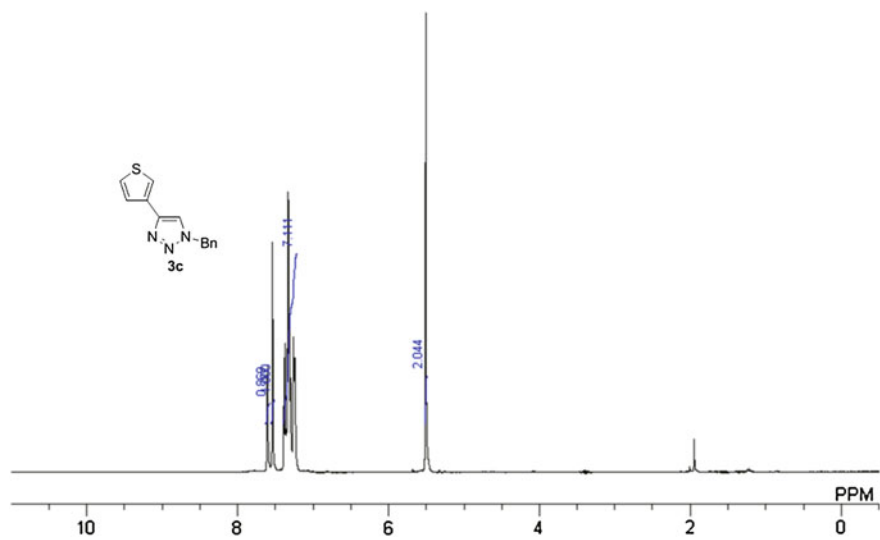
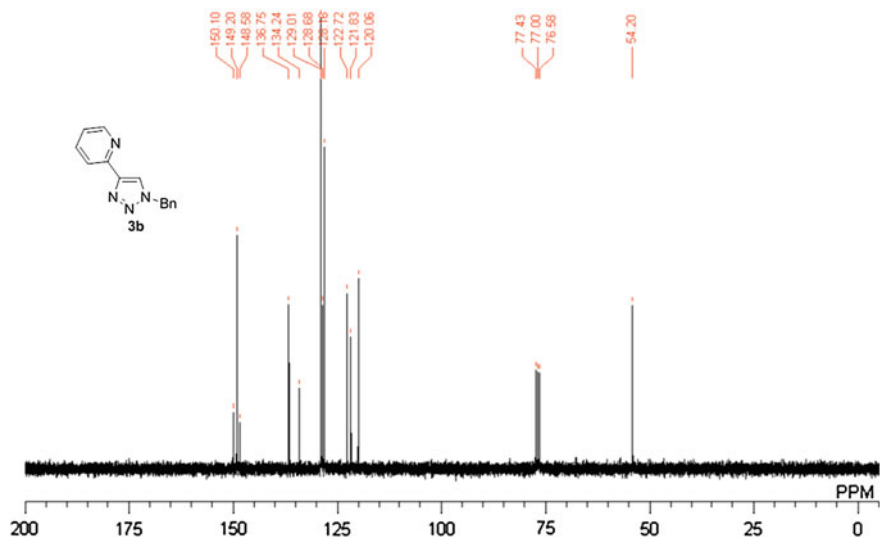
White solid;  $^1\text{H}$  NMR (300 MHz  $\text{CDCl}_3$ )  $\delta$  7.81 (d,  $J = 8.4$  Hz, 2H), 7.25 (d,  $J = 8.4$  Hz, 2H), 4.17-4.09 (m, 1H), 3.54-3.45 (m, 1H), 2.94 (d,  $J = 7.2$  Hz, 2H), 2.40 (s, 3H), 1.77-1.67 (m, 6H), 1.31-1.28 (m, 7H), 1.23-1.21 (m, 10H);  $^{13}\text{C}$  NMR (75 MHz,  $\text{CDCl}_3$ )  $\delta$  164.7, 142.0, 141.1, 128.8, 125.9, 50.2, 47.8, 38.6, 37.1, 32.5, 26.4, 25.9, 21.3, 20.5, 20.1; HRMS (ESI positive) calcd for  $\text{C}_{21}\text{H}_{34}\text{N}_2\text{O}_2\text{S}$   $[\text{M} + \text{Na}]^+$ : 401.2233, found: 401.2233.

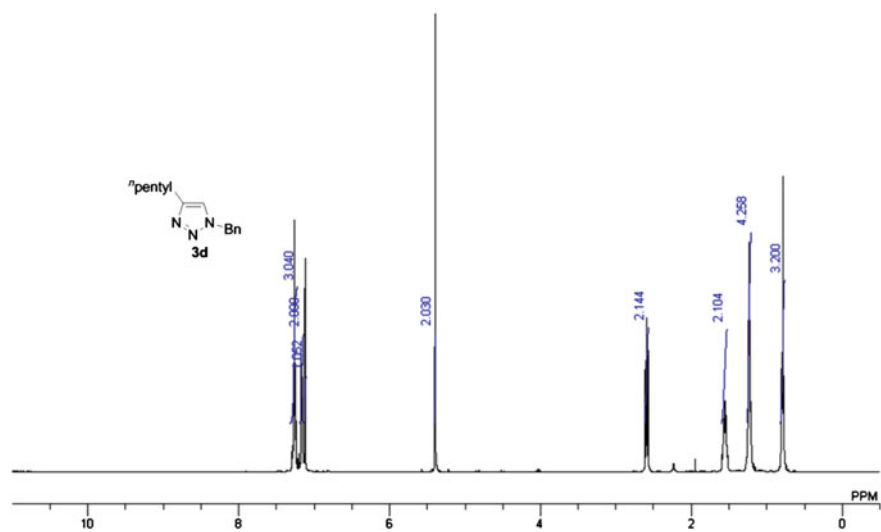
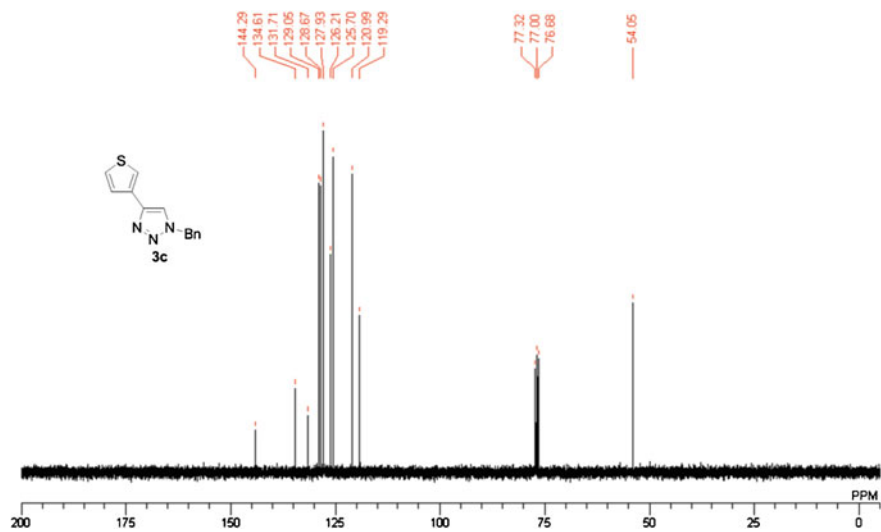
**N,N-diallyl-2-phenyl-N'-tosylacetimidamide**

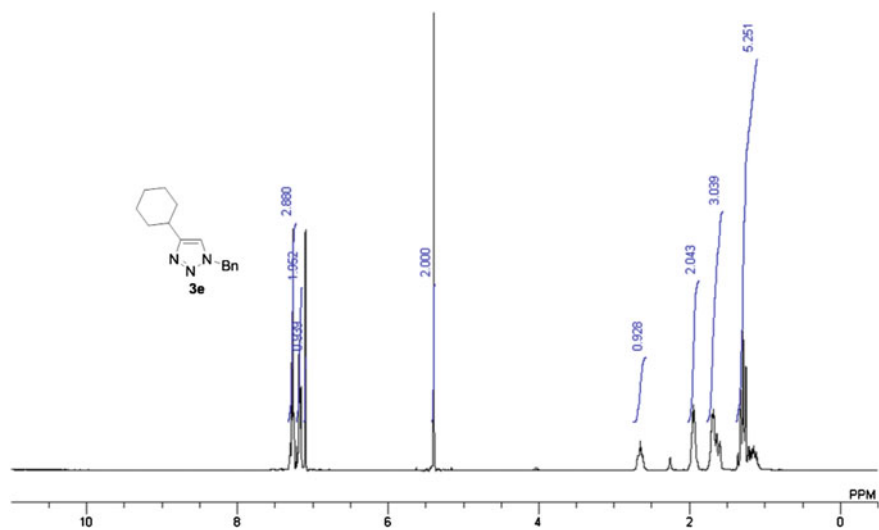
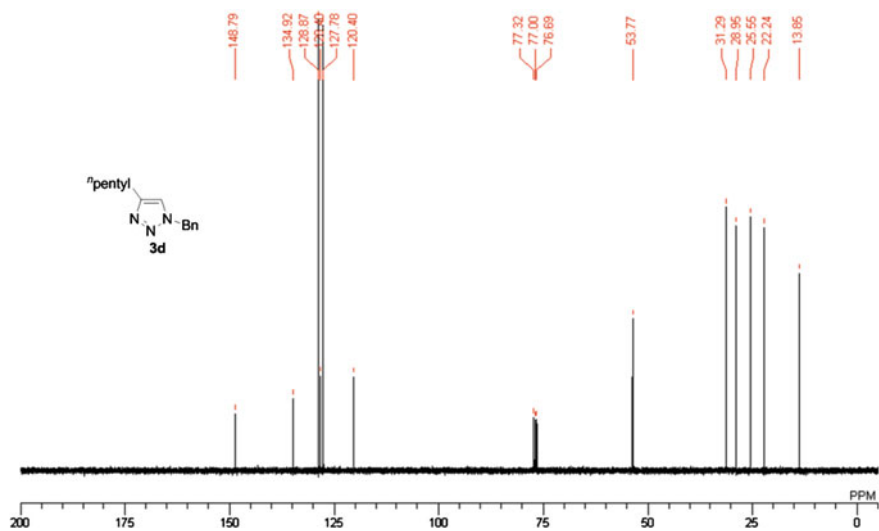
Yellow liquid;  $^1\text{H}$  NMR (300 MHz  $\text{CDCl}_3$ )  $\delta$  7.80 (d,  $J = 8.1$  Hz, 2H), 7.30-7.14 (m, 7H), 5.85-5.72 (m, 1H), 5.54-5.41 (m, 1H), 5.14 (dd,  $J = 10.2$  Hz, 17.1 Hz, 4H), 4.42 (s, 2H), 4.11 (d,  $J = 6.3$  Hz, 2H), 3.77 (d,  $J = 4.8$  Hz, 2H), 2.38 (s, 3H);  $^{13}\text{C}$  NMR (75 MHz,  $\text{CDCl}_3$ )  $\delta$  165.6, 141.7, 140.9, 133.9, 131.2, 131.1, 128.9, 128.8, 127.8, 126.7, 126.1, 118.4, 118.0, 50.6, 50.1, 36.5, 21.2; HRMS (ESI positive) calcd for  $\text{C}_{21}\text{H}_{24}\text{N}_2\text{O}_2\text{S}$   $[\text{M} + \text{Na}]^+$ : 391.1451, found: 391.1451.

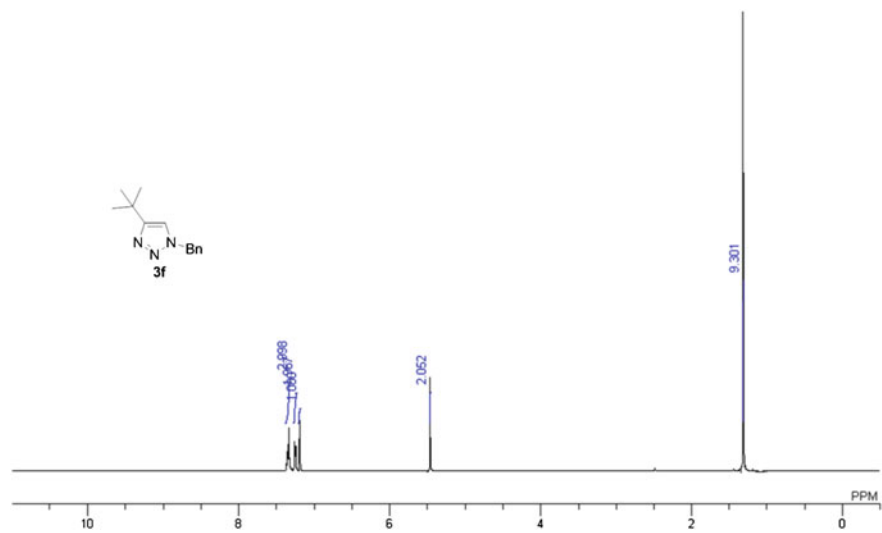
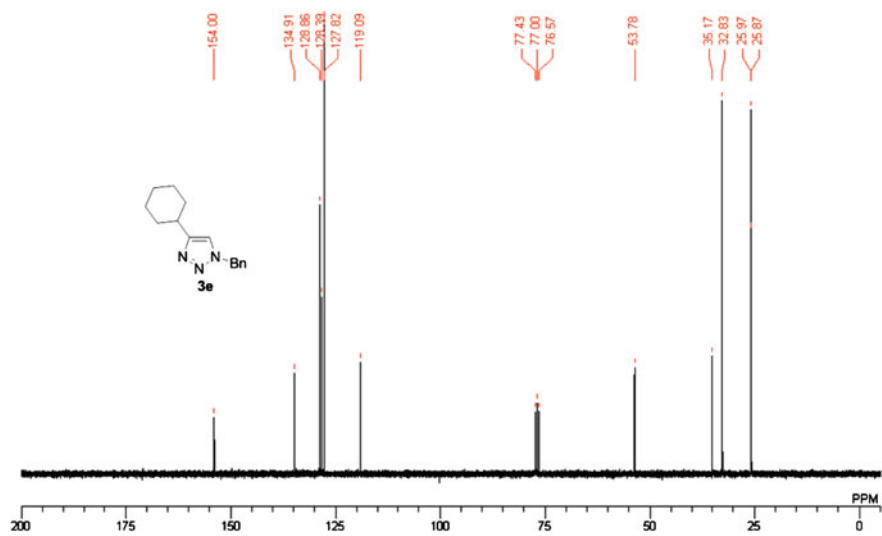
**2.4.12  $^1\text{H}$  and  $^{13}\text{C}$  NMR Spectra**



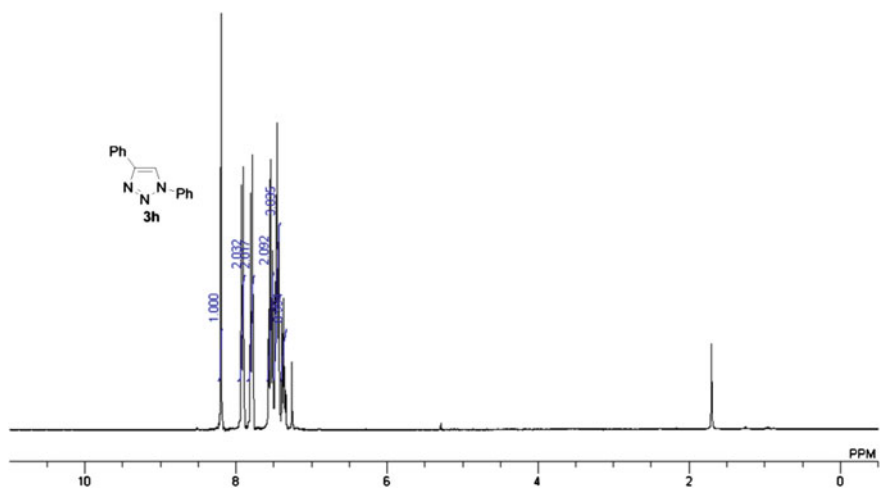
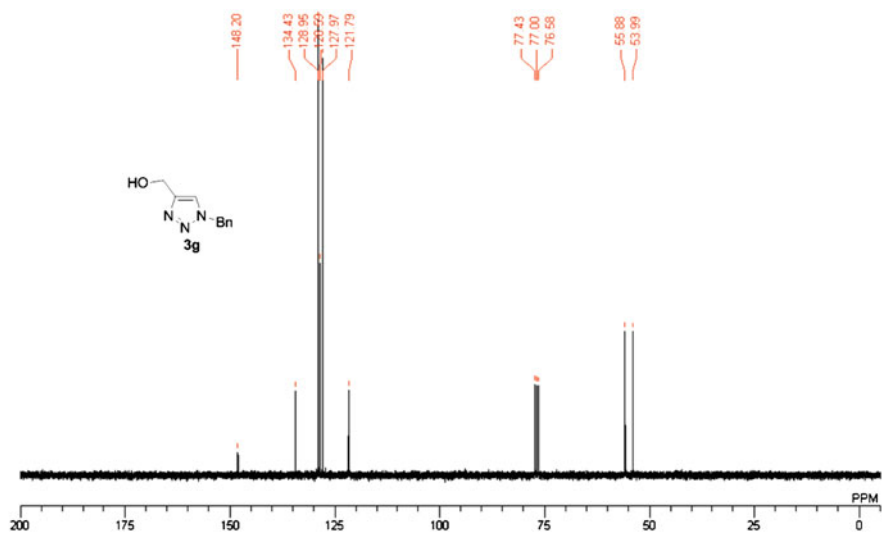


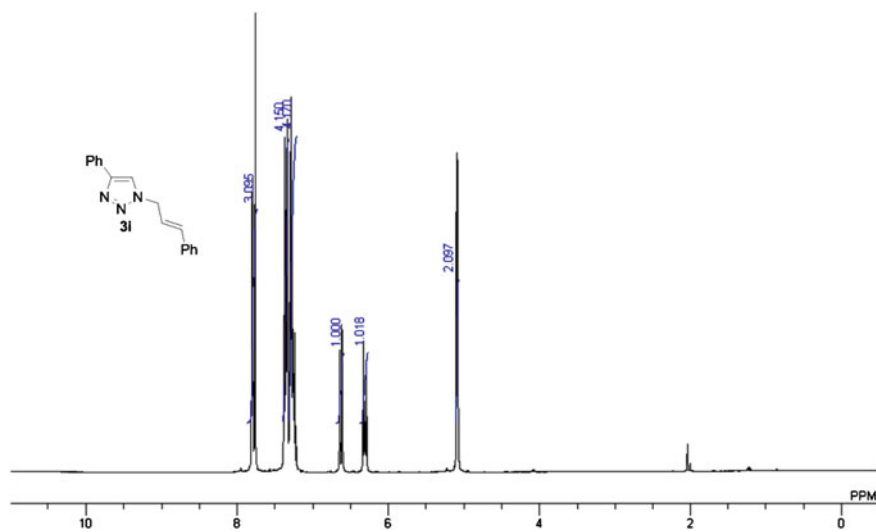
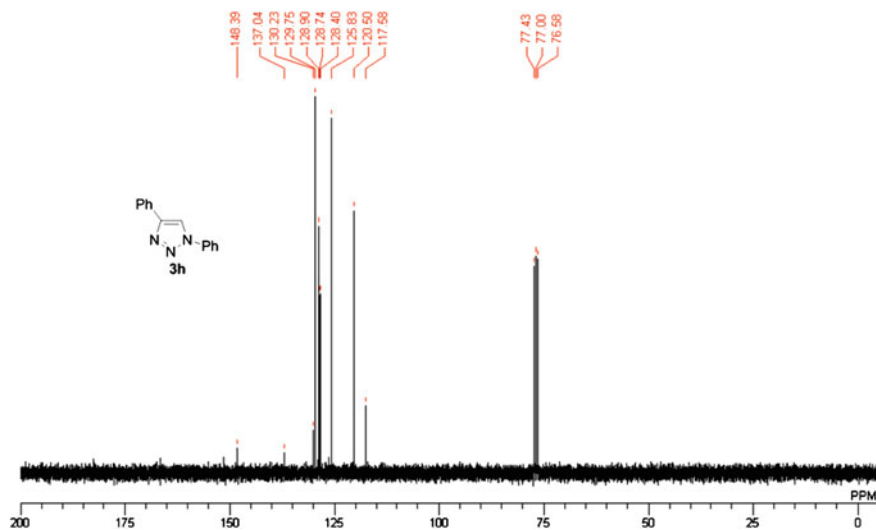


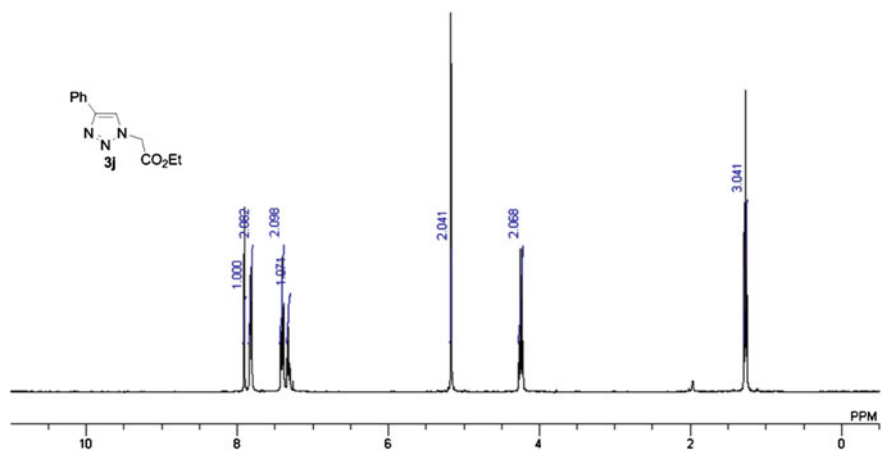
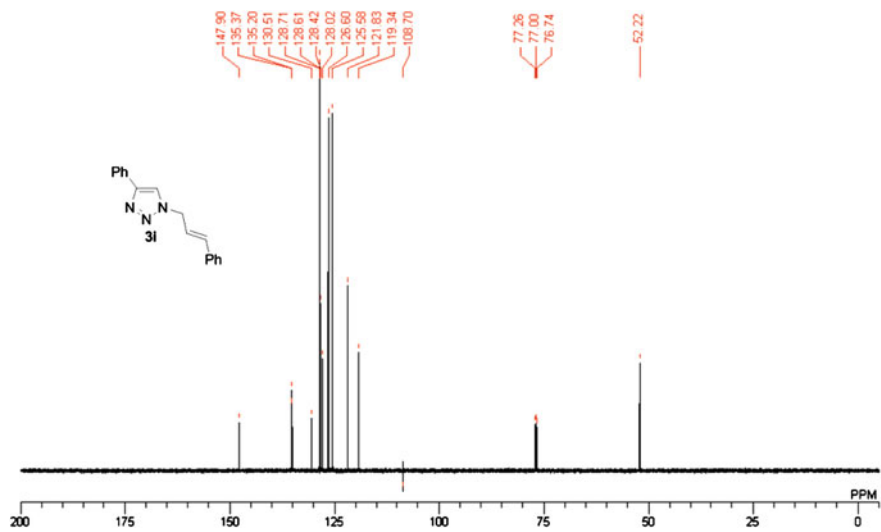




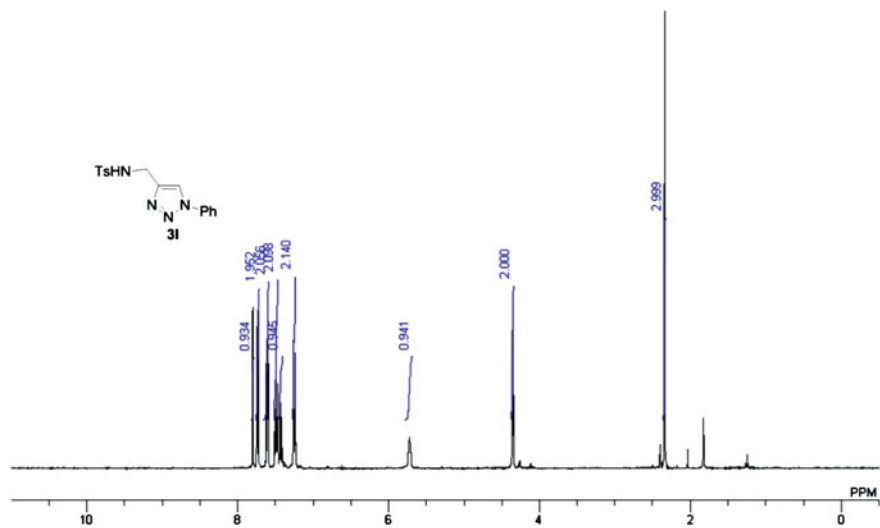
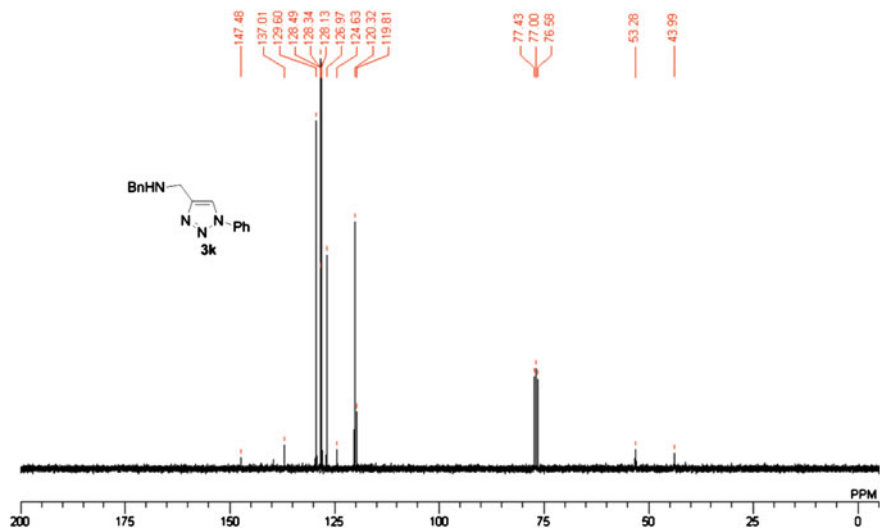


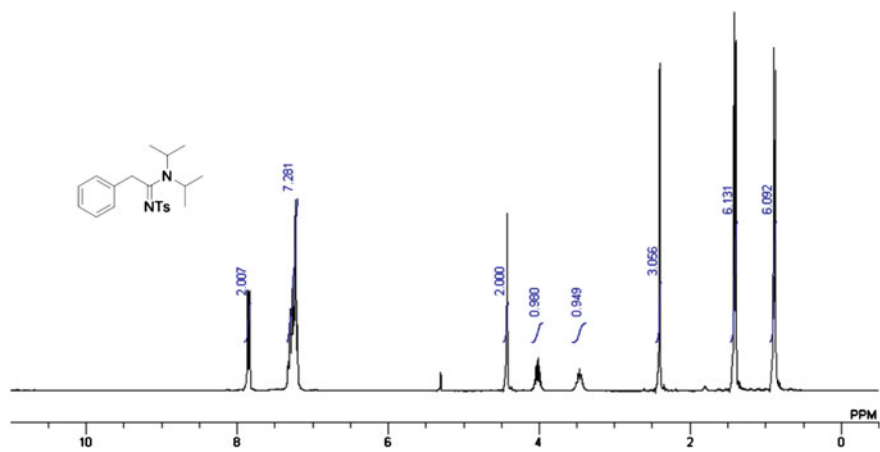
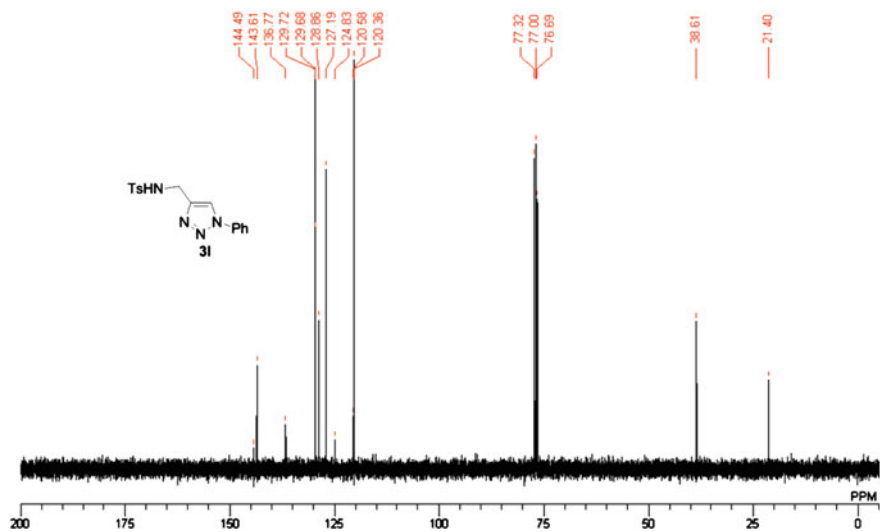


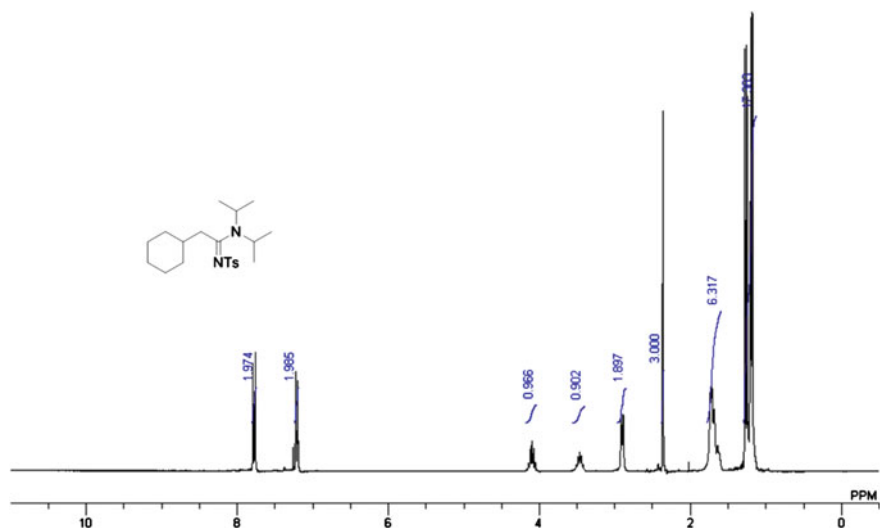
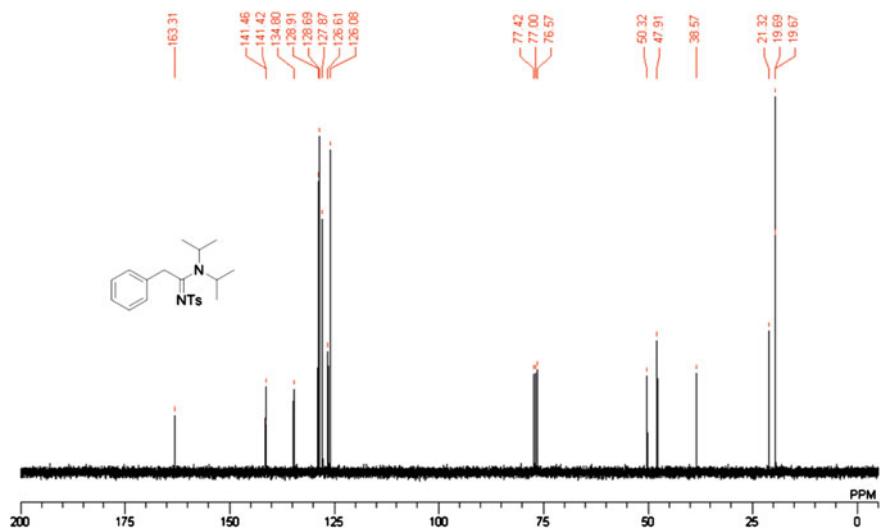


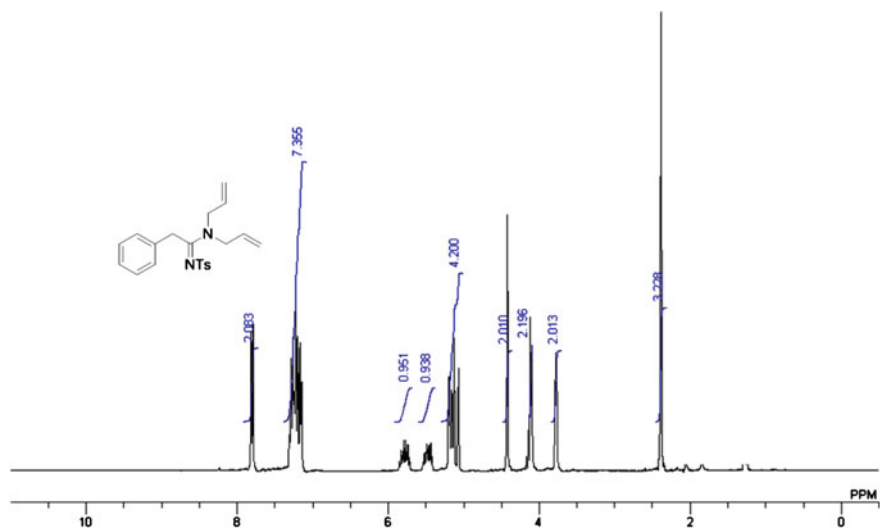
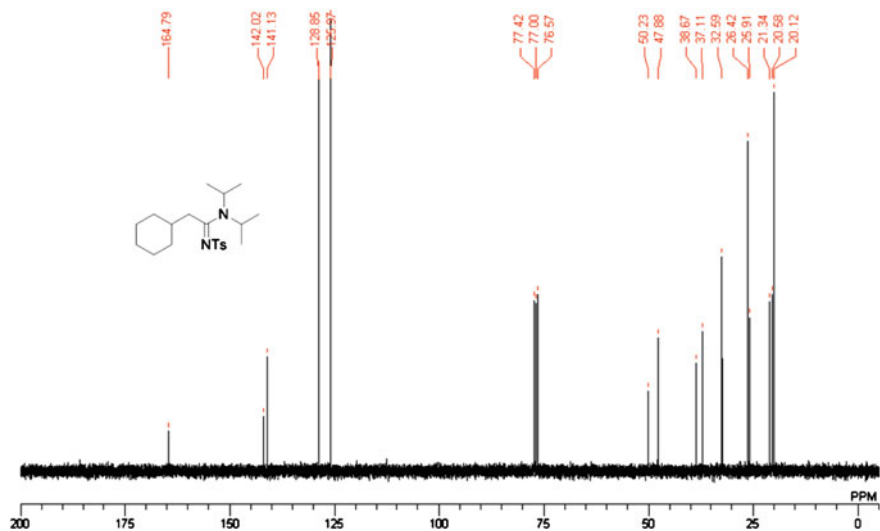


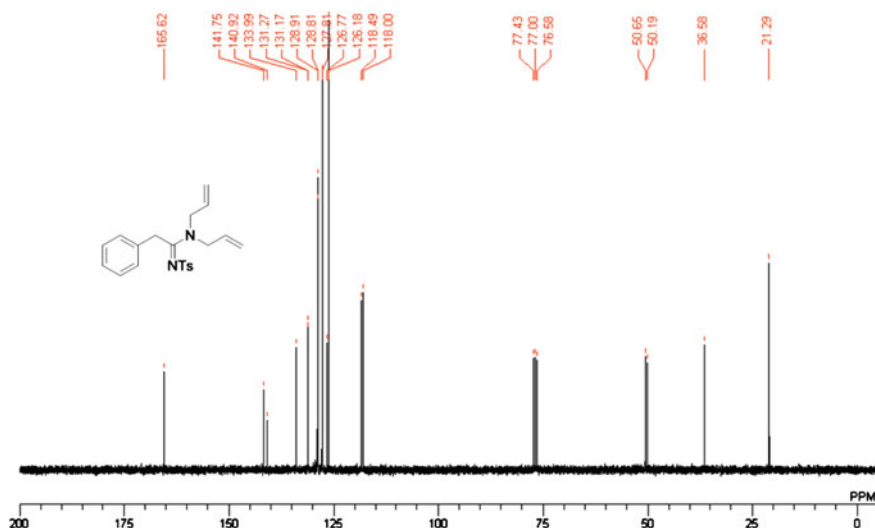












## References

- Zielasek V, Jürgens B, Schulz C et al (2006) Gold catalysts: nanoporous gold foams. *Angew Chem Int Ed* 45:8241–8244
- Xu C, Su J, Xu X et al (2007) Low temperature CO oxidation over unsupported nanoporous gold. *J Am Chem Soc* 129:42–43
- Xu C, Xu X, Su J et al (2007) Research on unsupported nanoporous gold catalyst for CO oxidation. *J Catal* 252:243–248
- Wittstock A, Neumann B, Schaefer A et al (2009) Nanoporous Au: an unsupported pure gold catalyst? *J Phys Chem C* 113:5593–5600
- Yin H, Zhou C, Xu C et al (2008) Aerobic oxidation of d-Glucose on support-free nanoporous gold. *J Phys Chem C* 112:9673–9678
- Wittstock A, Zielasek V, Biener J et al (2010) Nanoporous gold catalysts for selective gas-phase oxidative coupling of methanol at low temperature. *Science* 327:319–322
- Zhang J, Liu P, Ma H et al (2007) Nanostructured porous gold for methanol electro-oxidation. *J Phys Chem C* 111:10382–10388
- Yu C, Jia F, Ai Z et al (2007) Direct oxidation of methanol on self-supported nanoporous gold film electrodes with high catalytic activity and stability. *Chem Mater* 19:6065–6067
- Zeis R, Lei T, Sieradzki K et al (2008) Catalytic reduction of oxygen and hydrogen peroxide by nanoporous gold. *J Catal* 253:132–138
- Biener J, Nyce GW, Hodge AM et al (2008) Nanoporous plasmonic metamaterials. *Adv Mater* 20:1211–1217
- Bonroy K, Friedt JM, Frederix F et al (2004) A comparative plasmonic study of nanoporous and evaporated gold films. *Anal Chem* 76:4299–4306
- Hieda M, Garcia R, Dixon M et al (2004) Ultrasensitive quartz crystal microbalance with porous gold electrodes. *Appl Phys Lett* 84:628–630
- Kramer D, Viswanath RN, Wiessmueller J et al (2004) Surface-stress induced macroscopic bending of nanoporous gold cantilevers. *Nano Lett* 4:793–796
- Biener J, Wittstock A, Zepeda-Ruiz LA et al (2009) Surface-chemistry-driven actuation in nanoporous gold. *Nat Mater* 8:47–51

15. Asao N, Ishikawa Y, Hatakeyama N et al (2010) Nanostructured materials as catalysts: nanoporous-gold-catalyzed oxidation of organosilanes with water. *Angew Chem Int Ed* 49:10093–10095
16. Anaka S, Kaneko T, Asao N et al (2011) A nanostructured skeleton catalyst: Suzuki-coupling with a reusable and sustainable nanoporous metallic glass Pd-catalyst. *Chem Commun* 47:5985–5987
17. Rostovtsev VV, Green LG, Fokin VV et al (2002) Stepwise Huisgen cycloaddition process: copper(I)-catalyzed regioselective “Ligation” of azides and terminal alkynes. *Angew Chem Int Ed* 41:2596–2599
18. Tornøe CW, Christensen C, Meldal M (2002) Peptidotriazoles on solid phase: [1,2,3]-triazoles by regiospecific copper(I)-catalyzed 1,3-dipolar cycloadditions of terminal alkynes to azides. *J Org Chem* 67:3057–3062
19. Tron GC, Pirali T, Billington RA et al (2008) Regioselective intramolecular dipolar cycloaddition of azides and unsymmetrical alkynes. *Med Res Rev* 28:278–308
20. Melda M, Tornøe CW (2008) Cu-catalyzed azide-alkyne cycloaddition. *Chem Rev* 108:2952–3015
21. Amblard F, Cho JH, Schinazi RF (2009) Cu(I)-catalyzed Huisgen azide–alkyne 1,3-dipolar cycloaddition reaction in nucleoside, nucleotide, and oligonucleotide chemistry. *Chem Rev* 109:4207–4220
22. Pachon LD, van Maarseveen JH, Rothenberg G (2005) Click chemistry: copper clusters catalyze the cycloaddition of azides with terminal alkynes. *Adv Synth Catal* 347:811–815
23. Molteni G, Bianchi CL, Marinoni G et al (2006) Cu/Cu-oxide nanoparticles as catalyst in the “click” azide–alkyne cycloaddition. *New J Chem* 30:1137–1139
24. Lipshutz BH, Taft BR (2006) Terogeneous copper-in-charcoal-catalyzed click chemistry. *Angew Chem Int Ed* 45:8235–8238
25. Chassaing S, Kumarraja M, Sani Souna Sido A et al (2007) Click chemistry in CuI-zeolites: the Huisgen [3 + 2]-cycloaddition. *Org Lett* 9:883–886
26. Chassaing S, Sani Souna Sido A, Alix A et al (2008) “Click chemistry” in zeolites: copper(I) zeolites as new heterogeneous and ligand-free catalysts for the Huisgen [3+2] cycloaddition. *Chem Eur J* 14:6713–6721
27. Alix A, Chassaing S, Pale P et al (2008) ‘Click chemistry’ in CuI-zeolites: a convenient access to glycoconjugates. *Tetrahedron* 64:8922–8929
28. Miao T, Wang L (2008) Regioselective synthesis of 1,2,3-triazoles by use of a silica-supported copper(I) catalyst. *Synthesis* 2008:363–368
29. Sharghi H, Khalifeh R, Mahdi Doroodmand M (2009) Copper nanoparticles on charcoal for multicomponent catalytic synthesis of 1,2,3-triazole derivatives from benzyl halides or alkyl halides, terminal alkynes and sodium azide in water as a “green” solvent. *Adv Synth Catal* 351:207–218
30. Lee BS, Yi M, Chu SY et al (2010) Copper nitride nanoparticles supported on a superparamagnetic mesoporous microsphere for toxic-free click chemistry. *Chem Commun* 46:3935–3937
31. Himoto F, Lovell T, Hilgraf R et al (2005) Copper(I)-catalyzed synthesis of azoles. DFT study predicts unprecedented reactivity and intermediates. *J Am Chem Soc* 127:210–216
32. Hayes JR, Hodge AM, Biener J et al (2006) Monolithic nanoporous copper by dealloying Mn–Cu. *J Mater Res* 21:2611–2616
33. Qi Z, Zhao C, Wang X et al (2009) Formation and characterization of monolithic nanoporous copper by chemical dealloying of Al–Cu alloys. *J Phys Chem C* 113:6694–6698
34. Zhao C, Qi Z, Wang X et al (2009) Fabrication and characterization of monolithic nanoporous copper through chemical dealloying of Mg–Cu alloys. *Corros Sci* 51:2120–2125
35. Zhang Z, Wang Y, Qi Z et al (2009) Generalized fabrication of nanoporous metals (Au, Pd, Pt, Ag, and Cu) through chemical dealloying. *J Phys Chem C* 113:12629–12636
36. Chen LY, Yu JS, Fujita T et al (2009) Nanoporous copper with tunable nanoporosity for SERS applications. *Adv Funct Mater* 19:1221–1226

37. Mellor JR, Coville NJ, Sofianos AC et al (1997) Raney copper catalysts for the water-gas shift reaction: I. preparation, activity and stability. *Appl Catal A* 164:171–183
38. Mellor JR, Coville NJ, Durbach SH et al (1998) Acid leached Raney copper catalysts for the water-gas shift reaction. *Appl Catal A* 171:273–281
39. Liu WB, Zhao S, Li N et al (2010) Microstructure evolution of monolithic nanoporous copper from dual-phase Al 35 atom % Cu alloy. *J Electrochem Soc* 157:D666–D670
40. Liu WB, Zhang SC, Li N et al (2011) Influence of phase constituent and proportion in initial Al–Cu alloys on formation of monolithic nanoporous copper through chemical dealloying in an alkaline solution. *Corros Sci* 53:809–814
41. Bae I, Han H, Chang S (2005) Highly efficient one-pot synthesis of N-sulfonylamidines by Cu-catalyzed three-component coupling of sulfonyl azide, alkyne, and amine. *J Am Chem Soc* 127:2038–2039
42. Moulder JF, Stickle WF, Sobol PE et al (1995) Handbook of X ray photoelectron spectroscopy: a reference book of standard spectra for identification and interpretation of XPS data. Physical Electronics, Minnesota
43. Ahlquist M, Fokin VV (2007) Enhanced reactivity of dinuclear copper(I) acetylides in dipolar cycloadditions. *Organometallics* 26:4389–4391
44. Hein JE, Fokin VV (2010) Copper-catalyzed azide–alkyne cycloaddition (CuAAC) and beyond: new reactivity of copper(I) acetylides. *Chem Soc Rev* 39:1302–1315
45. Straub BF (2007) m-Acetylide and m-alkenylidene ligands in “click” triazole syntheses. *Chem Commun* 3868–3870
46. Zhou Y, Lecourt T, Micouin L (2010) Direct synthesis of 1,4-disubstituted-5-alumino-1,2,3-triazoles: copper-catalyzed cycloaddition of organic azides and mixed aluminum acetylides. *Angew Chem Int Ed* 49:2607–2610
47. Wang D, Li N, Zhao M et al (2010) Solvent-free synthesis of 1,4-disubstituted 1,2,3-triazoles using a low amount of Cu(PPh<sub>3</sub>)<sub>2</sub>NO<sub>3</sub> complex. *Green Chem* 12:2120–2123
48. Fletcher JT, Keeney ME, Walz SE (2010) 1-allyl- and 1-benzyl-3-methyl-1,2,3-triazolium salts via tandem click transformations. *Synthesis* 19:3339–3345
49. Alonso F, Moglie Y, Radivoy G (2010) Unsupported copper nanoparticles in the 1,3-dipolar cycloaddition of terminal alkynes and azides. *Eur J Org Chem* 10:1875–1884
50. Kamijo S, Jin T, Huo Z et al (2004) Highly N<sub>2</sub>-selective palladium-catalyzed arylation of 1,2,3-triazoles. *J Org Chem* 69:2386–2393
51. Qian LH, Yan XQ, Fujita T et al (2007) Surface enhanced Raman scattering of nanoporous gold: smaller pore sizes stronger enhancements. *Appl Phys Lett* 90:153120–153123
52. Mohanty A, Garg N, Jin R (2010) A universal approach to the synthesis of noble metal nanodendrites and their catalytic properties. *Angew Chem Int Ed* 49:4962–4966

## Chapter 3

# Nanoporous Gold Catalyst for Highly Selective Semihydrogenation of Alkynes: Remarkable Effect of Amine Additives

**Abstract** The unsupported nanoporous gold catalyst was firstly been reported for catalyzing the highly selective semihydrogenation of alkynes with organosilanes and water as the hydrogen source. Under the optimized reaction conditions, the present semihydrogenation of various terminal- and internal alkynes affords the corresponding alkenes in high chemical yields and excellent Z-selectivity without any over-reduction products. The use of DMF as solvent, which generates amines in situ, or pyridine as an additive is crucial to suppress the association of hydrogen atoms on AuNPore to form H<sub>2</sub> gas, which is unable to reduce alkynes on the unsupported gold catalysts. The AuNPore catalyst can be readily recovered and reused without any loss of catalytic activity. In addition, the SEM and TEM characterization of nanoporosity show that the AuNPore catalyst has a bicontinuous 3D structure and a high density of atomic steps and kinks on ligament surfaces, which should be one of the important origins of catalytic activity.

**Keywords** Nanoporous gold catalyst · Semihydrogenation of alkynes · Heterogeneous catalysis · Amine additives

### 3.1 Introduction

Catalysis using unsupported nanoporous gold (AuNPore) materials has attracted increasing attentions due to their fascinating green and sustainable catalytic properties [1–12]. The monolithic AuNPore can be fabricated by selective leaching of Ag from Au-Ag alloy [13, 14]. The outstanding merits of AuNPore, such as three-dimensional (3D) bicontinuous open pore network structure, high surface-to-volume ratio in comparison with bulk metals, distinguished electronic property, nontoxic nature, high recyclability and rather simple recovery, endow it to be an attractive candidate for upcoming heterogeneous catalyst. Moreover, in contrast to the supported gold nanoparticles (AuNPs) [15–19], thus, it is not surprising that the AuNPore free of supports should be an ideal catalyst system to

understand the intrinsic catalytic mechanism more easily and to extend the catalytic application widely by elimination of the support-effect problems and relaxation of aggregation [20].

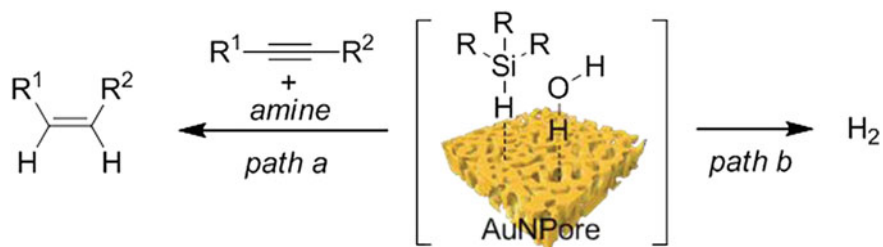
Recent advances on catalytic reactions using AuNPore catalyst, such as gas-phase CO oxidation and MeOH oxidation, liquid-phase oxidation of alcohols and glucose, as well as electrochemical oxidation of MeOH, demonstrated its excellent activity for selective oxidation reactions [1–12]. However, AuNPore catalyst has not been used for selective hydrogenation so far because of the limited ability of H<sub>2</sub> dissociation on gold as compared to its counterpart of the Pd-group metals [21, 22]. The HD formation studies using the TiO<sub>2</sub> supported AuNPs indicated that the small size of AuNPs and the gold/metal oxide interface play an important role for H<sub>2</sub> dissociation [23]; thus, it is not surprising that the hydrogenation reaction using the unsupported AuNPore as a catalyst is still unsuccessful.

Although some efficient homogenous catalytic systems are known for the semihydrogenation of alkynes [24–27], the development of a highly active and selective heterogeneous catalyst for these reactions would be very desirable from the viewpoint of organic synthesis and industrial interest. Heterogeneous catalysis based on Pd and Ni metals has been studied extensively to reduce alkynes to *Z*-alkenes with H<sub>2</sub> but suffer from *E/Z* isomerization and over-reduction of alkenes [28–37]. It was reported that the supported AuNPs catalysts are unique in the gas-phase hydrogenation of alkynes with H<sub>2</sub>, producing the corresponding alkenes with almost perfect selectivity due to the stronger adsorption of the alkynes as compared to the alkenes, but the activity was poor than PdNPs [38–42]. Most recently, our group reported that AuNPore was an effective catalyst for oxidation of organosilanes with water without any additives, producing organic silanols in high yields along with the vigorous liberation of H<sub>2</sub> gas (Scheme 3.1, path b) [43]. In the continuation of our interest in the development of new catalyst properties of nanoporous metals [7, 43–49], in this chapter, we report for the first time the highly selective semihydrogenation of alkynes catalyzed by the unsupported nanoporous gold using amines as an additive and organosilanes with water as a hydrogen source, affording the corresponding alkenes in excellent *Z*-selectivity without any over-reduced alkanes (Scheme 3.1, path a).

## 3.2 Results and Discussion

### 3.2.1 Nanoporosity Characterization of AuNPore

The unsupported AuNPore catalyst was prepared by dealloying of a homogeneous Au<sub>30</sub>Ag<sub>70</sub> alloy with thickness of 40 μm in 70 wt % of nitric acid as an electrolyte at room temperature for 18 h [43]. The scanning electron microscopy (SEM) image in Fig. 3.1a shows that ligaments and nanopore channels are formed uniformly across the entire AuNPore, and the average ligament size is around 30 nm.



**Scheme 3.1** AuNPore-catalyzed selective semihydrogenation of alkynes using hydrosilanes and  $\text{H}_2\text{O}$  as  $\text{H}_2$  source

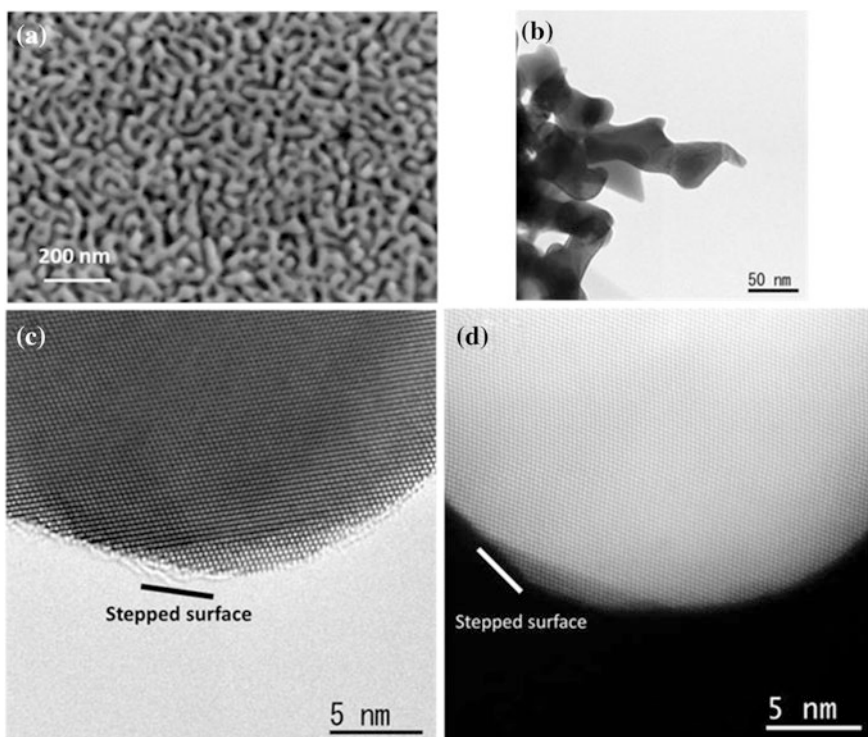


**Fig. 3.1** **a** SEM image of AuNPore, **b** representative bright-field TEM image, **c** HRTEM image with stepped surface, and **d** HAADF-STEM image with stepped surface

Energy dispersive X-ray (EDX) study shows that only elements of Au and Ag are observed in the spectra and the residual Ag composition in AuNPore is only 2 % (Fig. 3.2a). Figure 3.1b shows the representative bright-field transmission electron microscopy (TEM) image of AuNPore, which clearly reveals the multiple layers of gold ligaments with convex and concave columnar curvatures, indicating that the nanoporous structure is a bicontinuous 3D network. Moreover, the ligament size is

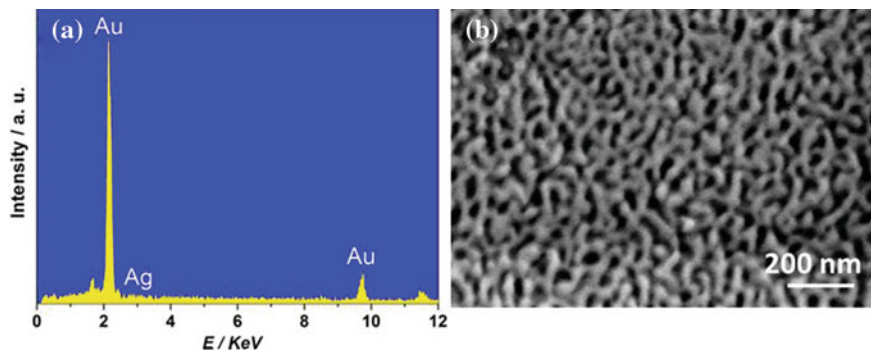
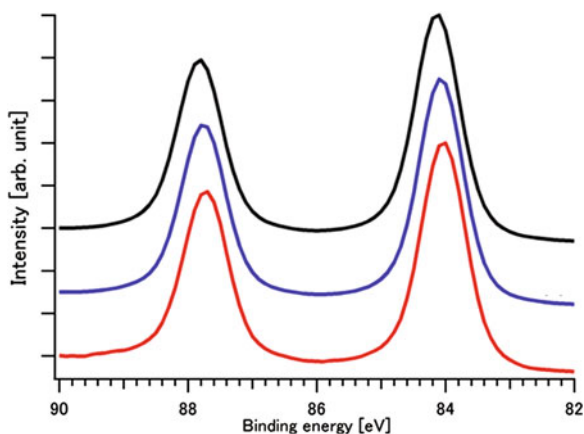


**Fig. 3.2** a EDX spectra of fresh AuNPore, Au<sub>98</sub>Ag<sub>2</sub>. b SEM image of after reaction

**Fig. 3.3** Normalized XPS spectra of a Au mica (*red*), b fresh AuNPore (*blue*), and c AuNPore treated with pyridine (*black*, see the control experiments section)



determined to be about 30 nm, which is consistent with the values estimated from the SEM image. Characterization of a convex region of ligament with high-resolution TEM (HRTEM) and scanning TEM (STEM) mode with high-angle annular dark-field (HAADF) detector shows a very high density of atomic steps and kinks at curved surfaces (Fig. 3.1c and d), implying the presence of a high concentration of low-coordination surface atoms. As the most recent observations on CO oxidation with AuNPore catalyst analyzed by in situ environmental HRTEM clearly indicated that the high density of low-coordination atoms on surface are the catalytically active sites [20], we predict that the obvious surface defects of AuNPore might be one of the most important origins of the catalytic activity in the present hydrogenation [50–52].

To gain more insight into the origin of catalytic property, the chemical state of AuNPore was measured by X-ray photoelectron spectroscopy (XPS). Analysis of AuNPore shows that AuNPore is composed of Au and Ag, while Au is predominant component. The difference of binding energy of Au 4f 7/2 between AuNPore (84.1 eV) and Au mica (84.0 eV) is very small, from which it can be concluded

**Table 3.1** AuNPore-catalyzed oxidation of organosilanes with water
$$R_{(4-n)}SiH_n + H_2O \xrightarrow[\text{acetone, room temp}]{\text{AuNPore (1~5 mol\%)}} R_{(4-n)}Si(OH)_n + nH_2$$

Entry	$R_{(4-n)}SiH_n$	AuNPore, mol%	t, h	$R_{(4-n)}Si(OH)_n$ yield, % <sup>a</sup>
1	Et <sub>3</sub> SiH	1	2	94
2	Bu <sub>3</sub> SiH	3	3	95
3	(i-Pr) <sub>3</sub> SiH	3	5	88
4	PhMe <sub>2</sub> SiH	1	1	100
5	Ph <sub>3</sub> SiH	1	5	99
6	Ph <sub>2</sub> SiH <sub>2</sub>	1	9	90
7	PhSiH <sub>3</sub>	5	6	80

*Reaction conditions* Organosilanes (1 mmol), H<sub>2</sub>O (0.1 mL), and AuNPore (1 ~ 5 mol%) in 1.5 mL acetone at room temperature

<sup>a</sup> Isolated yield

that the electronic states of AuNPore and Au mica are nearly the same (Fig. 3.3a vs. b). This suggests that AuNPore is metallic gold(0) that is playing as the catalytic species in the present reaction.

### 3.2.2 AuNPore-Catalyzed Oxidation of Organosilanes with Water

As aforementioned, recently, we observed that AuNPore has a remarkable catalytic activity in the oxidation of organosilanes with water, forming the corresponding silanols together with the evolution of hydrogen gas [43]. The reaction proceeds efficiently at room temperature without any formation of disiloxanes, and a wide range of organosilanes are compatible with the mild reaction systems. For examples, as shown in Table 3.1, not only aromatic silanes but also sterically less-hindered and hindered trialkylsilanes were oxidized effectively. The AuNPore catalyst was also applicable to the oxidations of tri-, di-, and mono-phenylsilanes, and the corresponding oxygenated products were obtained in high yields, respectively.

Taking the mechanism into consideration, we assumed that H<sub>2</sub> gas should be produced through the association of the in situ generated hydrogen atoms on AuNPore (Scheme 3.1, path b). If this is the case, we can imagine that the catalytic hydrogenation of the unsaturated multiple bonds such as alkynes by the hydrogen atoms on AuNPore should be achieved through the suppression of the quick association of these hydrogen atoms (Scheme 3.1, path a).

**Table 3.2** Screening of the reaction conditions using DMF as solvent catalyst (2 mol%)

Entry	Catalyst	R <sub>3</sub> SiH	2a yield/% <sup>a</sup>
1	AuNPore	H <sub>2</sub> (1 atm) <sup>b</sup>	0
2	AuNPore	PhMe <sub>2</sub> SiH	96 (96, <sup>c</sup> 98 <sup>d</sup> )
3	AuNPore	HMe <sub>2</sub> SiOSiMe <sub>2</sub> H	85
4	AuNPore	Et <sub>3</sub> SiH	79
5	AuNPore	(n-Bu) <sub>3</sub> SiH	47
6	AuNPore	(i-Pr) <sub>3</sub> SiH	9
7	AuCl	PhMe <sub>2</sub> SiH	18
8	Au <sub>30</sub> Ag <sub>70</sub> alloy	PhMe <sub>2</sub> SiH	0
9	none	PhMe <sub>2</sub> SiH	0
10 <sup>e</sup>	PdNPore	PhMe <sub>2</sub> SiH	54
11 <sup>f</sup>	Pd/C	PhMe <sub>2</sub> SiH	20

*Conditions* To a DMF solution (0.5 mL) of AuNPore (2 mol%) were added **1a** (0.5 mmol), H<sub>2</sub>O (1 mmol) and PhMe<sub>2</sub>SiH (0.75 mmol). The resulting mixture was stirred at 35 °C for 2 h

<sup>a</sup> <sup>1</sup>H NMR yield determined using anisole as an internal standard. For the yields lower than 96 %, some amounts of **1a** remained without formation of the over-reduced alkane

<sup>b</sup> H<sub>2</sub> gas (1 atm) was used instead of PhMe<sub>2</sub>SiH

<sup>c</sup> The yield of second use

<sup>d</sup> The yield of third use

<sup>e</sup> PdNPore was prepared from PdAl alloy

<sup>f</sup> The particle size was 5 nm

### 3.2.3 Optimization of AuNPore-Catalyzed Semihydrogenation of Phenyl Acetylene with Various Organosilanes and Water Using DMF as Solvent (Method A)

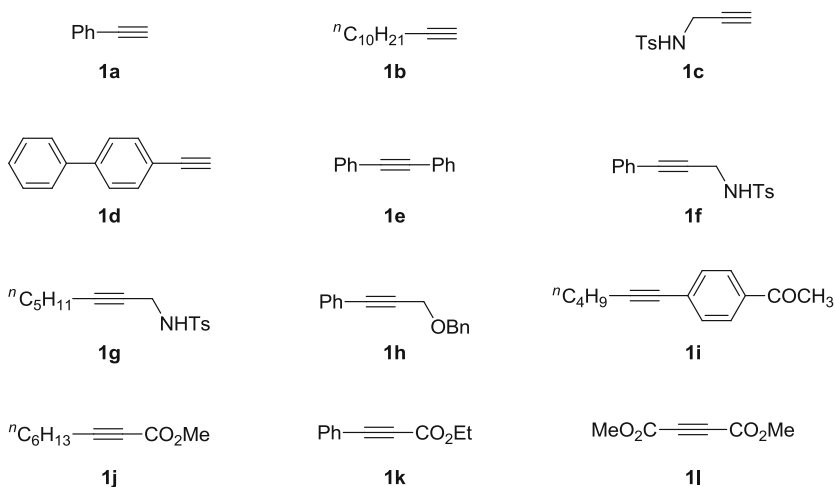
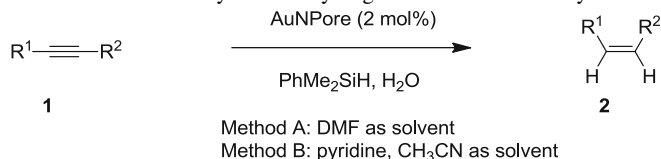
In the preliminary experiment, we found that the hydrogenation of phenylacetylene **1a** with H<sub>2</sub> in organic solvents by using AuNPore as a catalyst did not proceed at all (Table 3.2, entry 1). On the basis of the organosilane oxidation conditions and the new hypothesis, initially **1a** was treated with AuNPore catalyst, PhMe<sub>2</sub>SiH, and water in the presence of various organic solvents including acetone, CH<sub>2</sub>Cl<sub>2</sub>, THF (tetrahydrofuran), toluene, acetonitrile, and DMF (dimethylformamide). Surprisingly, only the use of DMF as solvent afforded the corresponding styrene **2a** in high yield (entry 2), and other solvents were almost ineffective, giving **2a** in less than 10 % yield. The AuNPore catalyst was recovered by simply picking the skeleton catalyst up and was reused for another two runs without any loss of catalytic activity (entry 2, in parenthesis). In addition, the SEM image in Fig. 3.2b showed that no significant changes of the nanoporous structure of AuNPore were observed after the third run. Further examination of other organosilanes using DMF as solvent showed that the steric hindrance of substituents on

silicon exhibited a significant influence on reaction efficiency; for examples, 1,1,3,3-tetramethyldisiloxane was still active, giving **2a** in 85 % yield, whereas with the use of triethylsilane, tributylsilane and triisopropylsilane, respectively, the yield of **2a** was decreased dramatically (entries 3–6). The homogeneous gold catalyst such as AuCl did not show a good catalytic activity (entry 7). It was noted that the reaction with the AuNPore precursor, Au<sub>30</sub>Ag<sub>70</sub> alloy as a catalyst, or without catalyst did not proceed (entries 8 and 9). Other catalysts such as nanoporous palladium (PdNPore) and Pd/C are also active, but the yields are much lower than that with AuNPore (entries 10 and 11).

### 3.2.4 Optimization of Amine Additives on AuNPore-Catalyzed Semihydrogenation (Method B)

The remarkable solvent effect in the present reaction led us to investigate the detailed role of DMF. During the reaction in DMF, we observed a foul odor from reaction mixture, which seems to be Me<sub>3</sub>N or Me<sub>2</sub>NH [53–55]. Consequently, *N*-methyl-*N*-phenylformamide (Ph(Me)NCHO) was used instead of DMF under method A. The <sup>1</sup>H NMR and gas chromatography (GC-MS) analysis showed the formation of a mixture of *N*-methyl-*N*-phenylamine (PhNHMe) and *N,N*-dimethyl-*N*-phenylamine (PhNMe<sub>2</sub>), which clearly indicated that amines generated in situ from DMF might play an important role in the semihydrogenation of alkynes. To gain further insight into the role of amines, we examined various amines (0.5 equiv) in the absence of DMF (Table 3.3). As expected, semihydrogenation of the dodec-1-yne **1b** with PhNHMe or PhNMe<sub>2</sub> as a base in acetonitrile at 80 °C gave the corresponding dodec-1-ene **2b** in 72 % and 57 % yields, respectively (entries 1 and 2). It seems that amines with a lower basicity exhibit a higher activity; for examples, the use of Et<sub>2</sub>NH gave a higher yield of **2b** than did Et<sub>3</sub>N (entries 3 and 4). Finally, we found that when pyridine was used, the yield of **2b** was increased up to 84 % yield together with a small amount of the recovered **1b** without formation of the over-reduced alkane (entry 5). Interestingly, we did not observe an obvious H<sub>2</sub> evolution in the presence of amines, but in the absence of amines, the reaction liberated a vigorous gas, giving **2b** in a very poor yield (entry 6), indicating the use of amines effectively suppressed the formation of H<sub>2</sub> gas, resulting in a significantly increased reaction efficiency. To investigate the influence of the amount of pyridine on reaction efficiency, further optimization was performed by changing the equivalent of pyridine. Reducing the equivalents of pyridine from 0.5 to 0.2 resulted in a lower yield of **2b** from 84 to 78 % (entries 5 and 7). Increasing the equivalent of pyridine to 1.0 afforded **2b** in 98 % yield, while the use of 1.5 equivalent of pyridine resulted in a decreased yield (entries 8 and 9). These results indicate that the use of proper amounts of pyridine efficiently suppress the association of hydrogen atoms, which are able to reduce alkyne to alkene in high yield. The catalytic loading can be reduced to 0.2 mol% without any influence on chemical yield and chemoselectivity of **2a**, while the prolonged reaction time is needed (45 h, entry 10).



**Table 3.4** AuNPore-catalyzed semihydrogenation of various alkynes

Entry	1	Method	T/°C	Time/ h	2	Conversion/ %	Yield/ % <sup>a</sup>	Z/E <sup>b</sup>
1	1a	A	35	3	2a	100	(96)	
2	1a	B	35	6	2a	100	(91) <sup>c</sup>	
3	1b	A	80	1	2b	<10	trace	
4	1b	B	80	8	2b	100	(98) <sup>d</sup>	
5	1c	A	55	8	2c	100	93	
6	1c	B	55	8	2c	100	91	
7	1d	A	55	8	2d	100	(67) <sup>e</sup>	
8	1d	B	55	8	2d	100	90	
9 <sup>f</sup>	1e	A	80	5	2e	100	(86)	100/0
10 <sup>g,h</sup>	1e	B	80	5	2e	100	85	100/0
11 <sup>f</sup>	1f	A	55	5	2f	100	96	100/0
12 <sup>f</sup>	1f	B	55	32	2f	92	(92)	100/0
13 <sup>f</sup>	1g	A	80	8	2g	100	81	100/0
14 <sup>g</sup>	1g	B	80	3	2g	40	(40)	100/0
15 <sup>f</sup>	1h	A	80	2.5	2h	78	(78)	100/0
16 <sup>g</sup>	1h	B	80	12	2h	60	(60)	100/0
17	1i	A	80	3	2i	100	(93)	100/0
18	1i	B	80	3	2i	100	98	100/0

(continued)

**Table 3.4** (continued)

Entry	1	Method	T/°C	Time/ h	2	Conversion/ %	Yield/ % <sup>a</sup>	Z/E <sup>b</sup>
19	1j	A	35	5	2j	100	95	100/0
20	1j	B	35	11	2j	100	(85)	100/0
21 <sup>g</sup>	1k	A	35	10	2k	100	90	>99/ 1
22 <sup>g</sup>	1k	B	35	15	2k	100	90	100/0
23 <sup>f</sup>	1l	B <sup>i</sup>	25	1.5	2l	100	(80)	100/0

*Conditions* AuNPore (2 mol%), alkyne (0.5 mmol), PhMe<sub>2</sub>SiH (0.75 mmol), H<sub>2</sub>O (1 mmol); method A, DMF (1 M); method B, pyridine (0.25 mmol), CH<sub>3</sub>CN (1 M)

<sup>a</sup> Isolated yield. <sup>1</sup>H NMR yield determined using CH<sub>2</sub>Br<sub>2</sub> as an internal standard is shown in parenthesis

<sup>b</sup> E/Z ratio was determined by H NMR spectroscopy

<sup>c</sup> Over-reduced product was obtained in 9 % yield

<sup>d</sup> Pyridine (0.5 mmol) was used

<sup>e</sup> Over-reduced product was obtained in 33 % yield

<sup>f</sup> PhMe<sub>2</sub>SiH (1.5 mmol) and H<sub>2</sub>O (1.75 mmol) were used

<sup>g</sup> PhMe<sub>2</sub>SiH (1.0 mmol) and H<sub>2</sub>O (1.25 mmol) were used

<sup>h</sup> Pyridine (0.35 mmol) was used

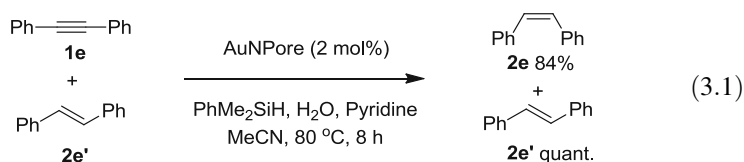
<sup>i</sup> The reaction was carried out in the absence of pyridine

To further explore the stereoselectivity, we examined several simple and functionalized internal alkynes. 1,2-Dipheylethyne (**1e**) is a suitable substrate for the present hydrogenation, providing the exclusive (*Z*)-stilbene (**2e**) in 85 % yield under the method A or B at 80 °C, which was difficult to obtain in high *Z*-selectivity in the case of Pd catalysts (entries 9 and 10) [56]. Note that 1,2-dialkyl-substituted internal alkyne such as dodec-6-yne did not participate in the present reaction conditions. During further investigation of other hydrosilanes having a strong hydride source, we found that the use of (EtO)<sub>3</sub>SiH instead of PhMe<sub>2</sub>SiH under both methods A and B gave almost quantitative yield of (*Z*)-dodec-6-ene. However, there is a problem on reproducibility of the reaction, probably due to the formation of an unknown turbid emulsion mixture during the reaction; sometimes the yield of (*Z*)-dodec-6-ene decreased dramatically. Hydrogenations of the functionalized alkynes were also tested. The reactions of *N*-tosyl-protected propargylamines bearing phenyl (**1f**) or *n*-pentyl (**1g**) substituent at the alkynyl terminus afforded the corresponding *Z*-alkenes **2f** and **2g** as a sole product in good to high yield under method A, respectively (entries 11 and 13), while the relatively lower conversion yields were observed under method B, especially for the reaction of **1g** (entries 12 and 14). Benzyl ethers are known to undergo hydrogenolysis of benzyl group in the presence of H<sub>2</sub>/Pd-C [57]. Our methods A and B show a remarkable selectivity at the alkyne moiety for reducing the benzyl-protected propargyl alcohol **1h** without cleavage of benzyl group, giving the desired *Z*-alkene **2h** in 78 % and 60 % yields, respectively (entries 15 and 16). A remarkable chemoselectivity toward semihydrogenation of the alkyne group only has been observed with the alkyne **1i** bearing a ketone functional group on

benzene ring, which produced the desired *Z*-alkene **2i** in excellent yield without reduction of carbonyl group (entries 17 and 18) [52]. It is known that the hydrogenation of  $\alpha$ ,  $\beta$ -unsaturated alkynyl esters gave the high amounts of the thermodynamically more stable *E*-alkenes in the presence of Pd catalysts [58]. Our method exhibits excellent *Z*-selectivity with hydrogenation of  $\alpha$ ,  $\beta$ -unsaturated alkynyl esters. The reaction of **1j** having *n*-hexyl group at the alkynyl terminus proceeded at 35 °C, giving the *Z*-alkene **2j** in high yield with 100 % *Z*-selectivity under method A, while a lower conversion was observed under method B (entries 19 and 20). Methyl 3-phenylpropiolate (**1k**) was also successfully hydrogenated to afford the desired *Z*-alkene **2k** in 90 % isolated yield under methods A and B (entries 21 and 22). It is noteworthy that the electron-poor alkyne dimethyl butynedioate (**1l**) is highly reactive; the reaction proceeded in the absence of pyridine under method B to afford the desired dimethyl maleate (**2l**) as a sole product in 80 % yield (entry 23), while **1l** was decomposed in the presence of pyridine in method B or under method A. For the examples with less than 90 % yield in Table 3.4, <sup>1</sup>H NMR and GC-MS of the crude reaction mixture showed no byproduct formation unless otherwise noted.

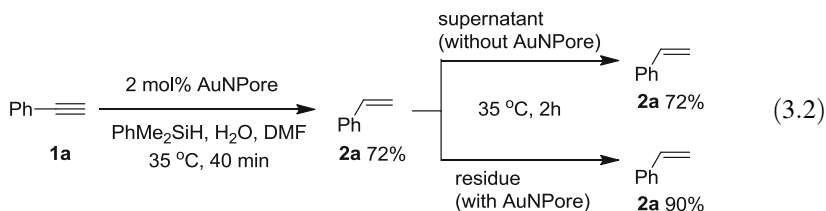
### 3.2.6 Control Experiments and Reaction Pathways

Several control experiments were conducted to understand the catalytic activity and selectivity that may support our proposed mechanism. As shown in Eq. (3.1), the reaction of a 1:1 mixture of diphenylethyne (**1e**) and *E*-stilbene under method B gave the corresponding *Z*-stilbene **2e** in 84 % yield along with the recovered *E*-stilbene in quantitative yield without any formation of over-reduced alkane. This result indicates that the AuNPore catalyst has a preferential chemoselectivity for alkynes over alkenes, which is consistent with the reported theoretical and experimental results that Au leads to the exothermic absorption for alkynes and endothermic absorption for alkenes [38, 59].

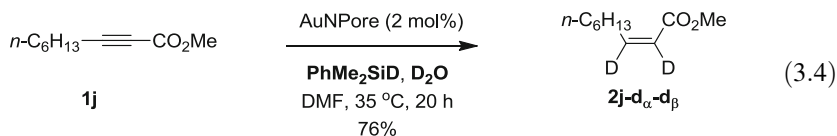
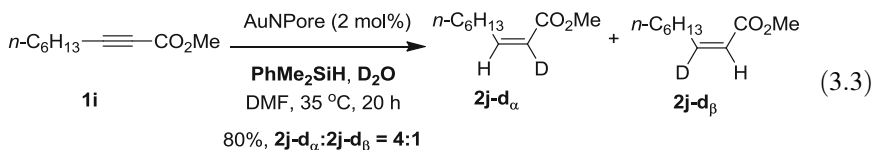


To clarify whether the AuNPore catalyst leached to the reaction mixture or not, we carried out the following leaching experiments (Eq. 3.2). Phenyl acetylene **1a** was treated with PhMe<sub>2</sub>SiH and water in the presence of AuNPore catalyst (2 mol%) in DMF at 35 °C (method A). After 40 min, a part of the supernatant was transferred to the other reaction vessel, and **2a** was produced in 72 % yield at

this time. The supernatant was continuously heated at 35 °C in the absence of the catalyst for 2 h, affording **2a** in 72 % yield. In contrast, the residual containing the AuNPore catalyst was completed in 2 h, giving **2a** in 90 % yield. These results clearly indicated that the present hydrogenation was catalyzed by the solid state of AuNPore without any leaching of gold.



To gain further insight into reaction details, we carried out the deuterium labeling experiments. The reaction of alkyne **1i** with PhMe<sub>2</sub>SiH and D<sub>2</sub>O in the presence of AuNPore catalyst in DMF gave a 4:1 mixture of the corresponding  $\alpha$ -D- and  $\beta$ -D-incorporated *Z*-alkenes **2j-d<sub>α</sub>** and **2j-d<sub>β</sub>** in 80 % yield (Eq. 3.3). The hydrogen derived from PhMe<sub>2</sub>SiH and deuterium derived from D<sub>2</sub>O are preferentially attached to the  $\beta$ - and  $\alpha$ -positions of  $\alpha$ ,  $\beta$ -unsaturated alkenyl ester to give **2j-d<sub>α</sub>** as a major product and the hydrogen and deuterium exchanged alkene **2j-d<sub>β</sub>** as a minor product. When PhMe<sub>2</sub>SiD and D<sub>2</sub>O were used, the corresponding **2j-d<sub>α</sub>-d<sub>β</sub>** having two D atoms at both  $\alpha$ - and  $\beta$ -positions was obtained in 76 % yield (Eq. 3.4). These results clearly indicate that the hydrogen atoms on *Z*-alkene moiety in product **2** were derived from PhMe<sub>2</sub>SiH and water, and the product proportion of **2j-d<sub>α</sub>** and **2j-d<sub>β</sub>** suggests the two reaction pathways; ionic and atomic hydrogenations (vide infra) [60, 61].



To investigate the interaction between pyridine and AuNPore, the pyridine-treated AuNPore was characterized using XPS analysis as shown in Fig. 3.3b versus c. The XPS of Au 4f 7/2 is slightly shifted to the higher binding energy as compared to the fresh AuNPore. However, this difference is very small, indicating

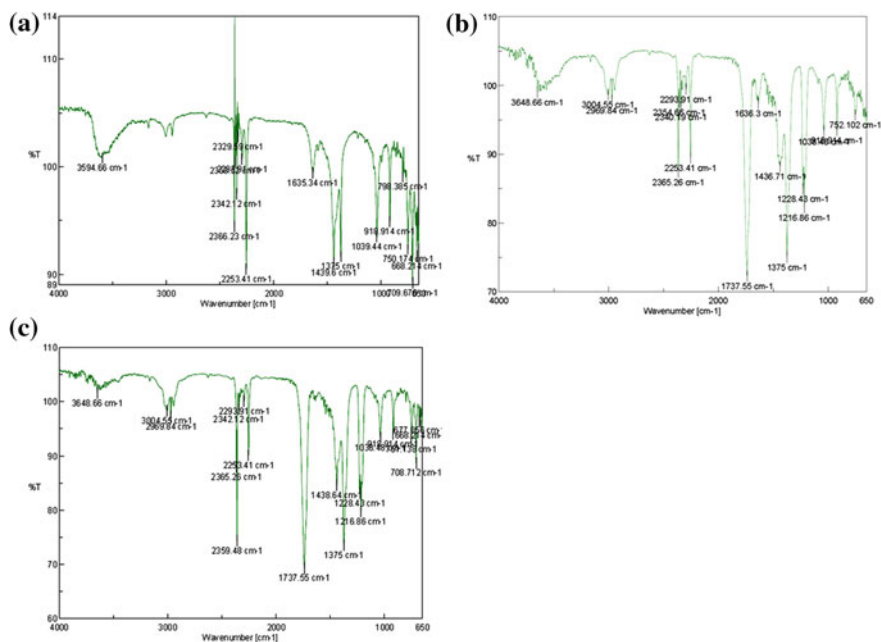
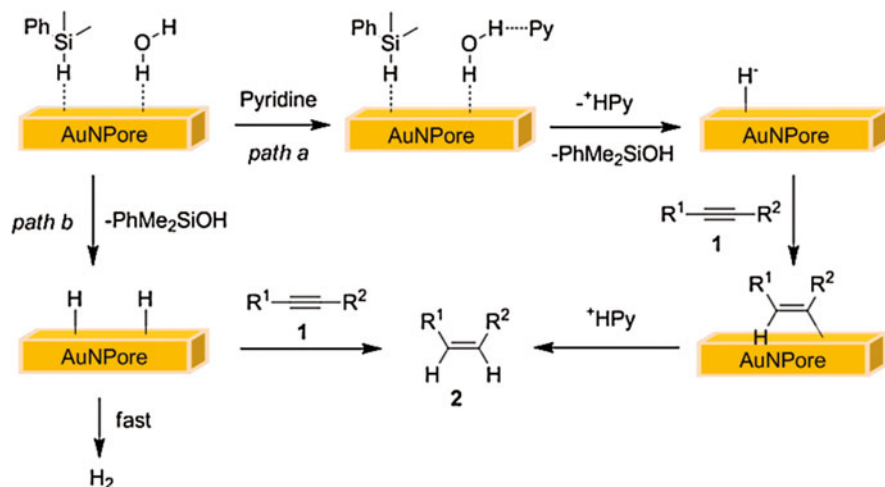


**Fig. 3.4** FTIR spectra of **a** pyridine and water in acetonitrile, **b** water in acetonitrile, **c** pyridine in acetonitrile

that the interaction between pyridine and AuNPore surface is weak. Furthermore, we found that, when pyridine was treated with water in acetonitrile solution, a strong broad band appeared at  $3594\text{ cm}^{-1}$  in the FTIR spectrum which is assigned as stretching vibration of  $\text{-OH}$  in the pyridine-water complex [62]. However, the water in acetonitrile and pyridine in acetonitrile did not show clear vibration in the same region (Fig. 3.4). These results suggest the strong interaction between pyridine and water through hydrogen bond formation.

On the basis of these experimental observations, two reaction pathways, ionic and atomic hydrogenations, are conceivable for the present catalytic semihydrogenation as shown in Scheme 3.2. Initially,  $\text{PhMe}_2\text{SiH}$  and  $\text{H}_2\text{O}$  get absorbed onto the low-coordinated Au atoms on the stepped surface of AuNPore catalyst. In path a, the hydrogen bond forms between pyridine and water followed by the reaction of hydrosilane and water to give  $[\text{AuNPore-H}]^-$  and  $[\text{HPy}]^+$  species. Next, the adsorbed alkyne reacts subsequently with  $[\text{AuNPore-H}]^-$  and  $[\text{HPy}]^+$  to form the corresponding  $Z$ -alkene. In contrast, as shown in path b, the reaction of the adsorbed hydrosilane and  $\text{H}_2\text{O}$  forms hydrogen atom on AuNPore surface. In the absence of amines, the hydrogen atom may rapidly associated together to liberate  $\text{H}_2$  gas, which inhibits the hydrogenation of alkyne to afford low yield of the desired alkene. Note that in the case of method A, the formed hydrogen atoms may reduce DMF to produce some amounts of  $\text{Me}_2\text{NH}$  or/and  $\text{Me}_3\text{N}$ , which act as



**Scheme 3.2** Reaction pathways for the AuNPore-catalyzed semihydrogenation of alkynes

amine base. We conclude that the ionic hydrogenation (path a) is the predominant pathway in the present semihydrogenation, which suppresses H<sub>2</sub> formation sufficiently in the presence of amines. In addition, the lower adsorption ability of the alkene on gold catalyst as compared to the alkyne inhibits its further hydrogenation to the alkane, leading to high chemoselectivity.

### 3.3 Conclusion

In summary, we have shown for the first time that the unsupported AuNPore catalyst is an efficient heterogeneous catalyst for the selective semihydrogenation of alkynes, whereas the unsupported gold was known to be inactive for hydrogenation so far. The labeling experiments clearly indicated that organosilanes and water were the hydrogen source. The use of DMF as a solvent that generates amines in situ, or pyridine as an additive, is required to suppress the formation of H<sub>2</sub>, leading to the efficient semihydrogenation. A wide range of terminal and internal alkynes can be reduced to the Z-alkenes in high yields with excellent chemo- and stereoselectivity. Moreover, the AuNPore catalyst is easily recoverable and can be reused several times without leaching and loss of activity. TEM characterization revealed that the AuNPore catalyst has a bicontinuous 3D structure and atomic steps and kinks on ligament surfaces with a high concentration of low-coordinated Au atoms, which should be one of the important origins of catalytic activity. Further extension of this hydrogenation method to other unsaturated multiple bonds is in progress.

## 3.4 Experimental Section

### 3.4.1 General Information

GC-MS analysis was performed on an Agilent 6890 N GC interfaced to an Agilent 5973 mass-selective detector (30 × 0.25 mm capillary column, HP-5MS). Scanning electron microscope (SEM) observation was carried out using a JEOL JSM-6500F instrument operated at an accelerating voltage of 30 kV. <sup>1</sup>H NMR and <sup>13</sup>C NMR spectra were recorded on JEOL JNM AL 400 (400 MHz) spectrometers. <sup>1</sup>H NMR spectra are reported as follows: chemical shift in ppm ( $\delta$ ) relative to the chemical shift of CDCl<sub>3</sub> at 7.26 ppm, integration, multiplicities (s = singlet, d = doublet, t = triplet, q = quartet, m = multiplet and br = broadened), and coupling constants (Hz). <sup>13</sup>C NMR spectra were recorded on JEOL JNM AL 400 (100.5 MHz) spectrometers with complete proton decoupling, and chemical shift reported in ppm ( $\delta$ ) relative to the central line of triplet for CDCl<sub>3</sub> at 77 ppm. IR spectra were recorded on JASCO FT/IR-4100 spectrometer; absorptions are reported in cm<sup>-1</sup>. High-resolution mass spectra were obtained on a BRUKER APEXIII spectrometer and JEOL JMS-700 MStation operator. Column chromatography was carried out employing silica gel 60 N (spherical, neutral, 40~100  $\mu$ m, KANTO Chemical Co.). Analytical thin-layer chromatography (TLC) was performed on 0.2 mm precoated plate Kieselgel 60 F254 (Merck).

### 3.4.2 Materials

The hydrosilanes and alkynes are commercially available, which are used as received. Au (99.99 %) and Ag (99.99 %) are purchased from Tanaka Kikinokuni Hanbai K.K. and Mitsuwa's Pure Chemicals, respectively. Alkyne **1f** was prepared following the reported literature [63, 64]. **2a** was identified by <sup>1</sup>H NMR comparing with the commercially available styrene. Structures of **2b** [65], **2c** [66], **2d** [67], **2e** [68], **2f** [69], **2h** [70], **2i** [71], **2k** [72], and **2l** [73] were determined by comparing with the reported authentic compounds. Products **2g** and **2j** were confirmed by <sup>1</sup>H, <sup>13</sup>C NMR and HRMS.

### 3.4.3 Fabrication of AuNPore Catalyst

Au (99.99 %) and Ag (99.99 %) were melted with electric arc-melting furnace under Ar atmosphere to form Au/Ag alloy (30:70, in at. %), which was rolled down to thickness of 0.04 mm. The resulting foil was annealed at 850 °C for 20 h. The foil was cut into small pieces (5 × 2 mm square). Treatment of the resulting chips (67.1 mg) with 70 wt% nitric acid (3.77 mL) for 18 h at room temperature in

a shaking apparatus resulted in the formation of the nanoporous structure by selective leaching of silver. The material was washed with a saturated aqueous solution of  $\text{NaHCO}_3$ , pure water, and acetone, successively. Drying of the material under reduced pressure gave the nanoporous gold (30.2 mg), and its composition was found to be  $\text{Au}_{98}\text{Ag}_2$  from EDX analysis.

#### ***3.4.4 Representative Procedure for the AuNPore-Catalyzed Semihydrogenation of 1j (Table 3.4, Entry 19):***

##### ***Method A***

To a DMF solution (1 M, 0.5 mL) of AuNPore (2 mol%, 2.0 mg) were added **1j** (84 mg, 0.5 mmol),  $\text{H}_2\text{O}$  (18  $\mu\text{l}$ , 1.0 mmol) and  $\text{PhMe}_2\text{SiH}$  (116  $\mu\text{l}$ , 0.75 mmol) subsequently at room temperature. The reaction mixture was stirred at 35 °C for 5 hours and was monitored by GC-MS analysis. The AuNPore catalyst was recovered by filtration, and the solution was extracted with diethyl ether and washed by water. The recovered AuNPore catalyst was washed with acetone and dried under vacuum. After concentration, the residue was purified with a silica gel chromatography to afford **2j** (81 mg, 95 %) as a yellow solid.

#### ***3.4.5 Representative Procedure for the AuNPore-Catalyzed Semihydrogenation of 1d (Table 3.4, Entry 8):***

##### ***Method B***

To a MeCN solution (1 M, 0.5 mL) of AuNPore (2 mol%, 2.0 mg) were added **1d** (89 mg, 0.5 mmol),  $\text{H}_2\text{O}$  (18  $\mu\text{l}$ , 1.0 mmol), pyridine (20  $\mu\text{l}$ , 0.25 mmol) and  $\text{PhMe}_2\text{SiH}$  (116  $\mu\text{l}$ , 0.75 mmol). The reaction mixture was stirred at 55 °C for 8 hours. The reaction was monitored by GC-MS analysis. The mixture was filtered and washed by diethyl ether. The recovered AuNPore catalyst was washed with acetone and dried under vacuum. After concentration of the filtrate, the residue was purified with silica gel chromatography, to afford **2d** (81 mg, 90 %) as a white solid.

#### ***3.4.6 Leaching Experiment***

Phenyl acetylene **1a** was treated with  $\text{PhMe}_2\text{SiH}$  and water in the presence of AuNPore catalyst (2 mol%) in DMF at 35 °C (method A). After 40 min, a part of supernatant was transferred to the other reaction vessel and **2a** was produced in 72 %  $^1\text{H}$  NMR yield at this time. The supernatant was continuously heated at 35

°C in the absence of the catalyst for 2 h, affording **2a** in 72 % <sup>1</sup>H NMR yield. In contrast, the residual containing the AuNPore catalyst was completed in 2 h, giving **2a** in 90 % <sup>1</sup>H NMR yield.

### 3.4.7 Synthesis of Starting Materials

#### 3.4.7.1 Synthesis of PhMe<sub>2</sub>SiD

To a Et<sub>2</sub>O solution (0.22 M) of LiAlD<sub>4</sub> (3 mmol) under argon atmosphere were added PhMe<sub>2</sub>SiCl (9 mmol). The reaction mixture was heated to reflux for 10 hours. Aqueous sodium hydroxide (10 ml, 10 wt %) was added to the reaction mixture, and extracted by Et<sub>2</sub>O and dried over anhydrous sodium sulfate. Filtration and evaporation of the solvent gave the crude product which was purified by silica gel column chromatography to give PhMe<sub>2</sub>SiD in 65 % yield.

#### 3.4.7.2 4-Methyl-N-(3-phenylprop-2-yn-1-yl)benzenesulfonamide (**1f**) [63, 64]

CBr<sub>4</sub> (1.2 equiv) was added in one portion to a solution of 3-phenylprop-2-yn-1-ol (1 equiv) in dry CH<sub>2</sub>Cl<sub>2</sub> (0.6 M) at 0 °C, and the reaction was stirred at 0 °C. After 10 min, a solution of Ph<sub>3</sub>P (1.5 equiv) in CH<sub>2</sub>Cl<sub>2</sub> (1.5 M) was added via cannula and stirred at 0 °C for 10 min. Then the reaction mixture was allowed to warm at rt and further stirred for 2 h. After reaction completed, the mixture was evaporated in vacuo. The residue was purified by silica gel column chromatography to give (3-bromoprop-1-yn-1-yl)benzene, 82 % yield.

To a 50 mL round-bottom flask was added 2.07 g (15 mmol) of K<sub>2</sub>CO<sub>3</sub>, TsNHBOC (*N*-(2,2-Dimethyl-propionyl)-4-methyl-benzenesulfonamide) 2.71 g (10 mmol) and DMF (12 mL). The solution was stirred at room temperature for 4 h. Then (3-bromoprop-1-yn-1-yl)benzene 1.95 g (10 mmol) was added in one portion. The reaction was monitored by TLC, after completion, Et<sub>2</sub>O (100 mL) was added. The solution was washed with 3 times of 15 mL portions of water. Then the solvent was removed at reduced pressure, leaving a yellow solid. The crude was dissolved in CH<sub>2</sub>Cl<sub>2</sub> (8 mL), then CF<sub>3</sub>COOH (3 mL) was added. The solution was stirred for overnight. The solvent was evaporated and the residue was purified by silica gel column chromatography to give 4-methyl-*N*-(3-phenylprop-2-yn-1-yl) benzenesulfonamide (**1f**) 2.6 g, 90 % yield.

#### 3.4.7.3 4-Methyl-N-(oct-2-yn-1-yl)benzenesulfonamide (**1g**)

4-Methyl-*N*-(oct-2-yn-1-yl)benzenesulfonamide (**1g**) was prepared according to the method of **1h** from 2.0 g (10 mmol) of 1-bromo-oct-2-yne. Yield: 2.0 g (71 %) of **1g** after purification of the crude product by silica gel column chromatography.

### 3.4.7.4 1-(4-(Hex-1-yn-1-yl)phenyl)ethanone (**1i**)

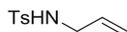
A mixture of 1-(4-bromophenyl)ethanone (995 mg, 10 mmol), Pd(PPh<sub>3</sub>)<sub>2</sub>Cl<sub>2</sub> (140 mg, 0.2 mmol), CuI (19 mg, 0.1 mmol) and hex-1-yne (2.5 g, 30 mmol) in triethylamine (40 mL) was heated to reflux for 4 h. After then, the mixture was cooled to room temperature. Filtration through celite and evaporation of the solvent gave the crude product which was purified by silica gel column chromatography to give 1-(4-(hex-1-yn-1-yl)phenyl) ethanone (**1i**) 1.7 g, 85 % yield.

## 3.4.8 Analytical Data of (1 and 2)

### 3.4.8.1 PhMe<sub>2</sub>SiD

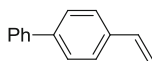
Colorless liquid; <sup>1</sup>H NMR (400 MHz, CDCl<sub>3</sub>) δ 7.26–7.54 (m, 2H), 7.38–7.36 (m, 3H), 0.35 (s, 6H); <sup>13</sup>C NMR (100 MHz, CDCl<sub>3</sub>) δ 137.3, 133.9, 129.1, 127.8, -3.8

### 3.4.8.2 *N*-Allyl-4-methylbenzenesulfonamide (**2c**)

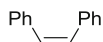


White solid; <sup>1</sup>H NMR (400 MHz, CDCl<sub>3</sub>) δ 7.71 (d, *J* = 8.0 Hz, 2H), 7.25 (d, *J* = 8.0 Hz, 2H), 5.70–5.62 (m, 1H), 5.13–4.96 (m, 3H), 3.53–3.49 (m, 2H), 2.37 (s, 3H); <sup>13</sup>C NMR (100 MHz, CDCl<sub>3</sub>) δ 143.2, 136.7, 132.7, 129.5, 126.9, 117.4, 45.6, 21.4; HRMS (ESI positive) calcd for C<sub>10</sub>H<sub>13</sub>NO<sub>2</sub>S [M + Na]<sup>+</sup>: 234.0559, found: 234.0559.

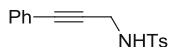
### 3.4.8.3 4-Phenylstyrene (**2d**)



White solid; <sup>1</sup>H NMR (400 MHz, CDCl<sub>3</sub>) δ 7.67–7.62 (m, 4H), 7.55–7.47 (m, 4H), 7.42–7.38 (m, 1H), 6.82 (dd, *J* = 17.6 Hz, 11.2 Hz, 1H), 5.86 (d, *J* = 17.6 Hz, 1H), 5.34 (d, *J* = 11.2 Hz, 1H); <sup>13</sup>C NMR (100 MHz, CDCl<sub>3</sub>) δ 140.5, 140.4, 136.4, 136.2, 128.6, 127.2, 127.1, 126.8, 126.5, 113.8; HRMS (APCI positive) calcd for C<sub>14</sub>H<sub>12</sub> [M + H]<sup>+</sup>: 181.1012, found: 181.1011.

**3.4.8.4 (Z)-1,2-Diphenylethene (2e)**

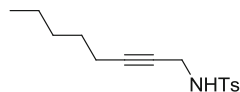
Colorless liquid;  $^1\text{H NMR}$  (400 MHz,  $\text{CDCl}_3$ )  $\delta$  7.28–7.18 (m, 10H), 6.61 (s, 2H);  $^{13}\text{C NMR}$  (100 MHz,  $\text{CDCl}_3$ )  $\delta$  137.1, 130.1, 128.7, 128.1, 126.9

**3.4.8.5 4-Methyl-N-(3-phenylprop-2-yn-1-yl)benzenesulfonamide (1f)**

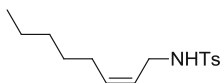
Light yellow solid;  $^1\text{H NMR}$  (400 MHz,  $\text{CDCl}_3$ )  $\delta$  7.82 (d,  $J = 7.2$  Hz, 2H), 7.29–7.12 (m, 5H), 7.11 (d,  $J = 8.4$  Hz, 2H), 5.02 (t,  $J = 6.0$  Hz, 1H), 4.06 (d,  $J = 6.0$  Hz, 2H), 2.33 (s, 3H);  $^{13}\text{C NMR}$  (100 MHz,  $\text{CDCl}_3$ )  $\delta$  143.5, 136.7, 131.4, 129.5, 128.3, 127.9, 127.3, 121.9, 84.5, 83.2, 33.7, 21.4.

**3.4.8.6 (Z)-4-Methyl-N-(3-phenylallyl)benzenesulfonamide (2f)**

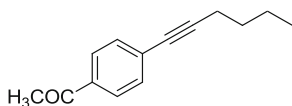
Colorless viscous liquid;  $^1\text{H NMR}$  (400 MHz,  $\text{CDCl}_3$ )  $\delta$  7.71 (d,  $J = 8.0$  Hz, 2H), 7.28–7.24 (m, 5H), 7.08 (d,  $J = 8.0$  Hz, 2H), 6.51 (d,  $J = 11.6$  Hz, 1H), 5.58–5.52 (m, 1H), 4.63 (bs, 1H), 3.84 (dd,  $J = 7.2, 6.4$  Hz, 2H), 2.42 (s, 3H);  $^{13}\text{C NMR}$  (100 MHz,  $\text{CDCl}_3$ )  $\delta$  143.4, 136.6, 135.6, 132.5, 129.6, 128.4, 128.2, 127.3, 127.0, 126.3, 41.3, 21.5; HRMS (ESI positive) calcd for  $\text{C}_{16}\text{H}_{17}\text{NO}_2\text{S}$  [ $\text{M} + \text{Na}$ ] $^+$ : 310.0872, found: 310.0872.

**3.4.8.7 4-Methyl-N-(oct-2-yn-1-yl)benzenesulfonamide (1g)**

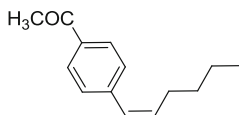
Yellow liquid;  $^1\text{H NMR}$  (400 MHz,  $\text{CDCl}_3$ )  $\delta$  7.73 (d,  $J = 8.0$  Hz, 2H), 7.25 (d,  $J = 8.0$  Hz, 2H), 4.96 (s, 1H), 3.75 (d,  $J = 6.0$  Hz, 2H), 2.37 (s, 3H), 1.87 (t,  $J = 6.8$  Hz, 2H), 1.25–1.14 (m, 6H), 0.81 (t,  $J = 6.8$  Hz, 3H);  $^{13}\text{C NMR}$  (100 MHz,  $\text{CDCl}_3$ )  $\delta$  143.2, 136.7, 129.3, 127.2, 85.3, 73.9, 33.3, 30.8, 27.9, 22.0, 21.4, 18.3, 13.8.

**3.4.8.8 (Z)-4-Methyl-N-(oct-2-en-1-yl)benzenesulfonamide (2g)**

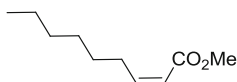
Colorless liquid;  $^1\text{H}$  NMR (400 MHz,  $\text{CDCl}_3$ )  $\delta$  7.70 (d,  $J = 8.0$  Hz, 2H), 7.25 (d,  $J = 8.0$  Hz, 2H), 5.45–5.39 (m, 1H), 5.23–5.17 (m, 1H), 4.45 (s, 1H), 3.52 (t,  $J = 6.8$  Hz, 2H), 2.37 (s, 3H), 1.84 (q,  $J = 6.8$  Hz, 2H), 1.24–1.11 (m, 6H), 0.80 (t,  $J = 6.8$  Hz, 3H);  $^{13}\text{C}$  NMR (100 MHz,  $\text{CDCl}_3$ )  $\delta$  143.2, 136.7, 134.6, 129.5, 127.0, 123.5, 40.1, 31.3, 28.9, 27.2, 22.4, 21.5, 14.0; HRMS (ESI positive) calcd for  $\text{C}_{15}\text{H}_{23}\text{NO}_2\text{S}$  [ $\text{M} + \text{Na}$ ] $^+$ : 304.1342, found: 304.1341.

**3.4.8.9 1-(4-(Hex-1-yn-1-yl)phenyl)ethanone (1i)**

Brown liquid;  $^1\text{H}$  NMR (400 MHz,  $\text{CDCl}_3$ )  $\delta$  7.87 (d,  $J = 8.0$  Hz, 2H), 7.44 (d,  $J = 8.0$  Hz, 2H), 2.57 (s, 3H), 2.42 (t,  $J = 7.2$  Hz, 2H), 1.61–1.44 (m, 4H), 0.94 (t,  $J = 7.2$  Hz, 3H);  $^{13}\text{C}$  NMR (100 MHz,  $\text{CDCl}_3$ )  $\delta$  197.1, 135.4, 131.5, 129.0, 128.0, 94.2, 80.0, 30.6, 26.5, 22.0, 19.2, 13.6.

**3.4.8.10 (Z)-1-(4-(hex-1-en-1-yl)phenyl)ethanone (2i)**

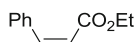
Colorless liquid;  $^1\text{H}$  NMR (400 MHz,  $\text{CDCl}_3$ )  $\delta$  7.91 (d,  $J = 8.0$  Hz, 2H), 7.34 (d,  $J = 8.0$  Hz, 2H), 6.42 (d,  $J = 12.0$  Hz, 1H), 5.80–5.74 (m, 1H), 2.58 (s, 3H), 2.36–2.30 (m, 2H), 1.48–1.30 (m, 4H), 0.89 (t,  $J = 7.2$  Hz, 3H);  $^{13}\text{C}$  NMR (100 MHz,  $\text{CDCl}_3$ )  $\delta$  197.3, 142.5, 135.4, 134.8, 128.6, 128.1, 127.7, 31.9, 28.4, 26.5, 22.3, 13.9; HRMS (ESI positive) calcd for  $\text{C}_{14}\text{H}_{18}\text{O}$  [ $\text{M} + \text{Na}$ ] $^+$ : 225.1250, found: 225.1249.

**3.4.8.11 (Z)-Methyl non-2-enoate (2j)**

Yellow liquid;  $^1\text{H}$  NMR (400 MHz,  $\text{CDCl}_3$ )  $\delta$  6.23–6.17 (m, 1H), 5.74 (d,  $J = 11.6$  Hz, 1H), 3.68 (s, 3H), 2.65–2.60 (m, 2H), 1.43–1.38 (m, 2H), 1.33–1.27 (m,

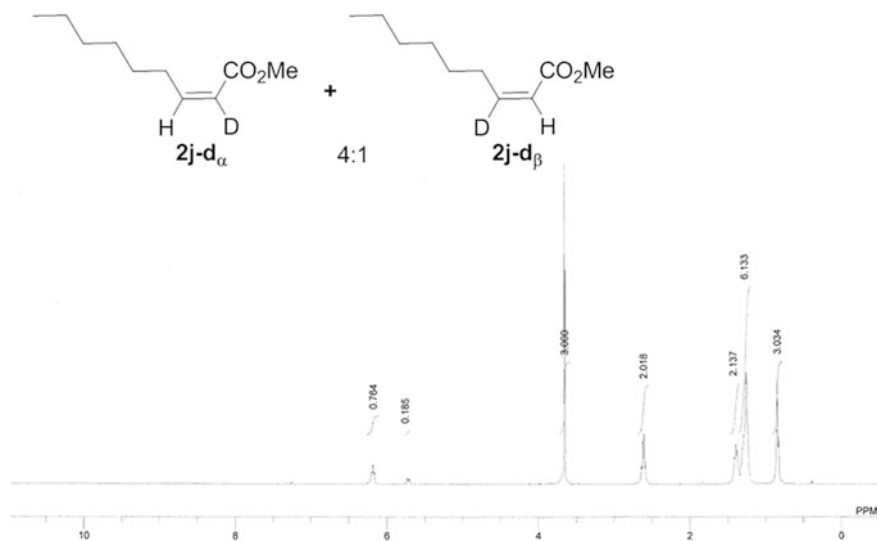
6H), 0.86 (t,  $J = 6.4$  Hz, 3H);  $^{13}\text{C}$  NMR (100 MHz,  $\text{CDCl}_3$ )  $\delta$  166.6, 150.8, 118.9, 50.8, 31.6, 29.0, 28.9, 28.9, 22.5, 14.0; HRMS (ESI positive) calcd for  $\text{C}_{10}\text{H}_{18}\text{O}_2$   $[\text{M} + \text{Na}]^+$ : 193.1199, found: 193.1199.

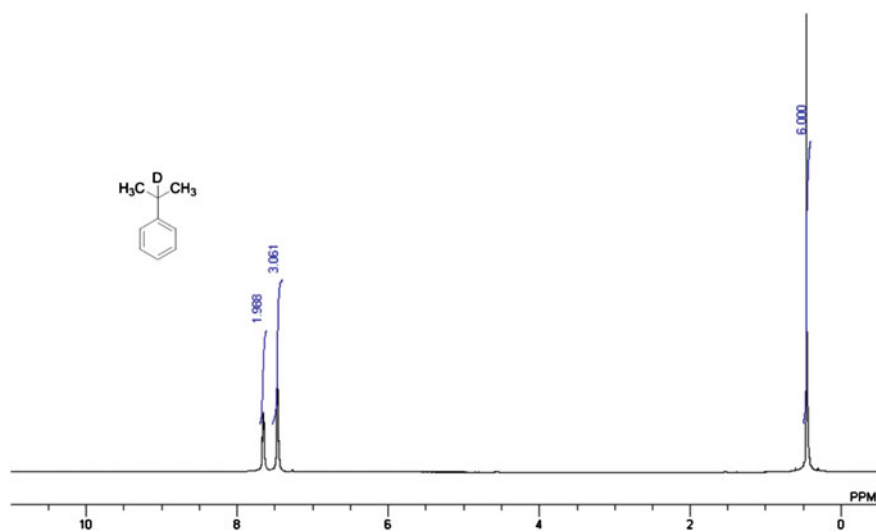
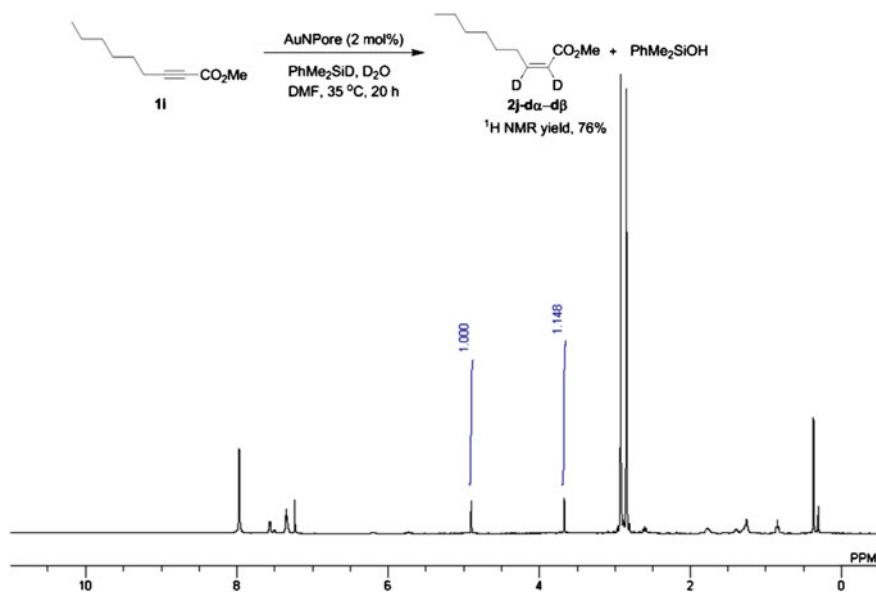
### 3.4.8.12 (Z)-Ethyl 3-phenylacrylate (2k)

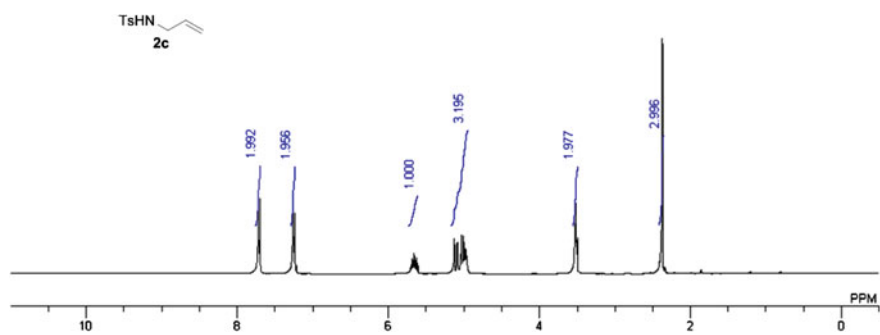
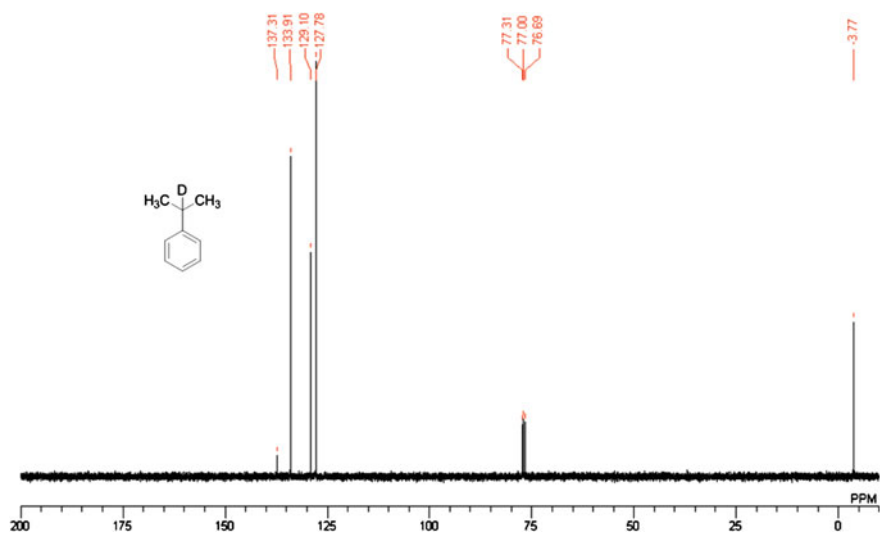


Yellow liquid;  $^1\text{H}$  NMR (400 MHz,  $\text{CDCl}_3$ )  $\delta$  7.55–7.53 (m, 2H), 7.33–7.27 (m, 3H), 6.90 (d,  $J = 12.4$  Hz, 1H), 5.91 (d,  $J = 12.4$  Hz, 1H), 4.13 (q,  $J = 7.2$  Hz, 2H), 1.20 (t,  $J = 7.2$  Hz, 3H);  $^{13}\text{C}$  NMR (100 MHz,  $\text{CDCl}_3$ )  $\delta$  166.0, 142.8, 134.7, 129.5, 128.8, 127.8, 119.7, 60.2, 14.0; HRMS (ESI positive) calcd for  $\text{C}_{10}\text{H}_{12}\text{O}_2$   $[\text{M} + \text{Na}]^+$ : 199.0730, found: 199.0729.

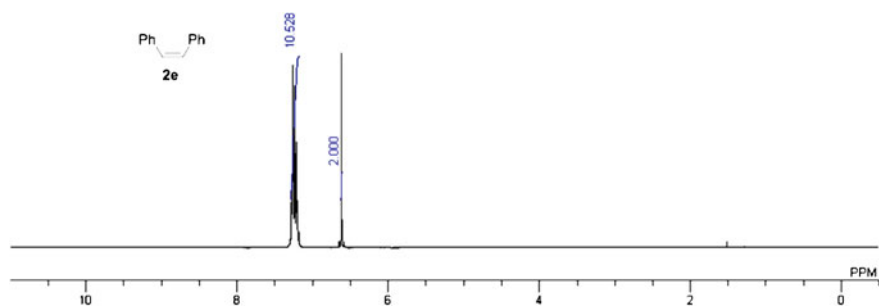
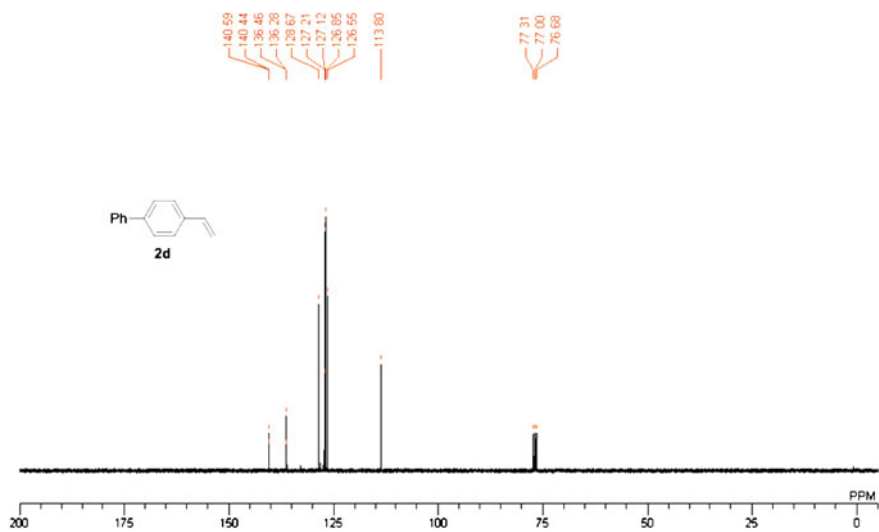
### 3.4.9 $^1\text{H}$ and $^{13}\text{C}$ NMR Spectra

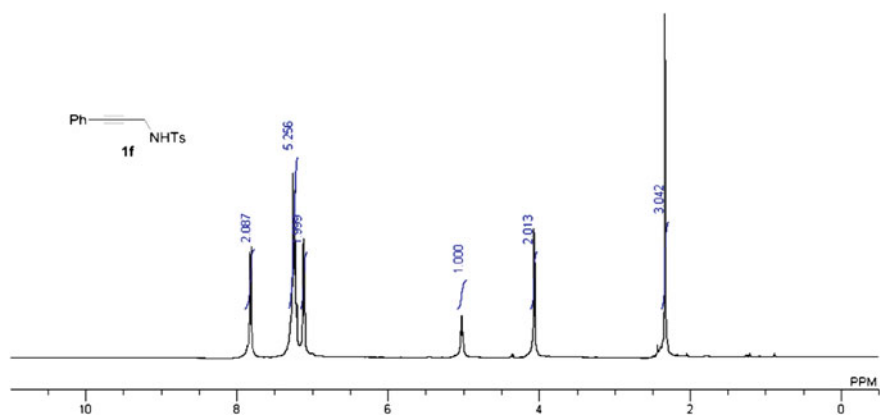
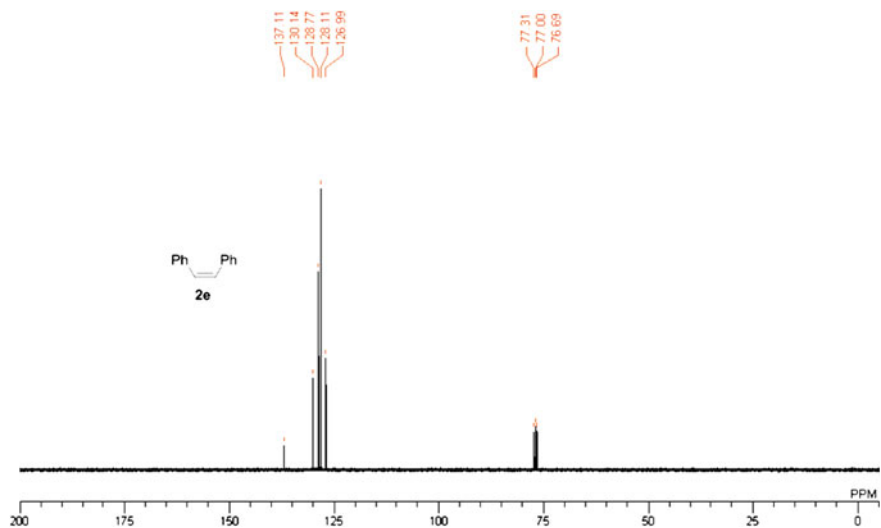




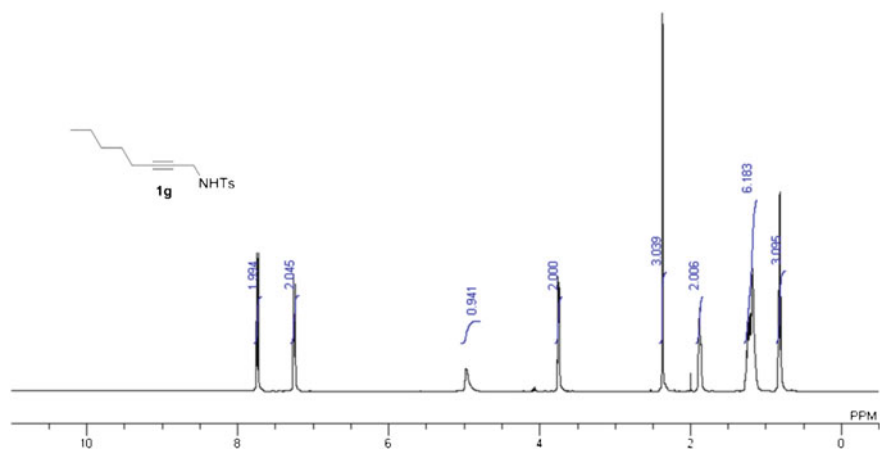
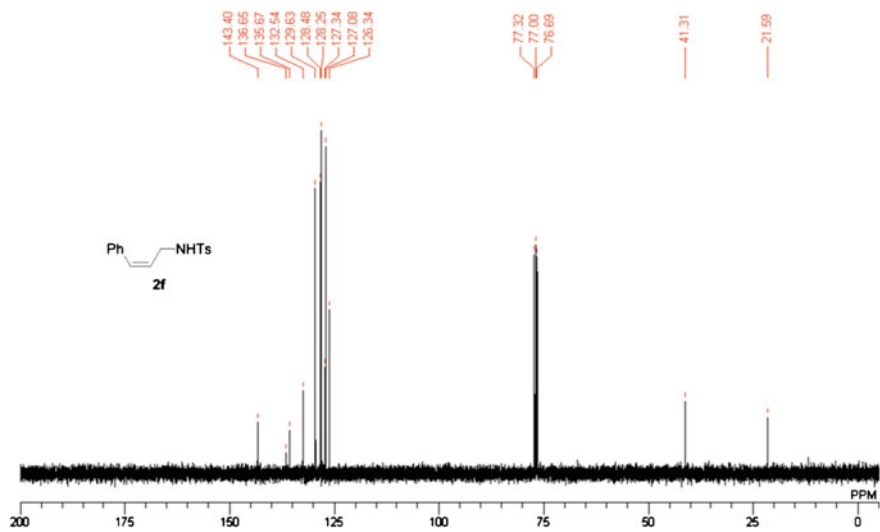


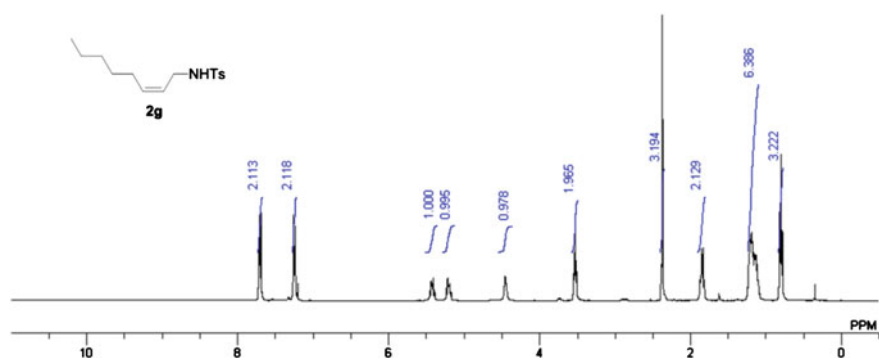
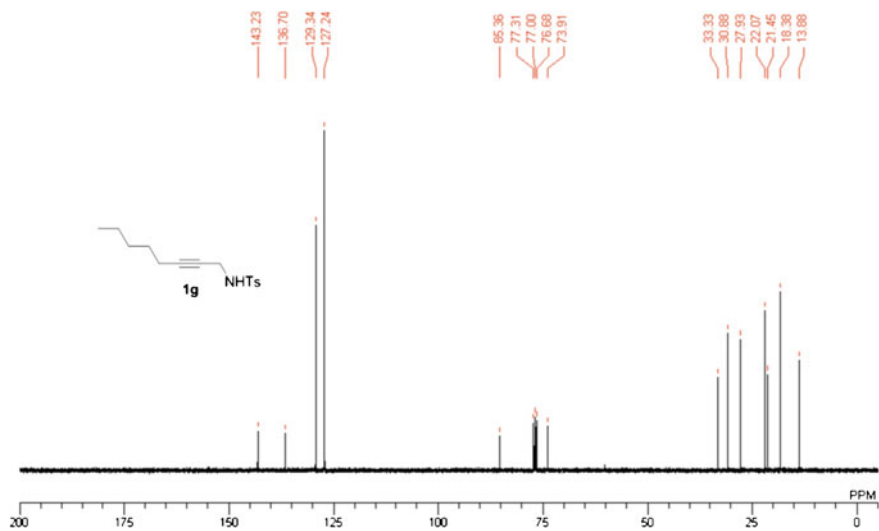


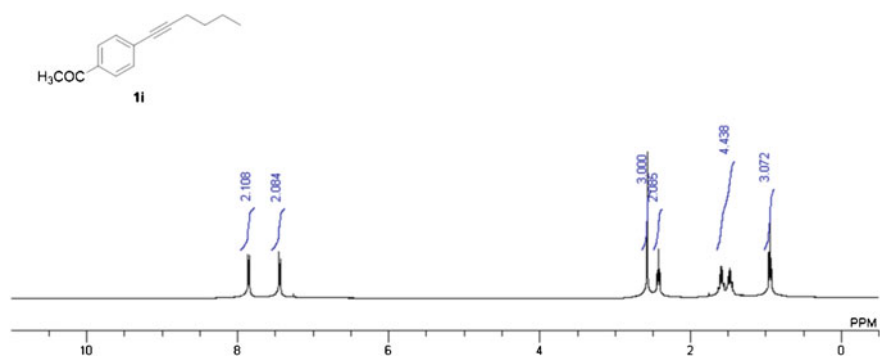
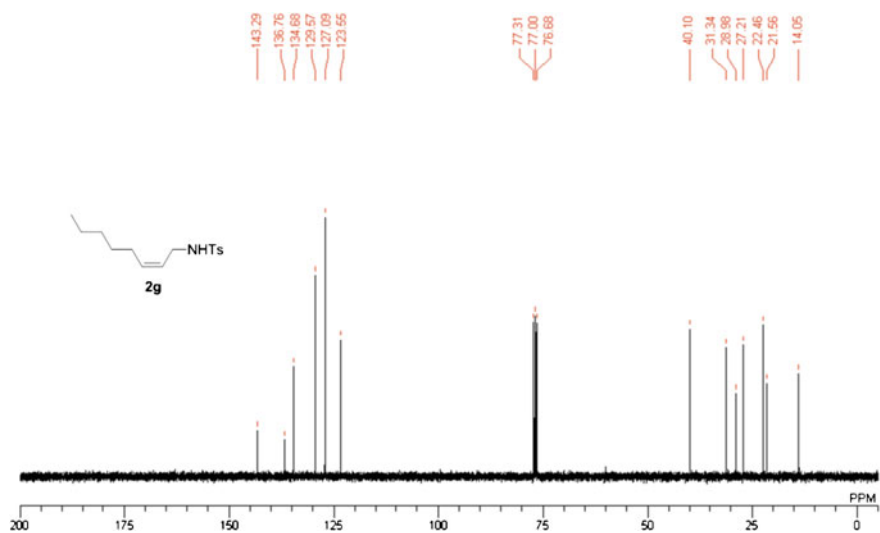


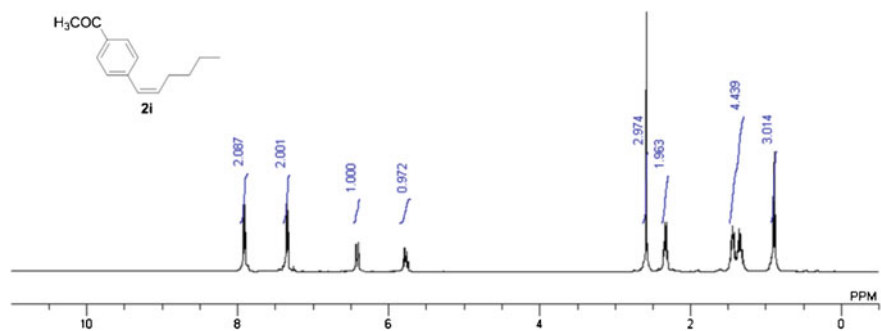
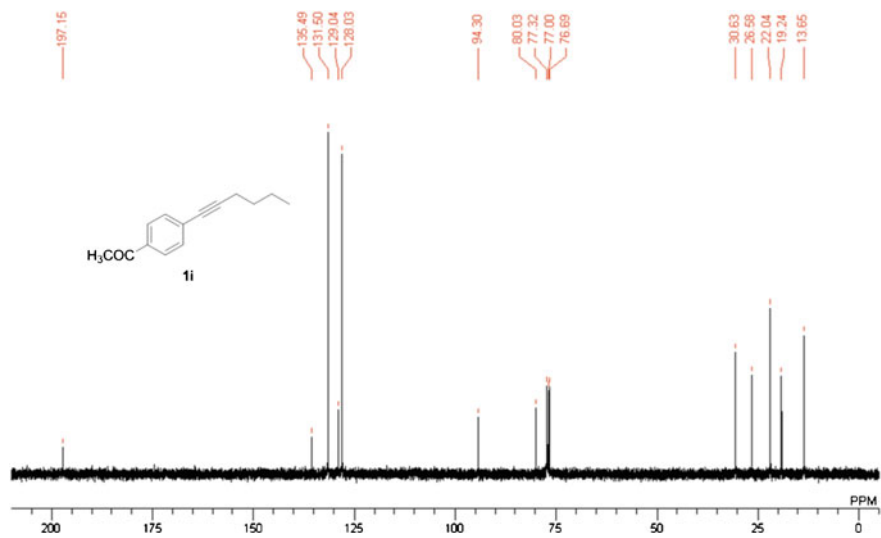


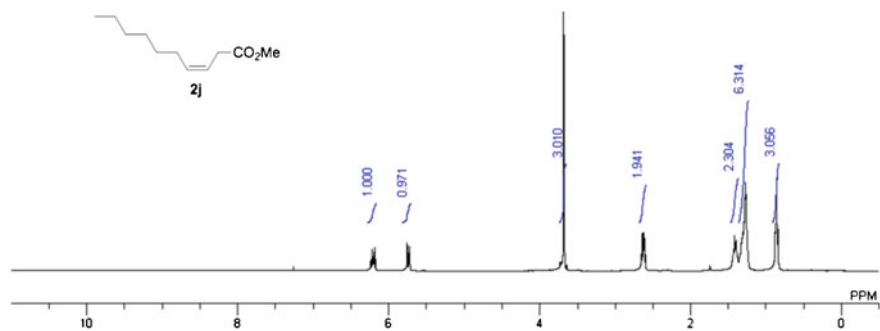
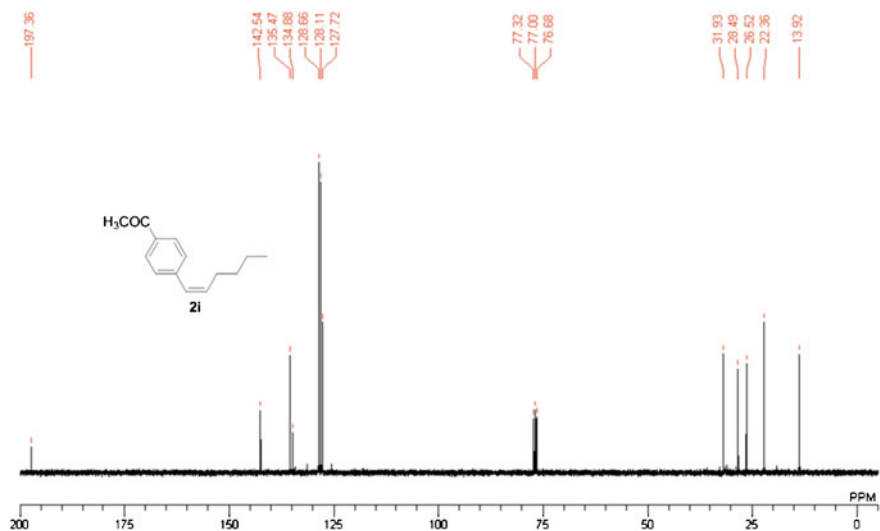


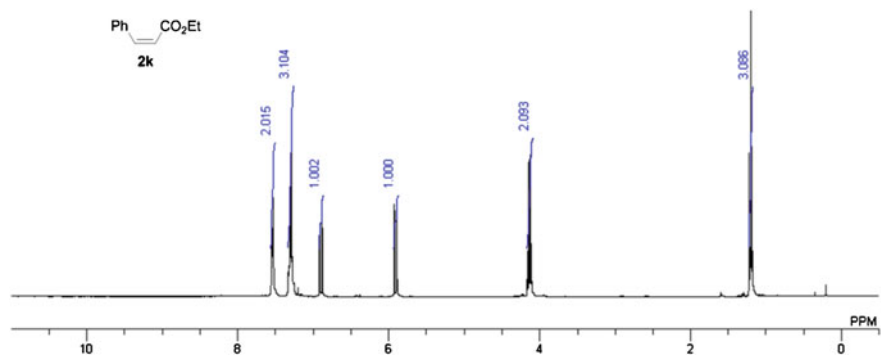
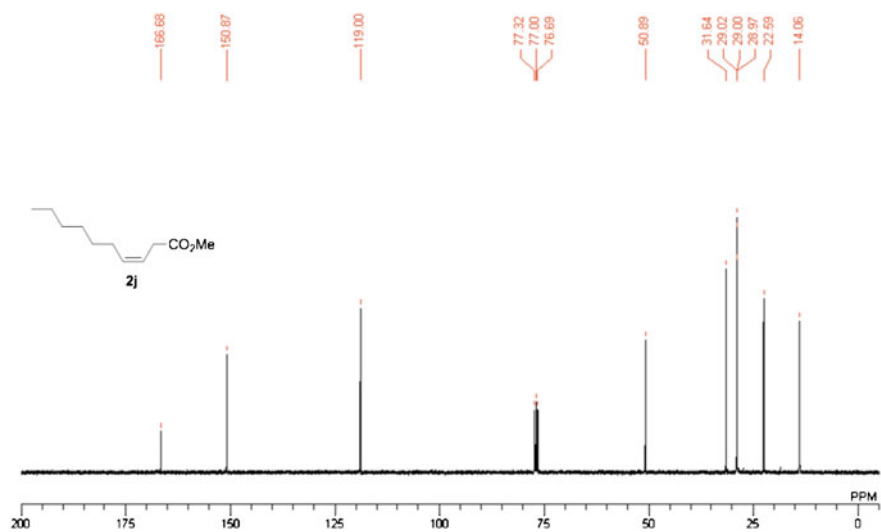


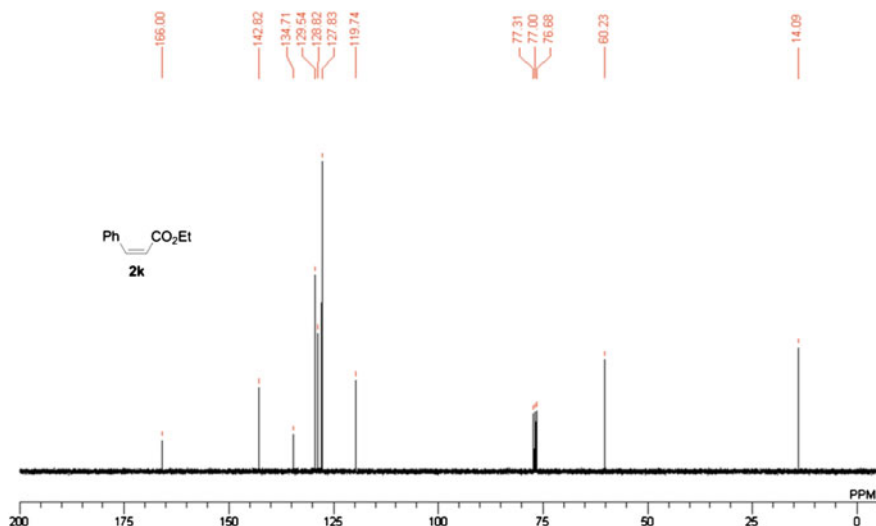












## References

- Zielasek V, Jürgens B, Schulz C et al (2006) Gold catalysts: nanoporous gold foams. *Angew Chem Int Ed* 45:8241–8244
- Xu C, Su J, Xu X et al (2007) Low temperature CO oxidation over unsupported nanoporous gold. *J Am Chem Soc* 129:42–43
- Xu C, Xu X, Su J et al (2007) Research on unsupported nanoporous gold catalyst for CO oxidation. *J Catal* 252:243–248
- Wittstock A, Neumann B, Schaefer A et al (2009) Nanoporous Au: an unsupported pure gold catalyst? *J Phys Chem C* 113:5593–5600
- Wang LC, Jin HJ, Widmann D et al (2011) Dynamic studies of CO oxidation on nanoporous Au using a TAP reactor. *J Catal* 278:219–227
- Wittstock A, Zielasek V, Biener J et al (2010) Nanoporous gold catalysts for selective gas-phase oxidative coupling of methanol at low temperature. *Science* 327:319–322
- Asao N, Hatakeyama N, Menggenbateer et al (2012) Aerobic oxidation of alcohols in the liquid phase with nanoporous gold catalysts. *Chem Commun* 48:4540–4542
- Yin H, Zhou C, Xu C, Liu P et al (2008) Aerobic oxidation of d-Glucose on Support-free nanoporous gold. *J Phys Chem C* 112:9673–9678
- Kosuda KM, Wittstock A, Friend CM et al (2012) Oxygen-mediated coupling of alcohols over nanoporous gold catalysts at ambient pressures. *Angew Chem Int Ed* 51:1698–1701
- Zhang J, Liu P, Ma H et al (2007) Nanostructured porous gold for methanol electro-oxidation. *J Phys Chem C* 111:10382–10388
- Yu C, Jia F, Ai Z et al (2007) Direct oxidation of methanol on self-supported nanoporous gold film electrodes with high catalytic activity and stability. *Chem Mater* 19:6065–6067
- Zeis R, Lei T, Sieradzki K et al (2008) Catalytic reduction of oxygen and hydrogen peroxide by nanoporous gold. *J Catal* 253:132–138
- Forty AJ (1979) Corrosion micromorphology of noble metal alloys and depletion gilding. *Nature* 282:597–598

14. Erlebacher J, Aziz MJ, Karma A et al (2001) Evolution of nanoporosity in dealloying. *Nature* 410:450–453
15. Hashmi ASK, Hutchings GJ (2006) Gold catalysis. *Angew Chem Int Ed* 45:7896–7936
16. Pina CD, Falletta E, Prati L et al (2008) Selective oxidation using gold. *Chem Soc Rev* 37:2077–2095
17. Corma A, Garcia H (2008) Supported gold nanoparticles as catalysts for organic reactions. *Chem Soc Rev* 37:2096–2126
18. Matsumoto T, Ueno M, Wang N et al (2008) Recent advances in immobilized metal catalysts for environmentally benign oxidation of alcohols. *Chem-Asian J* 3:196–214
19. Corma A, Leyva-Pérez A, Sabater MJ (2011) Gold-Catalyzed Carbon–Heteroatom Bond-Forming Reactions. *Chem Rev* 111:1657–1712
20. Fujita T, Guan P, McKenna K et al (2012) Atomic origins of the high catalytic activity of nanoporous gold. *Nature Mater* 11:775–780
21. Bond GC, Louis C, Thompson DT (2006) *Catalysis by gold*. Imperial College Press, London, Chapter 9, p. 244
22. McEwan L, Julius M, Roberts S et al (2010) A review of the use of gold catalysts in selective hydrogenation reactions Lynsey McEwana. *Gold Bull* 43:298–306
23. Fujitani T, Nakamura I, Akita T et al (2009) Hydrogen dissociation by gold clusters. *Angew Chem Int Ed* 48:9515–9518
24. Hauwert P, Maestri G, Sprengers J et al (2008) Transfer semihydrogenation of alkynes catalyzed by a zero-valent palladium N-heterocyclic carbene complex. *Angew Chem Int Ed* 47:3223–3226
25. La Pierre HS, Arnold J, Toste FD (2011) Selective semihydrogenation of alkynes catalyzed by a cationic vanadium bisimido complex. *Angew Chem Int Ed* 50:3900–3903
26. Gianetti TL, Tomson NC, Arnold J et al (2011) Z-selective, catalytic internal alkyne semihydrogenation under H<sub>2</sub>/CO mixtures by a niobium(III) imido complex. *J Am Chem Soc* 133:14904–14907
27. Shen R, Chen T, Zhao Y et al (2011) Facile regio- and stereoselective hydrometalation of alkynes with a combination of carboxylic acids and group 10 transition metal complexes: selective hydrogenation of alkynes with formic acid. *J Am Chem Soc* 133:17037–17044
28. Lindlar H (1952) Ein neuer katalysator für selektive hydrierungen. *Helv Chim Acta* 35:446–450
29. Savoia D, Tagliavini E, Trombini C et al (1981) Active metals from potassium-graphite. Highly dispersed nickel on graphite as a new catalyst for the stereospecific semihydrogenation of alkynes. *J Org Chem* 46:5340–5343
30. Brunet JJ, Caubere P (1984) Activation of reducing agents. Sodium hydride containing complex reducing agents. 20. Pd<sub>2</sub>, a new, very selective heterogeneous hydrogenation catalyst. *J Org Chem* 49:4058–4060
31. Gruttadauria M, Noto R, Deganello G et al (1999) Efficient semihydrogenation of the C–C triple bond using palladium on pumice as catalyst. *Tetrahedron Lett* 40:2857–2858
32. Gruttadauria M, Liotta LF, Noto R et al (2001) Palladium on pumice: new catalysts for the stereoselective semihydrogenation of alkynes to (Z)-alkenes. *Tetrahedron Lett* 42:2015–2017
33. Alonso F, Osante I, Yus M (2006) Highly stereoselective semihydrogenation of alkynes promoted by nickel(0) nanoparticles. *Adv Synth Catal* 348:305–308
34. Hori J, Murata K, Sugai T et al (2009) Highly active and selective semihydrogenation of alkynes with the palladium nanoparticles-tetrabutylammonium borohydride catalyst system. *Adv Synth Catal* 351:3143–3149
35. Venkatesan R, Prechtl MH, Scholten JD et al (2011) Palladium nanoparticle catalysts in ionic liquids: synthesis, characterisation and selective partial hydrogenation of alkynes to Z-alkenes. *J Mater Chem* 21:3030–3036
36. Wu J, Wang K, Li Y et al (2011) Semihydrogenation of phenylacetylene catalyzed by palladium nanoparticles supported on organic group modified silica. *Adv Mater Res* 233–235:2109–2112

37. Takahashi Y, Hashimoto N, Hara T et al (2011) Highly efficient Pd/SiO<sub>2</sub>-dimethyl sulfoxide catalyst system for selective semihydrogenation of alkynes. *Chem Lett* 40:405–407
38. Segura Y, López N, Pérez-Ramírez J (2007) Origin of the superior hydrogenation selectivity of gold nanoparticles in alkyne+alkene mixtures: Triple- versus double-bond activation. *J Catal* 247:383–386
39. Jia J, Haraki K, Kondo JN et al (2000) Selective hydrogenation of acetylene over Au/Al<sub>2</sub>O<sub>3</sub> catalyst. *J Phys Chem B* 104:11153–11156
40. Choudhary TV, Sivadinarayana C, Datye AK et al (2003) Acetylene hydrogenation on Au-based catalysts. *Catal Letters* 86:1–8
41. Azizi Y, Petit C, Pitchon V (2008) Formation of polymer-grade ethylene by selective hydrogenation of acetylene over Au/CeO<sub>2</sub> catalyst. *J Catal* 256:338–344
42. Nikolaev SA, Smirnov VV (2009) Synergistic and size effects in selective hydrogenation of alkynes on gold nanocomposites. *Catal Today* 147S:S336–S341
43. Asao N, Ishikawa Y, Hatakeyama N et al (2010) Nanostructured materials as catalysts: nanoporous-gold-catalyzed oxidation of organosilanes with water. *Angew Chem Int Ed* 49:10093–10095
44. Tanaka S, Kaneko T, Asao N et al (2011) A nanostructured skeleton catalyst: suzuki-coupling with a reusable and sustainable nanoporous metallic glass Pd-catalyst. *Chem Commun* 47:5985–5987
45. Kaneko T, Tanaka S, Asao N et al (2011) Reusable and sustainable nanostructured skeleton catalyst: heck reaction with nanoporous metallic glass Pd (PdNPore) as a support, stabilizer and ligand-free catalyst. *Adv Synth Catal* 353:2927–2932
46. Jin T, Yan M, Menggenbatee et al (2011) Nanoporous copper metal catalyst in click chemistry: nanoporosity-dependent activity without supports and bases. *Adv Synth Catal* 353:3095–3100
47. Asao N, Meggenbatee SY et al (2012) Nanoporous gold-catalyzed [4+2] benzannulation between ortho-alkynylbenzaldehydes and alkynes. *Synlett* 23:66–69
48. Asao N, Jin T, Tanaka S et al (2012) From molecular catalysts to nanostructured materials skeleton catalysts. *Pure Appl Chem* 84:1771–1784
49. Jin T, Yan M, Yamamoto Y (2012) Click chemistry of alkyne-azide cycloaddition using nanostructured copper catalysts. *ChemCatChem* 4:1217–1219
50. Mohr C, Hofmeister H, Radnik J et al (2003) Identification of active sites in gold-catalyzed hydrogenation of acrolein. *J Am Chem Soc* 125:1905–1911
51. Corma A, Boronat M, Gonzalez S et al (2007) On the activation of molecular hydrogen by gold: a theoretical approximation to the nature of potential active sites. *Chem Commun* 32:3371–3373
52. Zhu Y, Qian H, Drake BA et al (2010) Atomically precise Au<sub>25</sub>(SR)<sub>18</sub> nanoparticles as catalysts for the selective hydrogenation of  $\alpha$ ,  $\beta$ -unsaturated ketones and aldehydes. *Angew Chem Int Ed* 49:1295–1298
53. Schreiner S, Yu JY, Vaska L (1988) Carbon dioxide reduction via homogeneous catalytic synthesis and hydrogenation of *N,N*-dimethylformamide. *Inorg Chim Acta* 147:139–141
54. Sharma HK, Panel KH (2009) The photochemical irradiation of R<sub>3</sub>SiH in the presence of [( $\eta$ -5-C<sub>5</sub>H<sub>5</sub>)Fe(CO)<sub>2</sub>CH<sub>3</sub>] in DMF leads to disiloxanes not disilanes. *Angew Chem Int Ed* 48:7052–7054
55. Itazaki M, Ueda K, Nakazawa H et al (2009) Iron-catalyzed dehydrogenative coupling of tertiary silanes. *Angew Chem Int Ed* 48:3313–3316
56. Brunet JJ, Caubere P (1984) Activation of reducing agents. Sodium hydride containing complex reducing agents. 20. Pd<sub>c</sub>, a new, very selective heterogeneous hydrogenation catalyst. *J Org Chem* 49:4058–4060
57. Heathcock CH, Ratcliffe R (1971) Stereoselective total synthesis of the guaiazulenic sesquiterpenoids.  $\alpha$ -bulnesene and bulnesol. *J Am Chem Soc* 93:1746–1757
58. Hönig H, Seuffer-Wasserthal P, Weber H (1990) Chemo-enzymatic synthesis of all isomeric 3-phenylserines and -isoserines. *Tetrahedron* 46:3841–3850

59. Bridier B, López N, Pérez-Ramírez J (2010) Molecular understanding of alkyne hydrogenation for the design of selective catalysts. *Dalton Trans* 39:8412–8419
60. Noujima A, Mitsudome T, Mizugaki T et al (2011) Selective deoxygenation of epoxides to alkenes with molecular hydrogen using a hydrotalcite-supported gold catalyst: a concerted effect between gold nanoparticles and basic sites on a support. *Angew Chem Int Ed* 50:2986–2989
61. Fang M, Machalaba N, Sánchez-Delgado RA (2011) Hydrogenation of arenes and N-heteroaromatic compounds over ruthenium nanoparticles on poly(4-vinylpyridine): a versatile catalyst operating by a substrate-dependent dual site mechanism. *Dalton Trans* 40:10621–10632
62. Goethals M, Zeegers-Huyskens T (1995) FT-IR Study of the interaction between H<sub>2</sub>O, D<sub>2</sub>O, HOD, and pyridines. *Spectrosc Lett* 28:1125–1135
63. Okitsu T, Sato K, Potewar TM et al (2011) Iodocyclization of hydroxylamine derivatives based on the control of oxidative aromatization leading to 2,5-dihydroisoxazoles and isoxazoles. *J Org Chem* 76:3438–3449
64. Zhao L, Lu X, Xu W (2005) Palladium(II)-catalyzed enyne coupling reaction initiated by acetoxypalladation of alkynes and quenched by protonolysis of the carbon–palladium bond. *J Org Chem* 70:4059–4063
65. Huang JM, Lin JQ, Chen DS (2012) Electrochemically supported deoxygenation of epoxides into alkenes in aqueous solution. *Org Lett* 14:22–25
66. Woolven H, González-Rodríguez C, Marco I et al (2011) DABCO-bis(sulfur dioxide), DABSO, as a convenient source of sulfur dioxide for organic synthesis: utility in sulfonamide and sulfamide preparation. *Org Lett* 13:4876–4878
67. Yu JY, Kuwano R (2009) Rhodium-catalyzed cross-coupling of organoboron compounds with vinyl acetate. *Angew Chem Int Ed* 48:7217–7220
68. Shen R, Chen T, Zhao Y et al (2011) Facile regio- and stereoselective hydrometalation of alkynes with a combination of carboxylic acids and group 10 transition metal complexes: selective hydrogenation of alkynes with formic acid. *J Am Chem Soc* 133:17037–17044
69. Oppolzer W, Stammen B (1997) On the faciality of intramolecular palladium(0)-catalysed “metallo-ene-type” cyclisations. *Tetrahedron* 53:3577–3586
70. Kim IS, Dong GR, Jung YH (2007) Palladium(II)-catalyzed isomerization of olefins with tributyltin hydride. *J Org Chem* 72:5424–5426
71. Littke AF, Fu GC (2001) A versatile catalyst for heck reactions of aryl chlorides and aryl bromides under mild conditions. *J Am Chem Soc* 123:6989–7000
72. Walter C, Oestreich M (2008) Catalytic asymmetric C–Si bond formation to acyclic  $\alpha$ ,  $\beta$ -unsaturated acceptors by RhI-catalyzed conjugate silyl transfer using a Si–B linkage. *Angew Chem Int Ed* 47:3818–3820
73. Belger C, Neisius NM, Plietker BA (2010) Selective Ru-catalyzed semireduction of alkynes to Z olefins under transfer-hydrogenation conditions. *Chem Eur J* 16:12214–12220

# Chapter 4

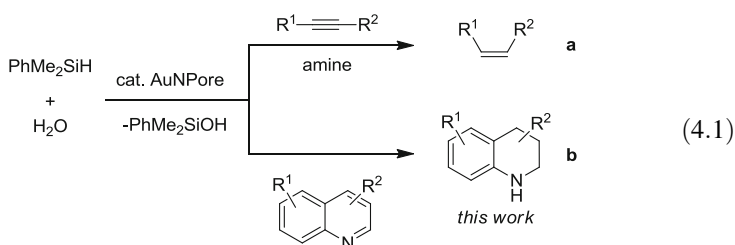
## Unsupported Nanoporous Gold Catalyst for Highly Selective Hydrogenation of Quinolines

**Abstract** We report for the first time the highly efficient and regioselective hydrogenation of quinoline derivatives to 1,2,3,4-tetrahydroquinolines using unsupported nanoporous gold as the catalyst and organosilane with water as the hydrogen source. The AuNPore catalyst can be readily recovered and reused without any loss of catalytic activity.

**Keywords** Nanoporous gold catalyst · Hydrogenation of quinolines · Heterogeneous catalysis

### 4.1 Introduction

Nanoporous gold (AuNPore) being of the three dimensional (3D) bicontinuous network structure, high surface area, nontoxic nature, high fabrication reproducibility, high recyclability, and rather simple recovery, is an attractive candidate as fascinating heterogeneous catalyst [1–14]. In contrast to gold nanoparticles loaded on the carrier [15–19], the unsupported AuNPore catalysts are more close to investigate the intrinsic catalytic activity, selectivity and mechanism as elimination of the supporting effect and to extend the catalytic area widely through relaxation of aggregation. Although recent advances on catalytic applications of AuNPore demonstrated that AuNPore possessed excellent catalytic performance on selective oxidation reactions [1–14], such as CO oxidation and alcohol oxidations as well as organosilane oxidation, it has not been employed for selective hydrogenation up to now due to the weak ability of H<sub>2</sub> dissociation of gold as compared to its counterpart of the Pd group metals [20, 21]. Recently, we have demonstrated for the first time that AuNPore was able to be used as a robust catalyst for the semihydrogenation of alkynes to alkenes with excellent Z-selectivity without over-reduced alkanes by using organosilane and water as a hydrogen source, and appropriate amine as an additive (Eq. 4.1a) [22].



1,2,3,4-Tetrahydroquinoline (py-THQ) is an important framework exists in numerous biologically active natural products and pharmacologically relevant therapeutic agents [23]. Direct hydrogenation of quinoline is regarded as an efficient and straightforward approach to access py-THQ. Both homogeneous and heterogeneous catalysis based on Ru, Rh, Pd, Pt and Ir have been studied extensively with H<sub>2</sub> but suffer from either high H<sub>2</sub> pressures (>1 atm) or high temperatures (>100 °C) [24–37]. Moreover, the strong adsorption of quinolines and their hydrogenated products on heterogeneous catalysts strongly inhibit catalytic activity and selectivity [30–37]. In contrast, gold metallic catalyst has attracted less attention for this reaction owing to its low adsorption ability toward quinoline [38, 39]. As a continuation of our research in the nanoporous metal catalysis [8, 40–45], in this chapter, it turns to present the highly regioselective hydrogenation of quinolines catalyzed by the unsupported AuNPore using organosilane and water to produce *in situ* hydrogen, affording the corresponding py-THQs in high yields (Eq. 4.1b).

## 4.2 Results and Discussion

### 4.2.1 Characterization of AuNPore

The unsupported AuNPore catalyst was prepared by dealloying a homogeneous Au<sub>30</sub>Ag<sub>70</sub> alloy with a thickness of 40 μm in 70 wt % of nitric acid as an electrolyte at room temperature for 18 h [22]. SEM image shown in Fig. 4.1 vividly reveals that ligament and nanopore channel are formed uniformly across the entire AuNPore with an average ligament size around 30 nm. The representative bright-field TEM image of AuNPore shows the multilayers of golds ligaments with convex and concave columnar curvatures, indicating the bicontinuous 3D network nanoporous structure (Fig. 4.2b). Ligament size is seen to be about 30 nm, which is consistent with the values estimated from the SEM image. The EDX analysis on fresh AuNPore shows that the residual Ag composition of AuNPore is 2 % indicating that most of silver is removed after dealloying (Fig. 4.2a).

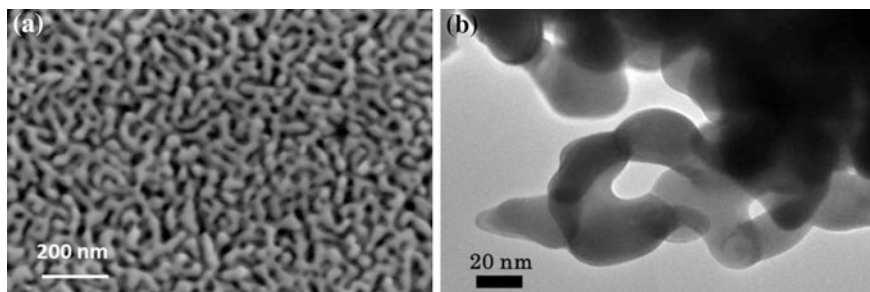


**Fig. 4.1** a SEM image of AuNPore. b Representative bright-field TEM image of AuNPore

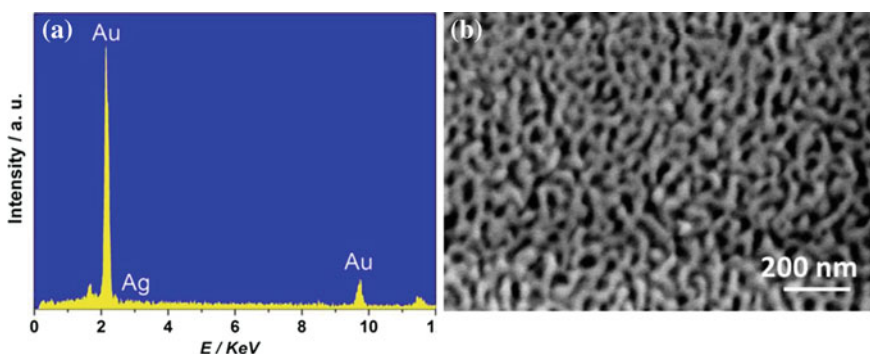


**Fig. 4.2** a EDX analysis of fresh AuNPore, Au<sub>0.8</sub>Ag<sub>0.2</sub>. b SEM image of AuNPore after 5th cycle

### 4.2.2 AuNPore-Catalyzed Hydrogenation of Quinolines

Recently we found that AuNPore was an effective catalyst for oxidation of organosilanes with water to produce organic silanols in high yields along with the vigorous liberation of H<sub>2</sub> gas [14]. In addition, as aforementioned in Eq. (4.1a), we have confirmed that the use of pyridine as an additive together with organosilane and water as a hydrogen source in the AuNPore-catalyzed semihydrogenation of alkynes, suppressed the evolution of H<sub>2</sub>, giving the corresponding alkenes in high selectivity [22]. During the screening of amine additives, it was found that py-THQ was produced as a by-product in 30 % yield when quinoline was used as an additive. This result encouraged us to further optimize the reaction conditions to achieve an efficient and selective hydrogenation of quinolines by using AuNPore as catalyst. Initially, quinoline (**1a**) was treated with AuNPore catalyst, PhMe<sub>2</sub>SiH and water in the presence of various organic solvents as shown in Table 4.1. The use of dimethylformamide (DMF) and acetonitrile (CH<sub>3</sub>CN), which were employed successfully in the previous alkyne hydrogenation, afforded the corresponding 1,2,3,4-tetrahydroquinoline (**2a**) as the only product but the yields were low

**Table 4.1** Screening of solvents for selective hydrogenation of quinoline (**1a**) to 1,2,3,4-tetrahydroquinoline (**2a**)

C1=CC=C2C=CC=NC2=C1 (1a)  $\xrightarrow[\text{solvent, } 80\text{ }^\circ\text{C}]{\text{AuNPore (2 mol\%), PhMe}_2\text{SiH, H}_2\text{O}}$  C1=CC=C2C=CCN2=C1 (2a)

Entry	Solvent	2a, Yield, % <sup>a</sup>
1	DMF	12
2	CH <sub>3</sub> CN	30
3	THF	26 <sup>b</sup>
4	EtOH	38
5	Toluene	91
6	Toluene	0 <sup>c</sup>
7 <sup>d</sup>	Toluene	0

Reaction conditions: quinoline (**1a**, 0.5 mmol), PhMe<sub>2</sub>SiH (1.25 mmol), H<sub>2</sub>O (1.5 mmol), solvent (0.5 mL), AuNPore (2 mol%), 80 °C for 24 h

<sup>a</sup> <sup>1</sup>H NMR yield determined using anisole as an internal standard

<sup>b</sup> Reaction temperature was 60 °C

<sup>c</sup> H<sub>2</sub> (1 atm) balloon was used instead of PhMe<sub>2</sub>SiH and H<sub>2</sub>O

<sup>d</sup> 2 mol% of AgNPore was used instead of AuNPore

(entries 1 and 2). Further examination with tetrahydrofuran (THF) and ethanol did not improve the yield of **2a** (entries 3 and 4). Fortunately, the use of nonpolar solvent such as toluene gave **2a** in high yield without formation of 5,6,7,8-tetrahydroquinoline (bz-THQ) and decahydroquinoline (DHQ) by-products (entry 5). It was noted that the hydrogenation of **1a** with H<sub>2</sub> in toluene by using AuNPore as a catalyst did not proceed at all (entry 6). It is noteworthy that a nanoporous silver (AgNPore) catalyst was totally inactive for the present hydrogenation of quinoline. AgNPore was fabricated by the dealloying of Ag<sub>23</sub>Al<sub>77</sub> alloy under basic conditions following the reported method (Fig. 4.3) [46]. When the reaction was treated with the AgNPore catalyst instead of AuNPore as shown in entry 7 in Table 4.1, the reaction did not proceed and **1a** was recovered in quantitative yield. This result implied that gold was a real catalytic species in the AuNPore catalyst for the present hydrogenation of quinoline and the residual Ag component in AuNPore was inactive.

To clarify whether the AuNPore catalyst leached to the reaction mixture or not, we carried out the leaching experiments in which (Eq. 4.2) **1a** was treated with PhMe<sub>2</sub>SiH and water in the presence of AuNPore catalyst (2 mol%) in toluene at 80 °C. After 8 h, the part of supernatant was transferred to the other reaction vessel and **2a** was produced in 51 % yield at this time. The supernatant was continuously heated at 80 °C in the absence of the catalyst for another 16 h, affording **2a** in 51 % yield as well. In contrast, the residual containing the AuNPore catalyst was completed in 16 h, giving **2a** in 90 % yield. These results, together with our previous X-ray photoelectron spectroscopy (XPS) analysis in

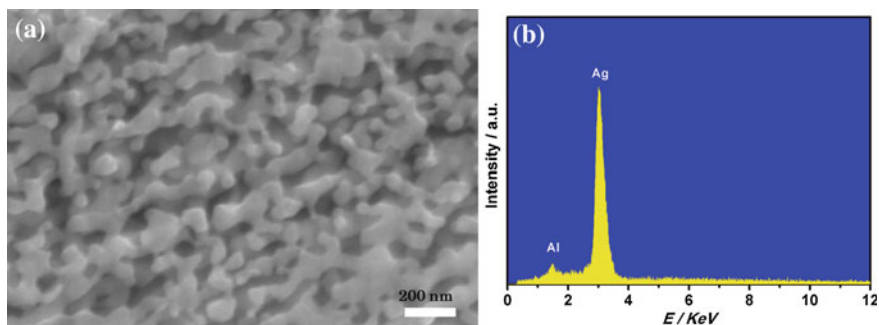
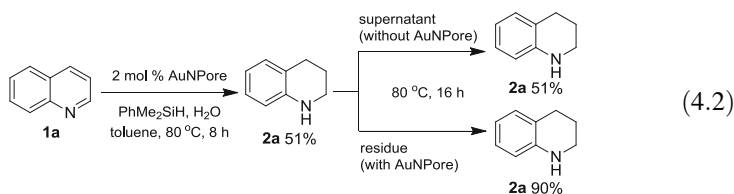


**Fig. 4.3** **a** SEM image of fresh AgNPore. **b** EDX analysis of fresh AgNPore,  $\text{Ag}_{88}\text{Al}_{12}$

which the binding energies of AuNPore and Au mica are almost same, clearly indicate that the present hydrogenation catalyzed by metallic gold(0) without any leaching of gold.



The catalytic activity of AuNPore was further examined with various substituted quinolines under the aforementioned conditions (Table 4.2). Mono-methyl-substituted quinolines were hydrogenated regioselectively to give the corresponding py-THQ in high isolated yields regardless of methyl substituent at benzene or pyridine ring (entries 2–4). Quinolines bearing 2,6-dimethyl (**1e**), 2-propyl (**1f**), and 2-phenyl (**1g**) were also the suitable substrates for the present hydrogenation, providing the corresponding py-THQs (**2e–g**) in high yields with exclusive regioselectivity (entries 5–7). Remarkably, AuNPore catalyst exhibited excellent selectivity with hydrogenation of 6-chloroquinoline (**1h**), affording the desired **2h** in high yield without formation of dehalogenated product (entry 8). When the 2,3-dimethyl-quinoline **1i** was employed in the standard conditions, the corresponding product **2i** was obtained in 78 % yield with a 2.5:1 mixture of *syn* and *anti* isomers, in which *syn*-isomer was obtained as a major product (entry 9). However, it should be noted that, quinoline derivatives with hydroxy or carbonyl group, such as quinoline-4-ol (poor solubility in toluene) or 2-quinolinecarbaldehyde was not compatible under the standard conditions, resulting in total recovery of substrates. Quinoline derivatives with alkynyl or alkenyl moiety did not show good chemoselectivity; 2-(oct-1-yn-1-yl)quinoline produced a mixture of products with alkyne-reduced quinoline<sup>7</sup> and alkynyl-tetrahydroquinoline as major

**Table 4.2** AuNPore-catalyzed hydrogenation of various quinolines

Entry	Substrate	1	Time, h	2	Yield, % <sup>a</sup>
1		1a	24	2a	86 <sup>b</sup>
2		1b	7	2b	91
3		1c	18	2c	96
4		1d	6	2d	83
5	to	1e	7	2e	98
6		1f	3	2f	97
7		1g	10	2g	98
8		1h	39	2h	97
9		1i	24	2i	78 <sup>c</sup>
10		1j	18	2j	85 <sup>d</sup>

Reaction conditions: quinoline (**1**, 0.5 mmol), PhMe<sub>2</sub>SiH (2.0 mmol), H<sub>2</sub>O (2.0 mmol), toluene (0.5 mL), AuNPore (2 mol%), 80 °C

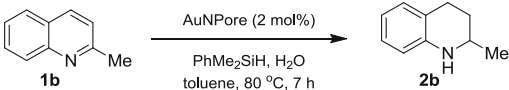
<sup>a</sup> Isolated yield

<sup>b</sup> PhMe<sub>2</sub>SiH (1.25 mmol) and H<sub>2</sub>O (1.5 mmol) were used

<sup>c</sup> A 2.5:1 mixture of *syn* and *anti* isomers

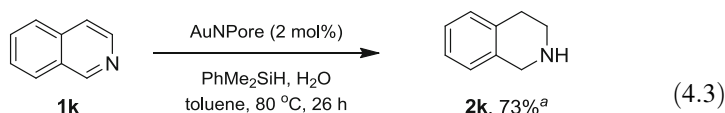
<sup>d</sup> The product is 2-phenethyl-1,2,3,4-tetrahydroquinoline

products, and 2-styrylquinoline (**1j**) afforded the both alkene and pyridine moieties reduced 2-phenethyl-1,2,3,4-tetrahydroquinoline(**2j**) in 85 % yield by using excess amounts of organosilane and water (entry 10). Note that isoquinoline (**1k**) showed a relatively lower reactivity compared with quinoline, affording the corresponding 1,2,3,4-tetrahydroisoquinoline (**2k**) in 70 % yield along with some amounts of recovered **1k** (Eq. 4.3). It was noted that no trace of bz-THQs or DHQs was detected in the present hydrogenation.

**Table 4.3** Reusability of AuNPore catalyst


Run	2b, Yield, % <sup>a</sup>
1st	95
2nd	98
3rd	98
4th	97
5th	98

<sup>a</sup> <sup>1</sup>H NMR yield determined using CH<sub>2</sub>Br<sub>2</sub> as an internal standard



<sup>a</sup> Yield was determined by <sup>1</sup>H NMR spectra using CH<sub>2</sub>Br<sub>2</sub> as an internal standard.

The AuNPore catalyst was reused for five cycles without any loss of catalytic activity and selectivity in the hydrogenation of 2-methylquinoline (**1b**) under the standard conditions; the yield was still 98 % even in the fifth cycle (Table 4.3). The catalyst was recovered through the simple filtration of the reaction mixture washing with acetone and reused without further purification. It is noteworthy that, the nanoporous structure of the recovered catalyst did not show the structural changes after the fifth cycle (Fig. 4.2b).

### 4.2.3 Proposed Reaction Pathway

To gain further insight into the reaction details, we carried out the deuterium labeling experiments. The reaction of quinoline **1a** with PhMe<sub>2</sub>SiH and D<sub>2</sub>O in the presence of the AuNPore catalyst in toluene gave the corresponding 3-D-tetrahydroquinoline **2a'** as the sole product in 60 % yield containing 100 % one deuterium atom and **1a** was recovered in 28 % yield (Eq. 4.4 and Fig. 4.4). This result clearly indicated that both PhMe<sub>2</sub>SiH and water are the hydrogen source in the present reaction.

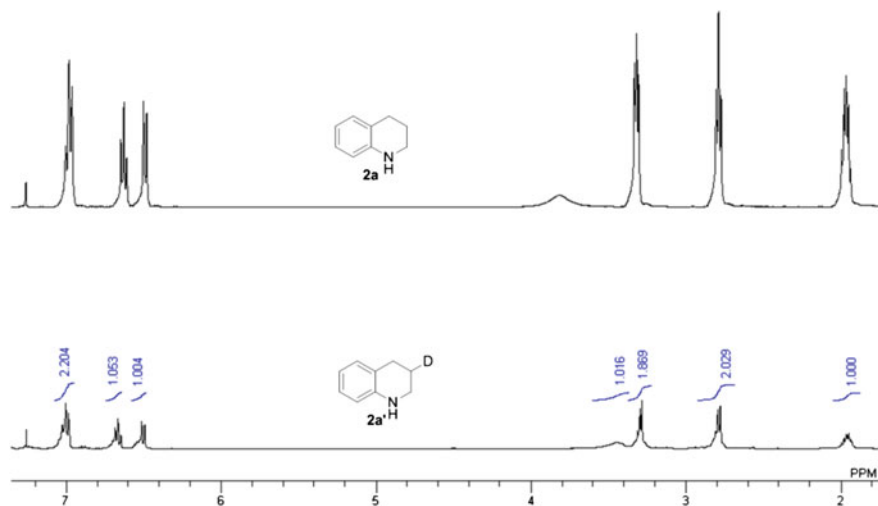
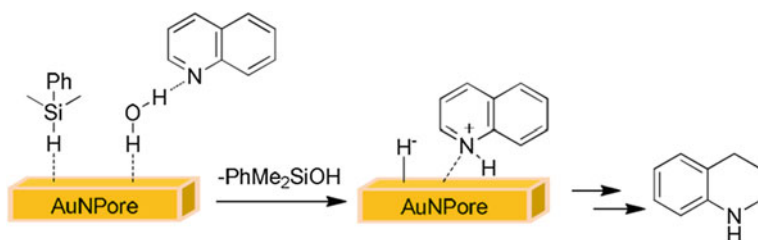
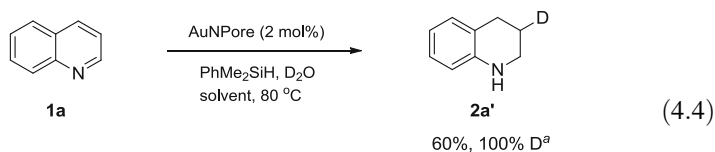


**Fig. 4.4**  $^1\text{H}$  NMR chart of Deuterium-labeling experiment for the reaction of quinoline with  $\text{PhMe}_2\text{SiH}$  and  $\text{D}_2\text{O}$  under standard conditions



**Scheme 4.1** Reaction pathway for the AuNPore-catalyzed hydrogenation of quinoline



<sup>a</sup> Yield was determined by  $^1\text{H}$  NMR spectra using  $\text{CH}_2\text{Br}_2$  as an internal standard.

On the basis of the present results and our previous study of the amine effect on the hydrogenation of alkynes [22], the ionic hydrogenation pathway is proposed as shown in Scheme 4.1. Due to the moderate adsorption energy of quinoline on Au [39], the hydrogen bond forms preferably between quinoline and water. The reaction of adsorbed  $\text{PhMe}_2\text{SiH}$  and water may produce  $[\text{AuNPore-H}]^-$  and  $[\text{H-quinoline}]^+$  species, in which the later reacts subsequently with hydride on

AuNPore to form the corresponding py-THQ. Although the detailed way of the following hydride addition into  $[\text{H-quinoline}]^+$ , such as 1,4-addition or 1,2-addition, remains unclear at this stage, the formation of hydrogen bond between quinoline and water is crucial for suppressing the vigorous liberation of  $\text{H}_2$  gas which is inactive toward the unsupported AuNPore catalyst.

### 4.3 Conclusion

We have demonstrated in this chapter that the unsupported AuNPore can catalyze the hydrogenation of quinolines. By using reaction between organosilane and water as a hydrogen source, various quinoline derivatives were hydrogenated to give the py-THQs in high yields with excellent regioselectivity. AuNPore catalyst can be easily recycled and reused for several times without any loss of catalytic activity and leaching. Further extension of this hydrogenation method to other unsaturated multiple bonds is in progress.

## 4.4 Experimental Section

### 4.4.1 General Information

GC-MS analysis was performed on an Agilent 6890 N GC interfaced to an Agilent 5973 mass-selective detector (30 m  $\times$  0.25 mm capillary column, HP-5MS). Scanning electron microscope (SEM) observation was carried out using a JEOL JSM-6500F instrument operated at an accelerating voltage of 30 kV.  $^1\text{H}$  NMR and  $^{13}\text{C}$  NMR spectra were recorded on JEOL JNM AL 400 (400 MHz) spectrometers.  $^1\text{H}$  NMR spectra are reported as follows: chemical shift in ppm ( $\delta$ ) relative to the chemical shift of  $\text{CDCl}_3$  at 7.26 ppm, integration, multiplicities (s = singlet, d = doublet, t = triplet, q = quartet, m = multiplet and br = broadened), and coupling constants (Hz).  $^{13}\text{C}$  NMR spectra were recorded on JEOL JNM AL 400 (100.5 MHz) spectrometers with complete proton decoupling, and chemical shift reported in ppm ( $\delta$ ) relative to the central line of triplet for  $\text{CDCl}_3$  at 77 ppm. Column chromatography was carried out employing silica gel 60 N (spherical, neutral, 40 ~ 100  $\mu\text{m}$ , KANTO Chemical Co.). Analytical thin-layer chromatography (TLC) was performed on 0.2 mm precoated plate Kieselgel 60 F254 (Merck).

### 4.4.2 Materials

The hydrosilanes and substituted quinolines are commercially available, which are used as received. Au (99.99 %) and Ag (99.99 %) are purchased from Tanaka Kikinzoku Hanbai K.K. and Mitsuwa's Pure Chemicals, respectively.

2-Propylquinoline **1f**, [47] **1i** [48] and **1j** [49] were prepared following the reported literature. **2i** was identified by  $^1\text{H}$  NMR comparing with the literature reported [50]. Structures of **2a**, [51] **2b**, [51] **2c**, [51] **2d**, [51] **2e**, [49] **1f**, [52] **2f**, [50] **2g**, [50] **2h**, [53] **2i**, [50] and **2j** [54] were determined by comparing with the reported authentic compounds. Nanoporous gold (AuNPore) [22] and nanoporous silver (AgNPore) [46] was fabricated following the reported method.

#### 4.4.3 Fabrication of AuNPore Catalyst

Au (99.99 %) and Ag (99.99 %) were melted with electric arc-melting furnace under Ar atmosphere to form Au/Ag alloy (30:70, in at. %), which was rolled down to thickness of 0.04 mm. The resulting foil was annealed at 850 °C for 20 h. The foil was cut into small pieces (5 × 2 mm square). Treatment of the resulting chips (67.1 mg) with 70 wt % nitric acid (3.77 mL) for 18 h at room temperature in a shaking apparatus resulted in the formation of the nanoporous structure by selective leaching of silver. The material was washed with a saturated aqueous solution of  $\text{NaHCO}_3$ , pure water, and acetone, successively. Drying of the material under reduced pressure gave the nanoporous gold (30.2 mg), and its composition was found to be  $\text{Au}_{08}\text{Ag}_2$  from EDX analysis.

#### 4.4.4 Representative Procedure for the AuNPore-Catalyzed Hydrogenation of **1a** (Table 4.1, Entry 5)

To a toluene solution (1 M, 0.5 mL) of AuNPore (2 mol%) were added **1a** (0.5 mmol),  $\text{H}_2\text{O}$  (1.5 mmol) and  $\text{PhMe}_2\text{SiH}$  (1.25 mmol) subsequently at room temperature. The reaction mixture was stirred at 80 °C for 24 h and was monitored by GC-MS analysis. The AuNPore catalyst was recovered by filtration, and washed by diethyl ether. The recovered AuNPore catalyst was washed with acetone and dried under vacuum. After concentration, the residue was purified with a silica gel chromatography to afford **2a** in 86 % yield.

#### 4.4.5 Reaction Procedure for the Hydrogenation of Isoquinoline (**1k**)

To a toluene solution (1 M, 0.5 mL) of AuNPore (2 mol%) were added **1k** (0.5 mmol),  $\text{H}_2\text{O}$  (2.0 mmol) subsequently at room temperature. The reaction mixture was stirred at 80 °C for 26 h and was monitored by GC-MS analysis. The AuNPore catalyst was recovered by filtration, and washed by diethyl ether. The recovered AuNPore catalyst was washed with acetone and dried under vacuum. After concentration, the residue showed that the corresponding **2k** [16] was

observed in 73 %  $^1\text{H}$  NMR yield using  $\text{CH}_2\text{Br}_2$  as an internal standard together with small amount of the recovered isoquinoline in 10 % yield.

#### 4.4.6 Deuterium-Labeling Experiment

To a toluene solution (1 M, 0.5 mL) of AuNPore (2 mol%) were added **1a** (0.5 mmol),  $\text{D}_2\text{O}$  (1.5 mmol) and  $\text{PhMe}_2\text{SiH}$  (1.25 mmol) subsequently at room temperature. The reaction mixture was stirred at 80 °C for 24 h and was monitored by GC-MS analysis. The AuNPore catalyst was recovered by filtration, and washed by diethyl ether. After concentration, the residue showed that the 3-position deuterated corresponding product **2a'** was obtained in 60 % NMR yield containing 100 % D and **1a** was recovered in 28 % yield.

#### 4.4.7 Leaching Experiments

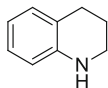
Quinoline **1a** was treated with  $\text{PhMe}_2\text{SiH}$  and water in the presence of AuNPore catalyst (2 mol%) in toluene at 80 °C. After 8 h, a part of supernatant was transferred to the other reaction vessel and **2a** was produced in 51 %  $^1\text{H}$  NMR yield at this time. The supernatant was continuously heated at 80 °C in the absence of the catalyst for 16 h, affording **2a** in 51 %  $^1\text{H}$  NMR yield. In contrast, the residual containing the AuNPore catalyst was completed in 16 h, giving **2a** in 90 %  $^1\text{H}$  NMR yield.

#### 4.4.8 Synthesis of Starting Material (2-propylquinoline 1f)

To a stirred solution of 2-methylquinoline (10.0 mmol) in ether at 0 °C was added n-BuLi (12.0 mmol, 1.62 M in hexane). After stirring 1.5 h at room temperature,  $\text{CH}_3\text{CH}_2\text{I}$  (15.0 mmol) was added at 0 °C. The resulting mixture was stirred at room temperature for 3 h. Water (10 mL) was added, and the product was extracted with ethyl acetate (30 mL  $\times$  3). The combined organic layer was dried over sodium sulfate, and concentrated in vacuo. Silica gel column purification afforded 2-propylquinoline [47].

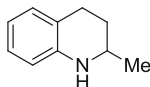
#### 4.4.9 Analytical Data of (1 and 2)

##### 1,2,3,4-tetrahydroquinoline (2a)



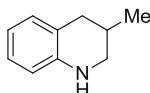
$^1\text{H}$  NMR (400 MHz,  $\text{CDCl}_3$ )  $\delta$  7.00–6.95 (m, 2H), 6.64–6.60 (m, 1H), 6.50–6.48 (m, 1H), 3.81 (br, 1H), 3.31 (t,  $J = 5.6$  Hz, 2H), 2.79 (t,  $J = 6.4$  Hz, 2H), 1.99–1.93 (m, 2H);  $^{13}\text{C}$  NMR (100 MHz,  $\text{CDCl}_3$ )  $\delta$  144.6, 129.3, 126.6, 121.3, 116.8, 114.0, 41.9, 26.9, 22.1 [51];

**2-methyl-1,2,3,4-tetrahydroquinoline (2b)** [51]



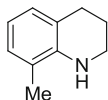
$^1\text{H}$  NMR (400 MHz,  $\text{CDCl}_3$ )  $\delta$  7.02–6.99 (m, 2H), 6.66–6.63 (m, 1H), 6.51 (d,  $J = 8.4$  Hz, 1H), 3.72 (br, 1H), 3.47–3.40 (m, 1H), 2.92–2.74 (m, 2H), 2.00–1.94 (m, 1H), 1.68–1.58 (m, 1H), 1.25 (d,  $J = 6.4$  Hz, 3H);  $^{13}\text{C}$  NMR (100 MHz,  $\text{CDCl}_3$ )  $\delta$  144.6, 129.1, 126.5, 120.9, 116.8, 113.8, 47.1, 30.1, 26.6, 22.6;

**3-methyl-1,2,3,4-tetrahydroquinoline (2c)** [51]



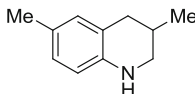
$^1\text{H}$  NMR (400 MHz,  $\text{CDCl}_3$ )  $\delta$  7.00–6.95 (m, 2H), 6.62 (t,  $J = 7.2$  Hz, 1H), 6.50 (d,  $J = 8.0$  Hz, 1H), 3.84 (br, 1H), 3.30–3.26 (m, 1H), 2.91 (t,  $J = 10.4$  Hz, 1H), 2.82–2.72 (m, 1H), 2.48–2.42 (m, 1H), 2.12–2.04 (m, 1H), 1.07 (d,  $J = 6.4$  Hz, 3H);  $^{13}\text{C}$  NMR (100 MHz,  $\text{CDCl}_3$ )  $\delta$  144.1, 129.4, 126.5, 121.0, 116.8, 113.7, 48.8, 35.5, 27.2, 19.0;

**8-methyl-1,2,3,4-tetrahydroquinoline (2d)** [51]

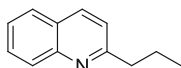


$^1\text{H}$  NMR (400 MHz,  $\text{CDCl}_3$ )  $\delta$  6.95 (dd,  $J = 8.0$  Hz, 10.0 Hz, 2H), 6.64 (t,  $J = 7.2$  Hz, 1H), 3.71 (br, 1H), 3.45 (t,  $J = 5.6$  Hz, 2H), 2.88 (t,  $J = 6.4$  Hz, 2H), 2.16 (s, 3H), 2.06–2.00 (m, 2H);  $^{13}\text{C}$  NMR (100 MHz,  $\text{CDCl}_3$ )  $\delta$  142.5, 127.6, 127.2, 121.0, 120.6, 116.2, 42.2, 27.2, 22.1, 17.1;

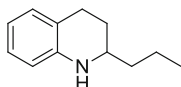
**2,6-dimethyl-1,2,3,4-tetrahydroquinoline (2e)** [49]



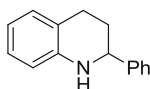
$^1\text{H}$  NMR (400 MHz,  $\text{CDCl}_3$ )  $\delta$  6.79 (d,  $J = 7.6$  Hz, 2H), 6.42 (d,  $J = 7.6$  Hz, 1H), 3.42–3.34 (m, 1H), 2.88–2.68 (m, 2H), 2.22 (s, 3H), 1.96–1.90 (m, 1H), 1.65–1.55 (m, 1H), 1.22 (d,  $J = 6.4$  Hz, 3H);  $^{13}\text{C}$  NMR (100 MHz,  $\text{CDCl}_3$ )  $\delta$  142.3, 129.7, 127.1, 126.1, 121.1, 114.1, 47.3, 30.4, 26.6, 22.6, 20.4;

**2-propylquinoline (1f)** [52]

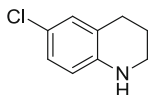
$^1\text{H}$  NMR (400 MHz,  $\text{CDCl}_3$ )  $\delta$  8.04–8.00 (m, 2H), 7.72 (d,  $J = 8.0$  Hz, 1H), 7.66–7.62 (m, 1H), 7.46–7.43 (m, 1H), 7.27–7.24 (m, 1H), 2.95–2.90 (m, 2H), 1.86–1.77 (m, 2H), 0.99 (t,  $J = 7.6$  Hz, 3H);  $^{13}\text{C}$  NMR (100 MHz,  $\text{CDCl}_3$ )  $\delta$  162.7, 147.7, 136.0, 129.1, 128.7, 127.3, 126.6, 125.5, 121.2, 41.3, 23.3, 14.0;

**2-propyl-1,2,3,4-tetrahydroquinoline (2f)** [50]

$^1\text{H}$  NMR (400 MHz,  $\text{CDCl}_3$ )  $\delta$  7.03–6.99 (m, 2H), 6.67–6.63 (m, 1H), 6.52 (dd,  $J = 8.4$  Hz, 1.2 Hz, 1H), 3.64 (br, 1H), 3.32–3.27 (m, 1H), 2.91–2.75 (m, 2H), 2.04–1.98 (m, 1H), 1.70–1.45 (m, 5H), 1.02 (t,  $J = 7.2$  Hz, 3H);  $^{13}\text{C}$  NMR (100 MHz,  $\text{CDCl}_3$ )  $\delta$  144.5, 129.1, 126.5, 121.2, 116.7, 113.9, 51.2, 38.8, 28.1, 26.4, 18.9, 14.2;

**2-phenyl-1,2,3,4-tetrahydroquinoline (2g)** [50]

$^1\text{H}$  NMR (400 MHz,  $\text{CDCl}_3$ )  $\delta$  7.36–7.20 (m, 5H), 6.99–6.95 (m, 2H), 6.61 (t,  $J = 7.6$  Hz, 1H), 6.49 (d,  $J = 8.4$  Hz, 1H), 4.40 (d,  $J = 9.2$  Hz, 1H), 4.00 (s, 1H), 2.93–2.85 (m, 1H), 2.73–2.68 (m, 1H), 2.11–2.06 (m, 1H), 2.00–1.91 (m, 1H);  $^{13}\text{C}$  NMR (100 MHz,  $\text{CDCl}_3$ )  $\delta$  144.6, 144.6, 129.1, 128.4, 127.3, 126.7, 126.4, 120.7, 117.0, 113.8, 56.2, 31.0, 26.4;

**6-chloro-1,2,3,4-tetrahydroquinoline (2h)** [53]

$^1\text{H}$  NMR (400 MHz,  $\text{CDCl}_3$ )  $\delta$  6.93–6.90 (m, 2H), 6.38 (d,  $J = 8.4$  Hz, 1H), 3.71 (br, 1H), 3.28 (t,  $J = 5.6$  Hz, 2H), 2.73 (t,  $J = 6.4$  Hz, 2H), 1.95–1.89 (m, 2H);  $^{13}\text{C}$  NMR (100 MHz,  $\text{CDCl}_3$ )  $\delta$  143.1, 128.8, 126.3, 122.6, 120.8, 114.9, 41.7, 26.8, 21.7;

**2,3-Methyl-1,2,3,4-tetrahydroquinoline (2i)** [50]

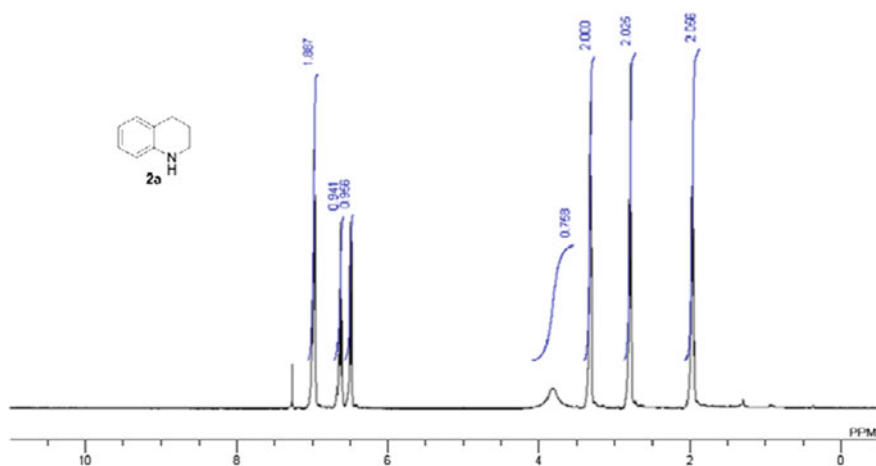
*Syn* : *anti* = 2.5 : 1;  $^1\text{H}$  NMR (400 MHz,  $\text{CDCl}_3$ )  $\delta$  7.00–6.96 (m, 2H, for *syn* and *anti* isomers), 6.64–6.60 (m, 1H), 6.49 (d,  $J = 8.0$  Hz, 1H, for *syn* and *anti* isomers), 3.71 (br, 1H, for *syn* and *anti* isomers), 3.55 (bs, 1H, for *syn* and *anti* isomers), 3.46 (dq,  $J = 6.4, 3.2$  Hz, 1H, for *syn* isomer), 3.01 (m, 1H, for *anti*

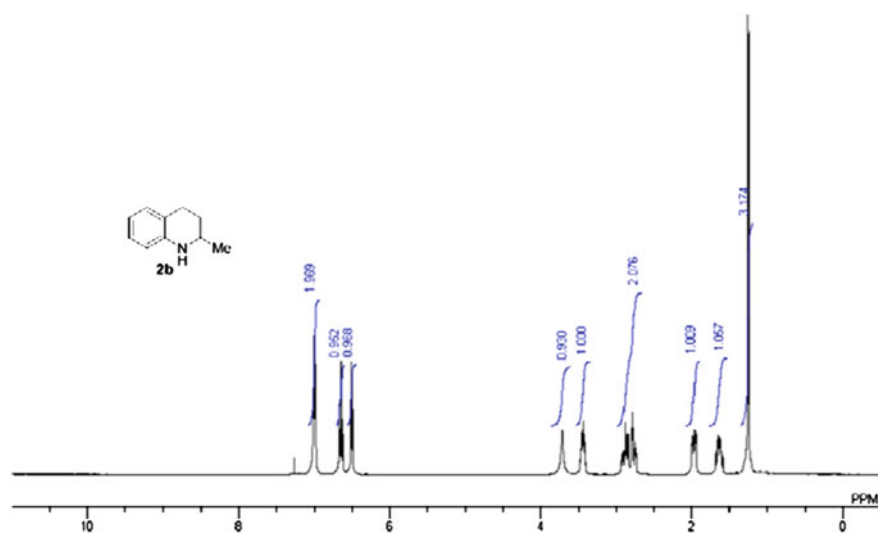
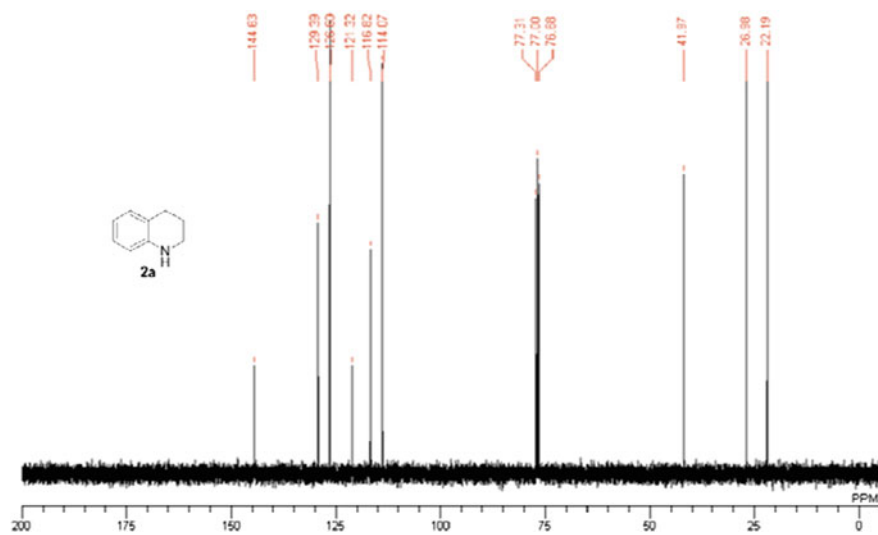
isomer), 2.92 (dd,  $J = 16.5, 5.2$  Hz, 1H, for *syn* isomer), 2.75 (dd,  $J = 16.0, 4.8$  Hz, 1H, for *anti* isomer), 2.50 (dd,  $J = 5.6$  Hz, 1H, for *syn* isomer), 2.50 (m, 1H, for *anti* isomer), 2.10–2.00 (m, 1H, for *syn* isomer), 1.70–1.58 (m, 1H, for *anti* isomer), 1.22 (d,  $J = 6.4$  Hz, 3H, for *anti* isomer), 1.13 (d,  $J = 6.8$  Hz, 3H, for *syn* isomer), 1.04 (d,  $J = 6.4$  Hz, 3H, for *anti* isomer), 0.96 (d,  $J = 6.8$  Hz, 3H, for *syn* isomer);  $^{13}\text{C}$  NMR (100 MHz,  $\text{CDCl}_3$ ) *syn* isomer:  $\delta$  143.7, 128.9, 126.4, 121.1, 116.6, 113.3, 49.9, 33.8, 30.5, 18.1, 14.4; *anti* isomer: 144.3, 128.9, 126.5, 121.2, 116.6, 113.3, 53.2, 35.5, 33.5, 20.8, 18.3;

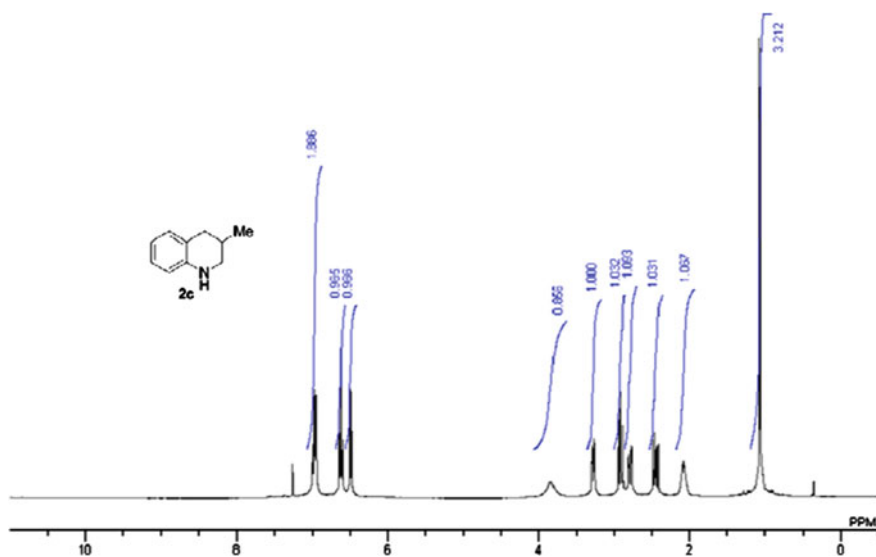
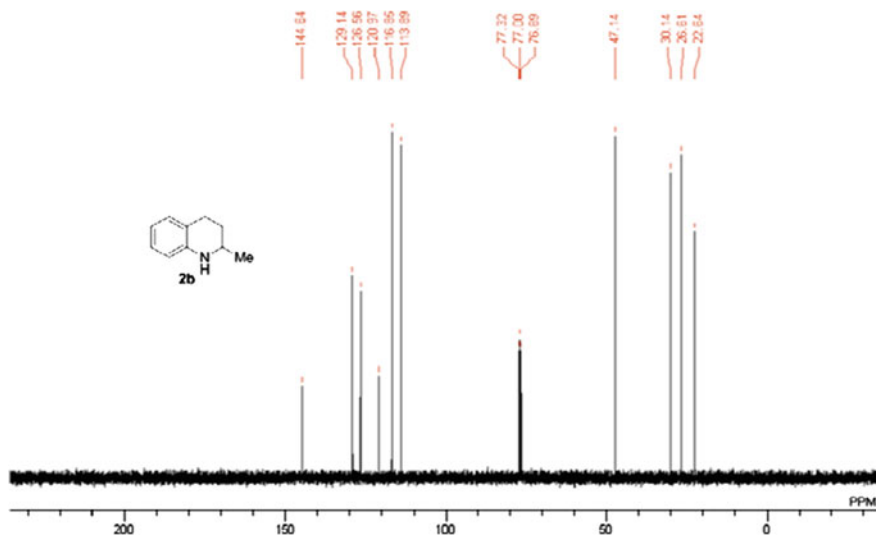
### 2-Phenethyl-1,2,3,4-tetrahydroquinoline (2j) [54]

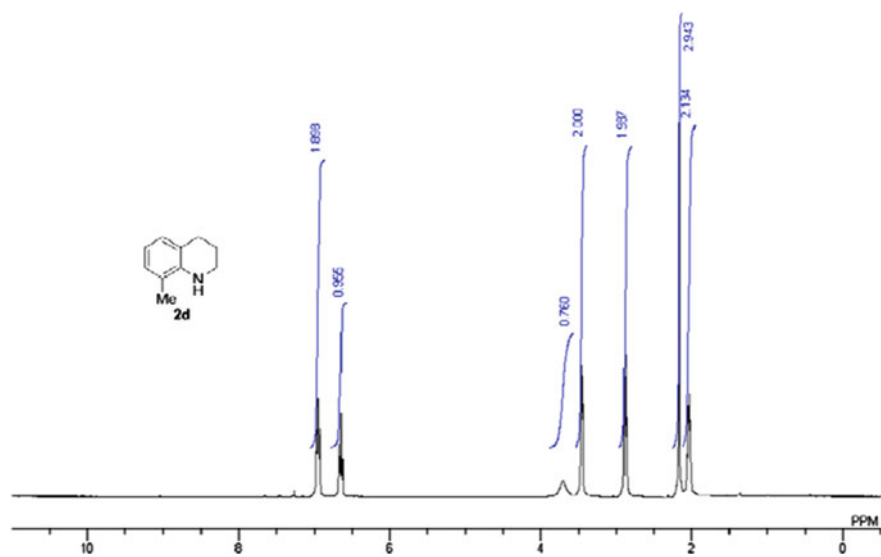
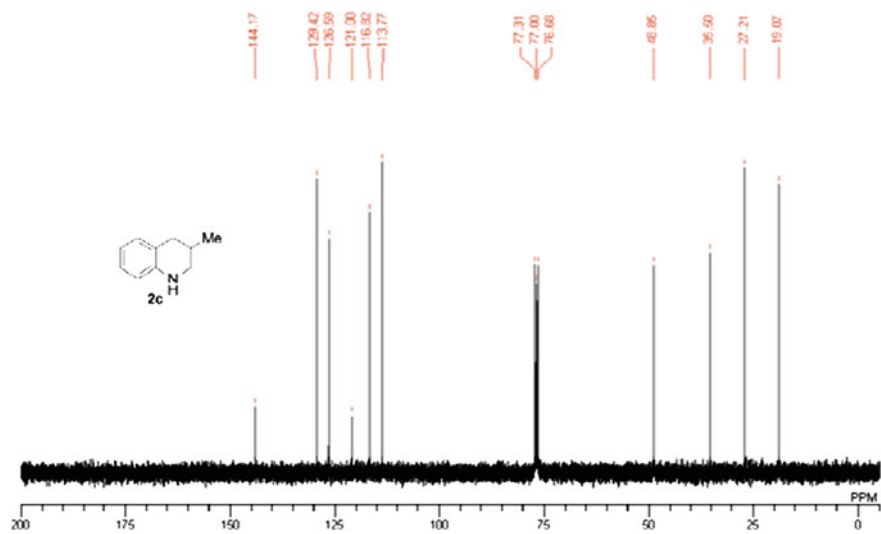
$^1\text{H}$  NMR (400 MHz,  $\text{CDCl}_3$ )  $\delta$  7.32–7.19 (m, 5H), 6.98–6.94 (m, 2H), 6.61 (dd,  $J = 7.6, 7.6$  Hz, 1H), 6.46 (d,  $J = 8.4$  Hz, 1H), 3.81 (bs, 1H), 3.33–3.28 (m, 1H), 2.82–2.73 (m, 4H), 2.04–1.97 (m, 1H), 1.87–1.82 (m, 2H), 1.73–1.66 (m, 1H);  $^{13}\text{C}$  NMR (100 MHz,  $\text{CDCl}_3$ )  $\delta$  144.3, 141.7, 129.1, 128.4, 128.2, 126.6, 125.8, 121.2, 116.9, 114.0, 51.1, 38.2, 32.2, 28.0, 26.2;

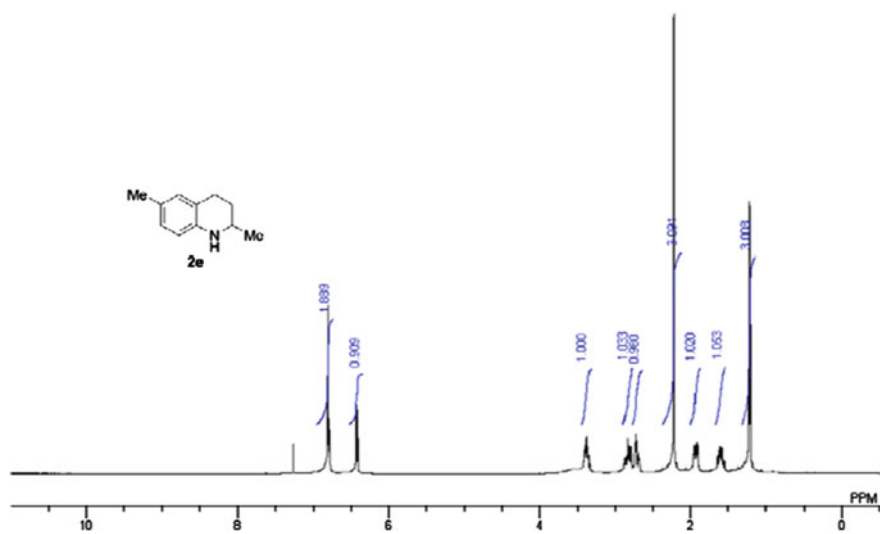
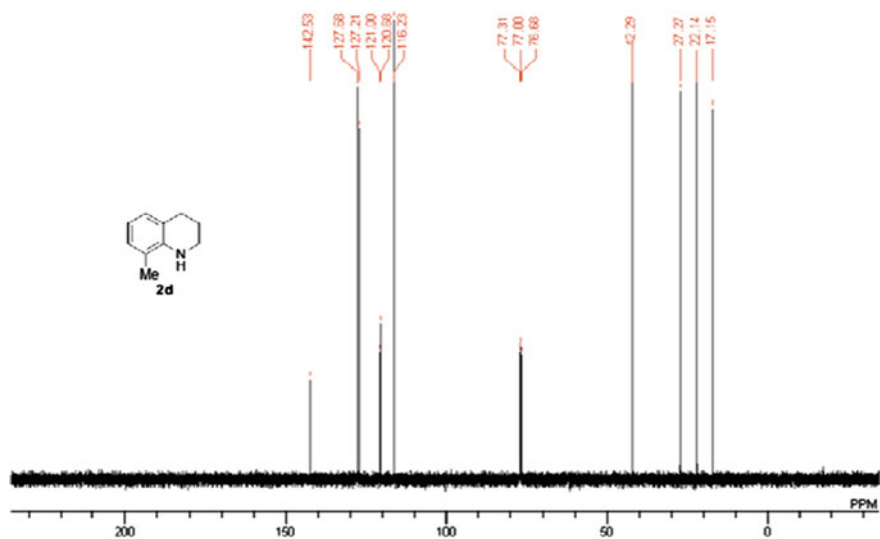
#### 4.4.10 $^1\text{H}$ and $^{13}\text{C}$ NMR Spectra

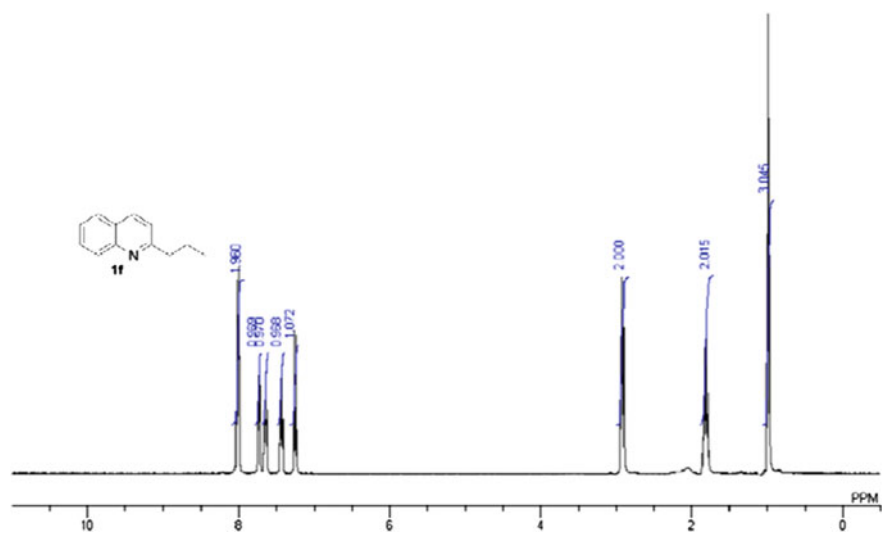
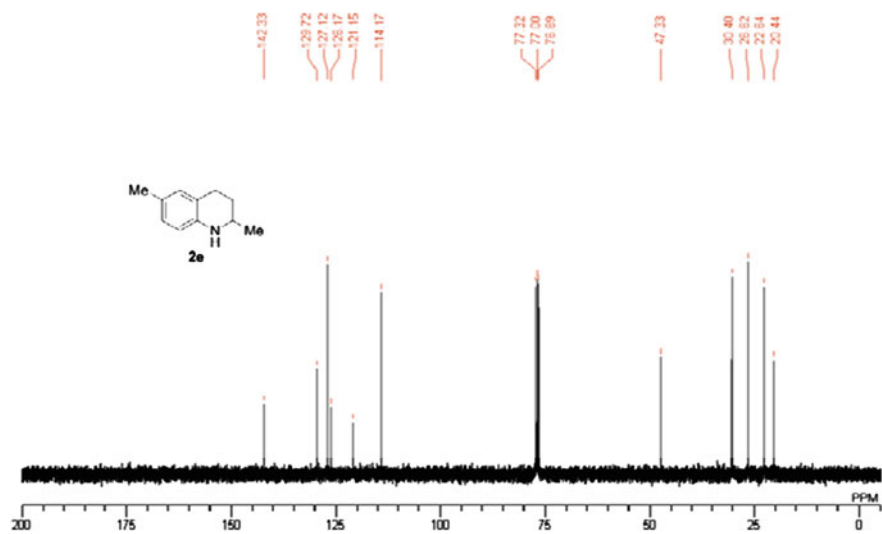


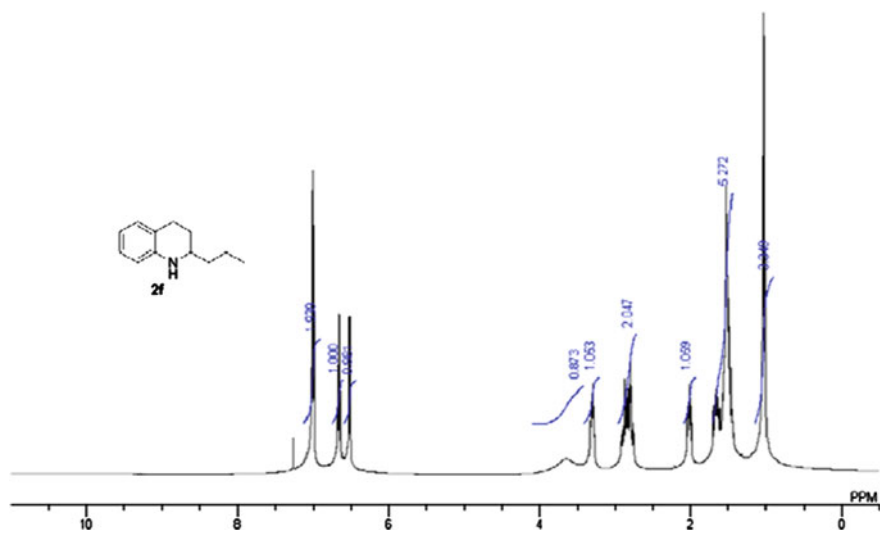
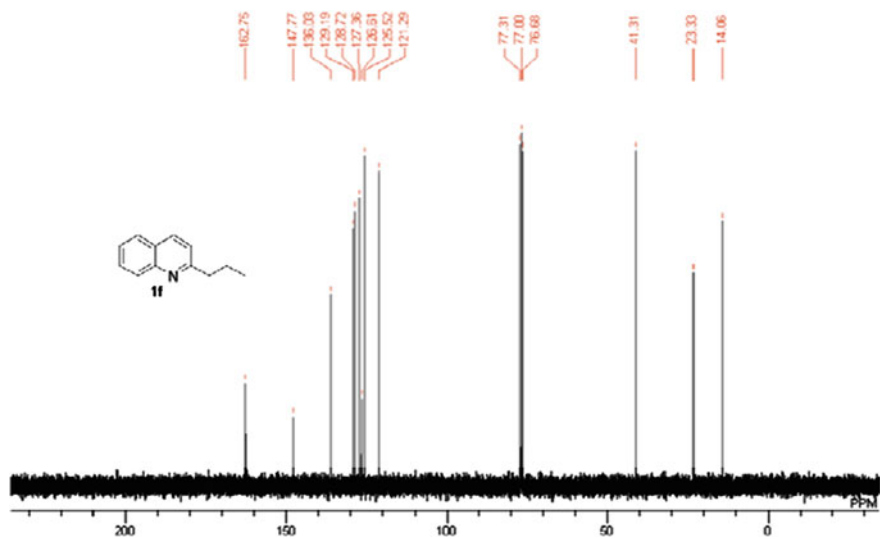


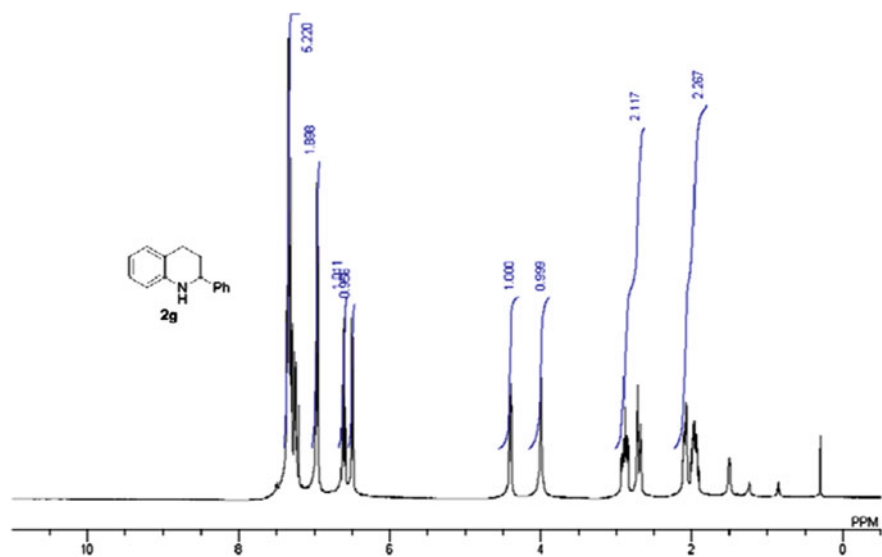
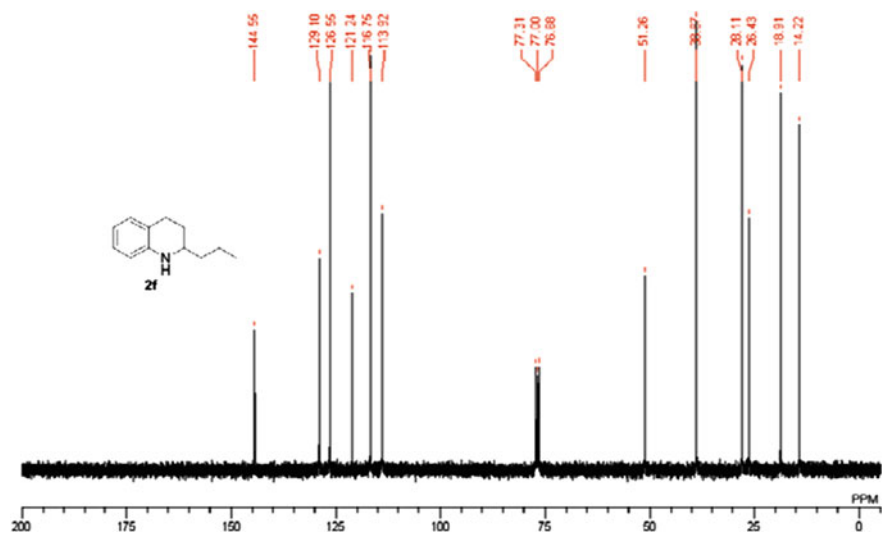


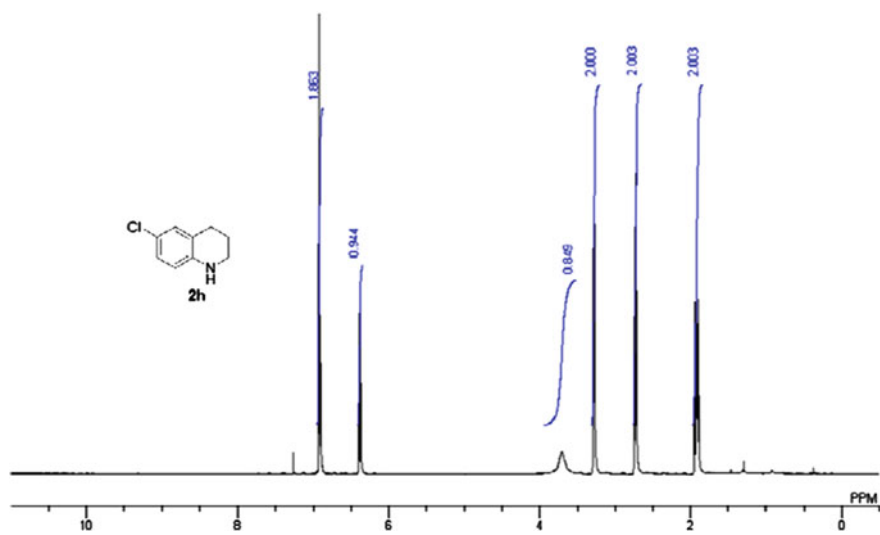
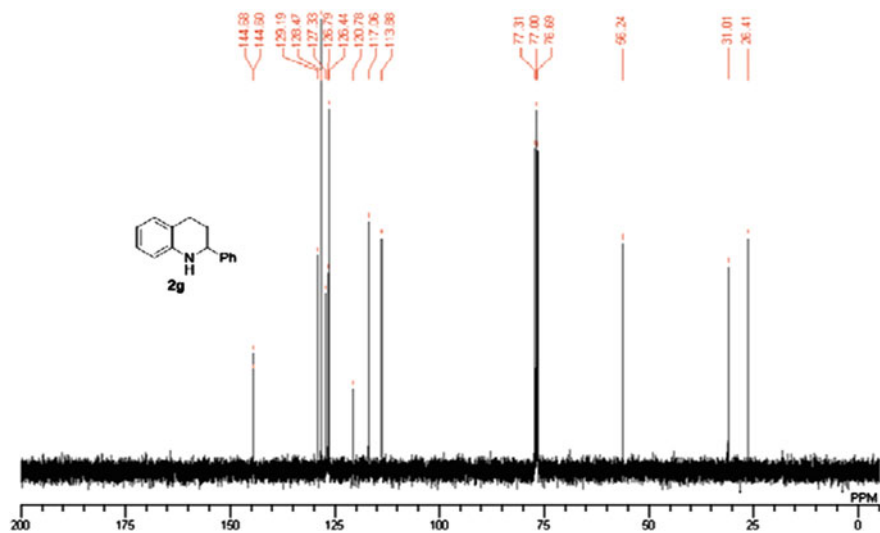


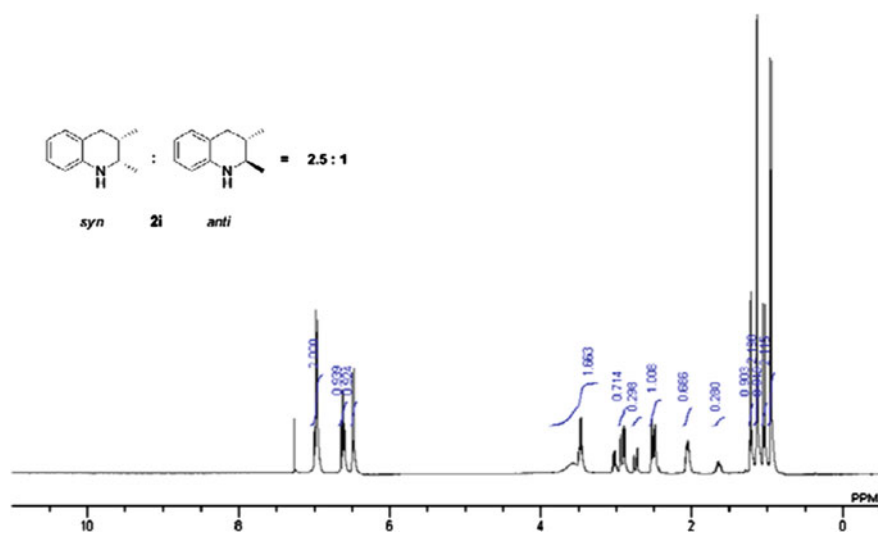
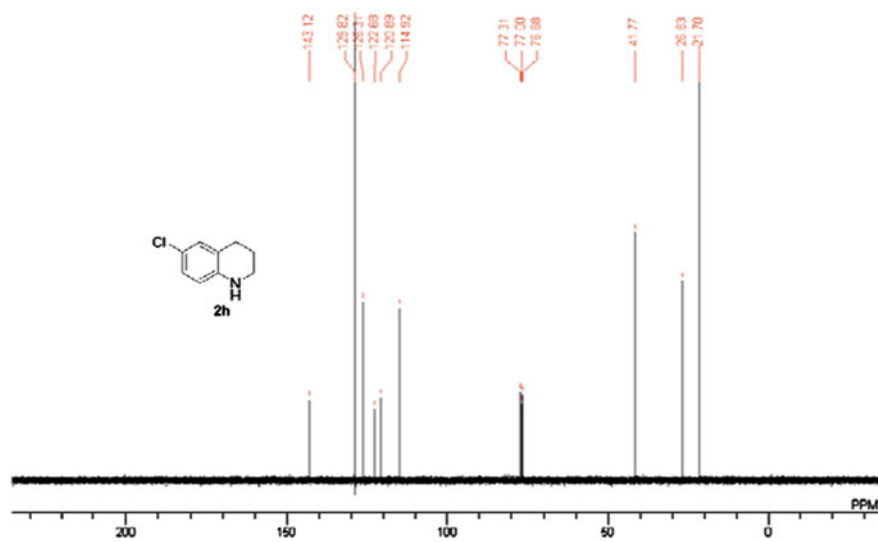


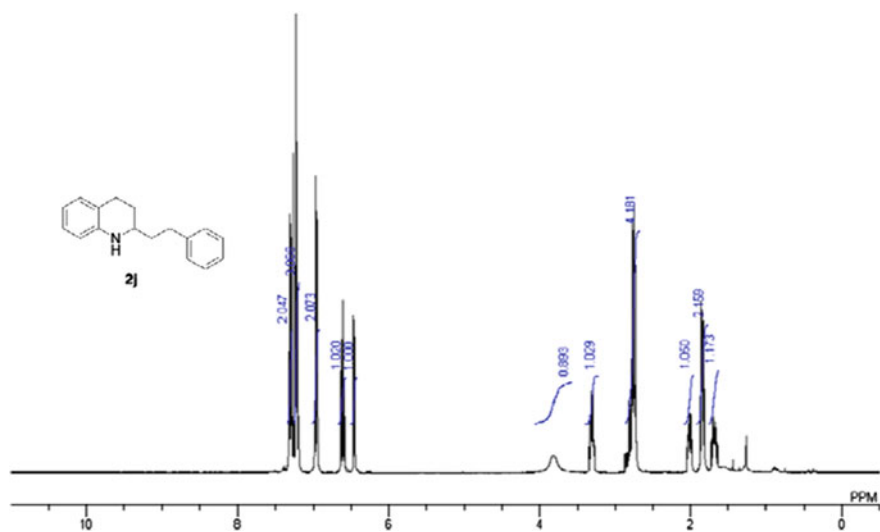
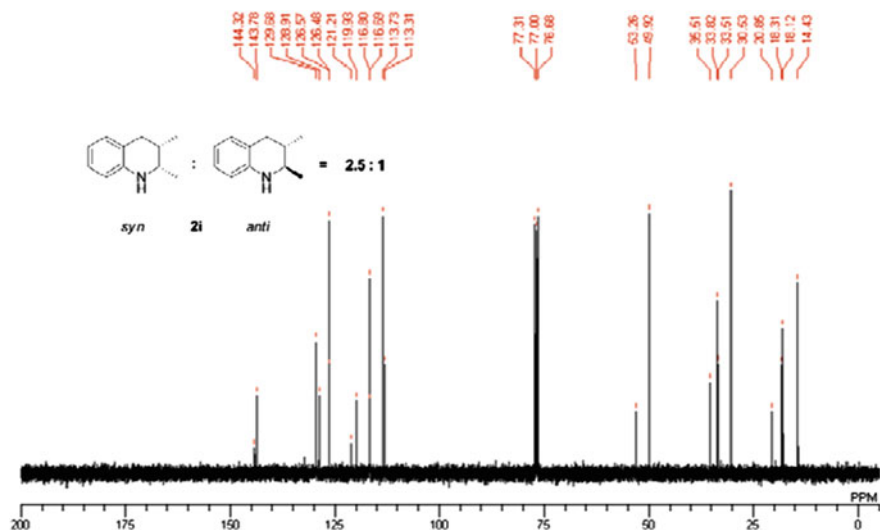


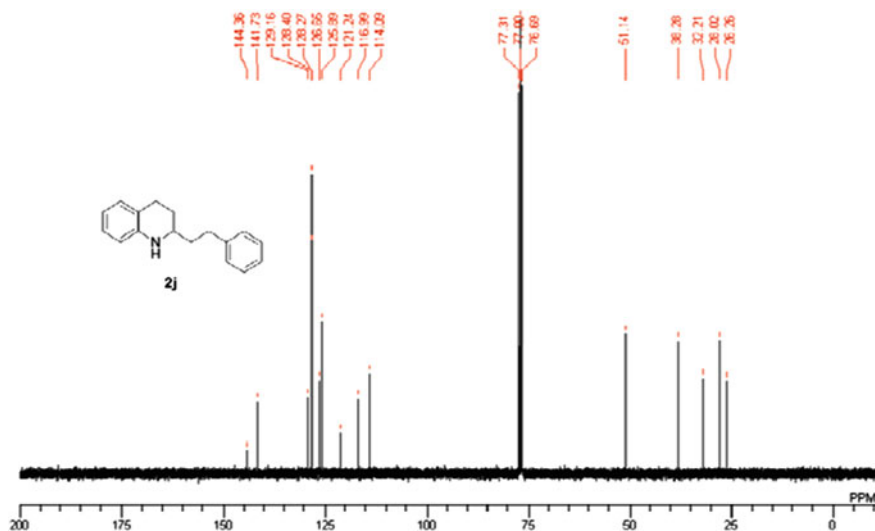












## References

- Zielasek V, Jürgens B, Schulz C et al (2006) Gold catalysts: nanoporous gold foams. *Angew Chem Int Ed* 45:8241–8244
- Xu C, Su J, Xu X et al (2007) Low temperature CO oxidation over unsupported nanoporous gold. *J Am Chem Soc* 129:42–43
- Xu C, Xu X, Su J et al (2007) Research on unsupported nanoporous gold catalyst for CO oxidation. *J Catal* 252:243–248
- Wittstock A, Neumann B, Schaefer A et al (2009) Nanoporous Au: an unsupported pure gold catalyst? *J Phys Chem C* 113:5593–5600
- Wang LC, Jin HJ, Widmann D et al Dynamic studies of CO oxidation on nanoporous Au using a TAP reactor. *J Catal* 278:219–227
- Fujita T, Guan P, McKenna K et al (2012) Atomic origins of the high catalytic activity of nanoporous gold. *Nat Mater* 11:775–780
- Wittstock A, Zielasek V, Biener J et al (2010) Nanoporous gold catalysts for selective gas-phase oxidative coupling of methanol at low temperature. *Science* 327:319–322
- Asao N, Hatakeyama N, Menggenbateer et al (2012) Aerobic oxidation of alcohols in the liquid phase with nanoporous gold catalysts. *Chem Commun* 48:4540–4542
- Yin H, Zhou C, Xu C et al (2008) Aerobic oxidation of d-glucose on support-free nanoporous gold. *J Phys Chem C* 112:9673–9678
- Kosuda KM, Wittstock A, Friend CM et al (2012) Oxygen-mediated coupling of alcohols over nanoporous gold catalysts at ambient Pressures. *Angew Chem Int Ed* 51:1698–1701
- Zhang J, Liu P, Ma H et al (2007) Nanostructured porous gold for methanol electro-oxidation. *J Phys Chem C* 111:10382–10388
- Yu C, Jia F, Ai Z et al (2007) Direct oxidation of methanol on self-supported nanoporous gold film electrodes with high catalytic activity and stability. *Chem Mater* 19:6065–6067
- Zeis R, Lei T, Sieradzki K et al (2008) Catalytic reduction of oxygen and hydrogen peroxide by nanoporous gold. *J Catal* 253:132–138

14. Asao N, Ishikawa Y, Hatakeyama N et al (2010) Nanostructured materials as catalysts: nanoporous-gold-catalyzed oxidation of organosilanes with water. *Angew Chem Int Ed* 49:10093–10095
15. Hashmi ASK, Hutchings (2006) Gold catalysis. *Angew Chem Int Ed* 45:7896–7936
16. Pina CD, Falletta E, Prati L et al (2008) Selective oxidation using gold. *Chem Soc Rev* 37:2077–2095
17. Corma A, Garcia H (2008) Supported gold nanoparticles as catalysts for organic reactions. *Chem Soc Rev* 37:2096–2126
18. Matsumoto T, Ueno M, Wang N et al (2008) Recent advances in immobilized metal catalysts for environmentally benign oxidation of alcohols. *Chem-Asian J* 3:196–214
19. Corma A, Leyva-Pérez A, Sabater MJ (2011) Gold-catalyzed carbon–heteroatom bond-forming reactions. *Chem Rev* 111:1657–1712
20. Bond GC, Louis C, Thompson DT (2006) *Catalysis by gold*. Imperial College Press, London, p 244
21. McEwan L, Julius M, Roberts S et al (2010) A review of the use of gold catalysts in selective hydrogenation reactions Lynsey McEwana. *Gold Bull* 43:298–306
22. Yan M, Jin T, Ishikawa Y et al (2012) Nanoporous gold catalyst for highly selective semihydrogenation of alkynes: remarkable effect of amine additives. *J Am Chem Soc* 134:17536–17542
23. Sridharan V, Suryavanshi P, Menendez JC (2011) Advances in the chemistry of tetrahydroquinolines. *Chem Rev* 111:7157–7259
24. Fish RH, Tan JL, Thormodsen AD (1984) Homogeneous catalytic hydrogenation. 2. Selective reductions of polynuclear heteroaromatic compounds catalyzed by chlorotris(triphenylphosphine)rhodium(I). *J Org Chem* 49:4500–4505
25. Fish RH, Tan JL, Thormodsen AD (1985) Homogeneous catalytic hydrogenation. 4. Regioselective reduction of polynuclear heteroaromatic compounds catalyzed by hydridochlorotris (triphenylphosphine)ruthenium(II). *Organometallics* 4:1743–1747
26. Wang WB, Lu SM, Yang PY et al (2003) Highly enantioselective iridium-catalyzed hydrogenation of heteroaromatic compounds, quinolones. *J Am Chem Soc* 125:10536–10537
27. Zhu G, Pang K, Parkin G (2008) New modes for coordination of aromatic heterocyclic nitrogen compounds to molybdenum: catalytic hydrogenation of quinoline, isoquinoline, and quinoxaline by Mo(PMe<sub>3</sub>)<sub>4</sub>H<sub>4</sub>. *J Am Chem Soc* 130:1564–1565
28. Zhou H, Li Z, Wang Z et al (2008) Hydrogenation of quinolines using a recyclable phosphine-free chiral cationic ruthenium catalyst: enhancement of catalyst stability and selectivity in an ionic liquid. *Angew Chem Int Ed* 47:8464–8467
29. Dobreiner GE, Nova A, Schley ND (2011) Iridium-catalyzed hydrogenation of n-heterocyclic compounds under mild conditions by an outer-sphere pathway. *J Am Chem Soc* 133:7547–7562
30. Fache F (2004) Solvent dependent regioselective hydrogenation of substituted quinolines. *Synlett* 15:2827–2829
31. Zhandarev VV, Goshin ME, Kazin VN et al (2006) Catalytic synthesis of new halogen-containing tetrahydroquinolin-8-ols. *J Org Chem* 42:1093–1094
32. Sánchez-Delgado RA, Machalaba N, Ng-a-qui N (2007) Hydrogenation of quinoline by ruthenium nanoparticles immobilized on poly(4-vinylpyridine). *Catal Commun* 8:2115–2118
33. Hashimoto N, Takahashi Y, Hara T et al Fine tuning of Pd<sub>0</sub> nanoparticle formation on hydroxyapatite and its application for regioselective quinoline hydrogenation. *Chem Lett* 39:832–834
34. Sun YP, Fu HY, Zhang DL et al (2010) Complete hydrogenation of quinoline over hydroxyapatite supported ruthenium catalyst. *Catal Commun* 12:188–192
35. Fang M, Machalaba N, Sánchez-Delgado RA (2011) Hydrogenation of arenes and N-heteroaromatic compounds over ruthenium nanoparticles on poly(4-vinylpyridine): a versatile catalyst operating by a substrate-dependent dual site mechanism. *Dalton Trans* 40:10621–10632

36. Mao H, Chen C, Liao X et al (2011) Catalytic hydrogenation of quinoline over recyclable palladium nanoparticles supported on tannin grafted collagen fibers. *J Mol Catal A: Chem* 341:51–56
37. Rueping M, Koenigs RM, Borrmann R et al (2011) Size-selective, stabilizer-free, hydrogenolytic synthesis of iridium nanoparticles supported on carbon nanotubes. *Chem Mater* 23:2008–2010
38. Cao Y and co-authors reported the quinoline hydrogenation using Au/HAS-TiO<sub>2</sub> catalyst under high pressure of H<sub>2</sub> (2 MPa), see: Ren D, He L, Yu L et al (2012) An Unusual Chemoselective Hydrogenation of Quinoline Compounds Using Supported Gold Catalysts. *J Am Chem Soc* 134:17592–17598 (During our manuscript in preparation)
39. Ferri D, Burgi T, Baiker A (2001) Pt and Pt/Al<sub>2</sub>O<sub>3</sub> thin films for investigation of catalytic solid–liquid interfaces by ATR-IR spectroscopy: CO adsorption, H<sub>2</sub>-induced reconstruction and surface-enhanced absorption. *J Phys Chem B* 105:3187–3195
40. Tanaka S, Kaneko T, Asao N et al (2011) A nanostructured skeleton catalyst: Suzuki-coupling with a reusable and sustainable nanoporous metallic glass Pd-catalyst. *Chem Commun* 47:5985–5987
41. Kaneko T, Tanaka S, Asao N et al (2011) Reusable and sustainable nanostructured skeleton catalyst: heck reaction with nanoporous metallic glass Pd (PdNPore) as a support, stabilizer and ligand-free catalyst. *Adv Synth Catal* 353:2927–2932
42. Jin T, Yan M, Menggenbateer et al (2011) Nanoporous copper metal catalyst in click chemistry: nanoporosity-dependent activity without supports and bases. *Adv Synth Catal* 353:3095–3100
43. Asao N, Meggenbateer, Seya Y et al (2012) Nanoporous Gold-Catalyzed [4+2] Benzannulation between ortho-alkynylbenzaldehydes and alkynes. *Synlett* 23:66–69
44. Asao N, Jin T, Tanaka S et al (2012) From molecular catalysts to nanostructured materials skeleton catalysts. *Pure Appl Chem* 84:1771–1784
45. Jin T, Yan M, Yamamoto Y (2012) Click chemistry of alkyne-azide cycloaddition using nanostructured copper catalysts. *ChemCatChem* 4:1217–1229
46. Xu C, Li Y, Tian F et al (2010) Dealloying to nanoporous silver and its implementation as a template material for construction of nanotubular mesoporous bimetallic nanostructures. *ChemPhysChem* 11:3320–3328
47. Qian B, Guo S, Shao J et al (2010) Palladium-catalyzed benzylic addition of 2-methyl azaarenes to N-sulfonyl aldimines via C–H bond activation. *J Am Chem Soc* 132:3650–3651
48. Wang DW, Wang XB, Wang DS et al (2009) Highly enantioselective iridium-catalyzed hydrogenation of 2-benzylquinolines and 2-functionalized and 2,3-disubstituted quinolines. *J Org Chem* 74:2780–2787
49. Wang T, Zhou LG, Li Z et al (2011) Highly enantioselective hydrogenation of quinolines using phosphine-free chiral cationic ruthenium catalysts: scope, mechanism, and origin of enantioselectivity. *J Am Chem Soc* 133:9878–9891
50. Wu J, Wang C, Tang W et al (2012) The remarkable effect of a simple ion: iodide-promoted transfer hydrogenation of heteroaromatics. *Chem Eur J* 18:9525–9529
51. Hashimoto N, Takahashi Y, Hara T et al (2010) Fine tuning of Pd<sub>0</sub> nanoparticle formation on hydroxyapatite and its application for regioselective quinoline hydrogenation. *Chem Lett* 39:832–834
52. Parekh V, Ramsden JA, Wills M et al (2010) Asymmetric transfer hydrogenation of quinolines using tethered Ru(II) catalysts. *Tetrahedron Asymmetry* 21:1549–1556
53. Mccall JM, Romero DL (2012) PCT Int Appl WO 2012094462:A2
54. Patil NT, Wu H, Yamamoto YA (2007) Route to 2-substituted tetrahydroquinolines via palladium-catalyzed intramolecular hydroamination of anilino-alkynes. *J Org Chem* 72:6577–6579

# Curriculum Vitae



## Mei Yan

Harbin 150080, P. R. China  
Key Laboratory of Microsystems  
and Micronanostructures Manufacturing,  
Ministry of Education,  
Harbin Institute of Technology  
Tel.: +86-451-86403493  
Fax: +86-451-86403483  
e-mail: yanmei@hit.edu.cn  
Web: <http://homepage.hit.edu.cn/pages/meiyan>

## Education

### Tohoku University Sendai, Japan

Degree: Ph.D. March 2013

Thesis advisor: Naoki Asao

Thesis topic: Development of New Catalytic Performances of Nanoporous Metals for Molecular Transformations

### Dalian Institute of Technology Dalian, China

Degree: M.S. July 2009

### Daqing Petroleum Institute Daqing, China

Degree: B.S. July 2006

## Major Honors and Awards

- The Presidential Prize, 2013.
- Aoba Society for the Promotion of Science Award, 2013.
- Research assistant (RA) in WPI-Advanced Institute for Materials Research, 2012–2013.
- The Scholarship supported by China Scholarship Council, 2009–2013.

## Research Interests

I am interested in novel nano-metal materials especially high catalytic nano-catalysts for heterogeneous molecular transformations. Recently, I have largely focused on nanoporous metals and their application in heterogeneous organic reactions. What excites me most is the high catalytic activity and selectivity of nanoporous gold for the semihydrogenation of alkynes affording the corresponding alkenes in high chemical yields and excellent Z-selectivity without any over-reduced alkanes. Moreover, in contrast to the supported metal nanoparticles, nanoporous metals without supports are challenging catalyst systems to understand the intrinsic catalytic activity more easily and to extend the catalytic application widely by elimination of the support-effect problems and relaxation of aggregation. These make me to explore new catalytic performances of nanoporous metals for molecular transformations.

## Relevant Employment History

July 2013—present. Harbin Institute of Technology

Lecturer

Nano-metal catalysts and their application in catalysis.

# Publications

1. Yan, M.; Jin, T.; Ishikawa, Y.; Minato, T.; Fujita, T.; Chen, L-Y.; Bao, M.; Asao, N.; Chen, M-W.; Yamamoto, Y. Nanoporous Gold Catalyst for Highly Selective Semihydrogenation of Alkynes: Remarkable Effect of Amine Additives. *J. Am. Chem. Soc.* **2012**, *134*, 17536–17542.
2. Yan, M.; Jin, T.; Chen, Q.; Ho, H. E.; Fujita, T.; Chen, L-Y.; Bao, M.; Chen, M-W.; Asao, N.; Yamamoto, Y. Unsupported Nanoporous Gold Catalyst for Highly Selective Hydrogenation of Quinolines. *Org. Lett.* **2013**, *15*, 1484–1487.
3. Jin, T.; Yan, M.; Menggenbateer.; Minato, T.; Bao, M.; Yamamoto, Y. Nanoporous Copper Metal Catalyst in Click Chemistry: Nanoporosity Dependent Activity without Supports and Bases. *Adv. Synth. Catal.* **2011**, *353*, 3095–3100.
4. Jin, T.; Yan, M.; Yamamoto, Y. Click Chemistry of Alkyne-Azide Cycloaddition Using Nano-structured Copper Catalysts. *ChemCatChem.* **2012**, *4*, 1217–1229.
5. Feng, X.; Yan, M.; Zhang, X.; Bao, M. Preparation and application of SBA-15-supported palladium catalyst for Heck reaction in supercritical carbon dioxide. *Chinese Chemical Letters.* **2011**, *22*, 643–646.
6. Feng, X.; Yan, M.; Zhang, T.; Liu, Y.; Bao, M. Preparation and application of SBA-15-supported palladium catalyst for Suzuki reaction in supercritical carbon dioxide. *Green Chem.* **2010**, *12*, 1758–1766.
7. Guo, C.; Wu, X.; Yan, M.; Dong, Q.; Yin, S.; Sato, T.; Liu, S. The visible-light driven photocatalytic destruction of NO<sub>x</sub> using mesoporous TiO<sub>2</sub> spheres synthesized via a “water-controlled release process”. *Nanoscale.* **2013**, *5*, 8184–8191.
8. Guo, C.; Yin, S.; Yan, M.; Kobayashi, M.; Kakihana, M.; Sato, T. Morphology-controlled Synthesis of W18O49 Nanostructures and Their Near-infrared Absorption Properties. *Inorganic Chemistry.* **2012**, *51*, 4763–4771.
9. Guo, C.; Yin, S.; Yan, M.; Sato, T. Facile synthesis of homogeneous Cs<sub>x</sub>WO<sub>3</sub> nanorods with excellent low-emissivity and NIR shielding property by a water controlled-release process. *J. Mater. Chem.* **2011**, *21*, 5099–5105.
10. Guo, C.; Yin, S.; Zhang, P.; Yan, M.; Adachi, K.; Chonan, T.; Sato, T. Novel synthesis of homogenous Cs<sub>x</sub>WO<sub>3</sub> nanorods with excellent NIR shielding properties by a water controlled-release solvothermal process. *J. Mater. Chem.* **2010**, *20*, 8227–8229.
11. Liu, P.; Yan, M.; He, R. Bis(imino)pyridine palladium(II) complexes as efficient catalysts for the Suzuki–Miyaura reaction in water. *Appl. Organometal. Chem.* **2010**, *24*, 131–134.